ADVANCED MATERIALS
www.advmat.de

# Self-Healing Hydrogel Bioelectronics

*Zhikang Li, Jijian Lu, Tian Ji, Yumeng Xue,* Libo Zhao,* Kang Zhao, Boqing Jia, Bin Wang, Jiaxiang Wang, Shiming Zhang,* and Zhuangde Jiang*

**Hydrogels have emerged as powerful building blocks to develop various soft bioelectronics because of their tissue-like mechanical properties, superior bio-compatibility, the ability to conduct both electrons and ions, and multiple stimuli-responsiveness. However, hydrogels are vulnerable to mechanical damage, which limits their usage in developing durable hydrogel-based bioelectronics. Self-healing hydrogels aim to endow bioelectronics with the property of repairing specific functions after mechanical failure, thus improving their durability, reliability, and longevity. This review discusses recent advances in self-healing hydrogels, from the self-healing mechanisms, material chemistry, and strategies for multiple properties improvement of hydrogel materials, to the design, fabrication, and applications of various hydrogel-based bioelectronics, including wearable physical and biochemical sensors, supercapacitors, flexible display devices, triboelectric nanogenerators (TENGs), implantable bioelectronics, etc. Furthermore, the persisting challenges hampering the development of self-healing hydrogel bioelectronics and their prospects are proposed. This review is expected to expedite the research and applications of self-healing hydrogels for various self-healing bioelectronics.**

Z. Li, J. Lu, T. Ji, L. Zhao, K. Zhao, B. Jia, B. Wang, J. Wang, Z. Jiang
State Key Laboratory for Manufacturing Systems Engineering
International Joint Laboratory for Micro/Nano Manufacturing and Measurement Technologies
Xi'an 710049, China
E-mail: libozhao@xjtu.edu.cn

Z. Li, J. Lu, T. Ji, L. Zhao, K. Zhao, B. Jia, B. Wang, J. Wang, Z. Jiang
School of Instrument Science and Technology
Xi'an Jiaotong University
Xi'an 710049, China

Z. Li, J. Lu, T. Ji, L. Zhao, K. Zhao, B. Jia, B. Wang, J. Wang, Z. Jiang
School of Mechanical Engineering
Xi'an Jiaotong University
Xi'an 710049, China

Y. Xue
State Key Laboratory of Solidification Processing
School of Materials Science and Engineering
Northwestern Polytechnical University and Shaanxi Joint Laboratory of Graphene
Xi'an 710072, China
E-mail: ymxue@nwpu.edu.cn

S. Zhang
Department of Electrical and Electronic Engineering
The University of Hong Kong
Hong Kong SAR 999077, China
E-mail: szhang@eee.hku.hk

The ORCID identification number(s) for the author(s) of this article can be found under https://doi.org/10.1002/adma.202306350

**DOI: 10.1002/adma.202306350**

## 1. Introduction

In recent years, soft bioelectronics have ushered in a booming development era because of their promising applications in personalized healthcare monitoring, point-of-care clinical diagnostics, prostheses, and human-machine interface, which will essentially improve the efficiency of precise theranostics, and alter the way that people interact with machines.[1–3] This prosperity hinges on the unique functions of soft electronic devices: 1) soft and sensitive to perceive tiny changes in ambient stimulus, such as strain (0.1%) and pressure (≈0.01 Pa);[1,4] 2) flexible and stretchable (≈1000%) to be conformably adhered to any curved surfaces,[5] such as human skin; 3) thin (≈1 μm) and lightweight (3 g $m^{-2}$) to allow imperceptible integration and readily movement.[6,7] These prominent features enable soft bioelectronics to seamlessly integrate with humans and prostheses to realize real-time, long-term, and low-cost sensing of various physical and biological information. To date, a variety of soft bioelectronics have been developed, including electronic skin, wearable sensors, flexible triboelectric nanogenerators (TENGs), soft super-capacitors, and implantable electronics. Their applications spread from tactile sensing, vital physiological signal monitoring,[8,9] and biomarker detection (e.g., sweat, tear, and urine)[10,11] to in vivo drug delivery,[12] cell manipulation,[13] neuromodulation and therapy.[14] Superior functionalities that conventional solid devices cannot achieve have been successfully implemented. For instance, battery-free epidermal electronics have emerged for wireless, continuous, and real-time measurement of electrocardiogram (ECG) and photoplethysmogram (PPG) signals from fragile neonates, which can significantly reduce injuries to the neonatal skin and constraints on the natural movement of babies compared with conventional, hard-wired monitoring systems.[15] Wearable biochemical sensors have been developed for in situ and real-time analysis of glucose, lactate, and sodium and potassium ions in sweat, enabling real-time assessment of human physiological conditions.[16] Implantable tissue-like electronics have been invented to conformally interface with nerve tissues for localized neuromodulation through electrical stimulation.[17]

Although soft bioelectronics are bringing about rapid revolutions in human life and society, the majority of currently developed bioelectronics are based on textiles,[18] elastomers[19] (such as polydimethylsiloxane (PDMS), polyurethane (PU), and

 

Ecoflex), polymer-nanomaterials composites,[20,21] which generally feature much larger Young's modulus (typically, 2 MPa–1 GPa) and non-intrinsic biological compatibility. The large mechanical mismatch with human skin or tissues and severe issues of biocompatibility significantly hinder their practical biomedical applications. Compared with these materials, hydrogel, a three-dimensional (3D) polymer network infiltrated with plenty of water (≥80 wt%),[17,22] has been widely considered as a promising material for developing both soft wearable and implantable electronics for biomedical applications because of their tissue-mimicking Young's modulus, superior biocompatibility, biologically-similar ionic conductivity, and multiple stimuli-responsiveness.[23,24] Specifically, the close Young's modulus (≈1 Pa to ≈1 MPa) of hydrogels to that (≈1 kPa to ≈100 kPa) of human skin or tissues can enable excellent mechanical matching at electronic-tissue interfaces, contributing to conformable integration of electronics with biology.[25–28] Their superior extracellular matrix-mimetic structure renders soft bioelectronics with native tissue-like physiological properties, i.e., excellent cytocompatibility and histocompatibility, which can avoid unexpected biological immune reactions during long-term attachment.[29] Meanwhile, the ionic conductive mechanism of hydrogels enables electronic devices to be capable of readily electrical communication with biological tissues.[27] Additionally, their diverse stimuli-responsiveness endows hydrogels with the capabilities to react to various external stimuli (e.g., light, pH, heat, etc.), which can be harnessed to develop bioactuators for drug delivery.[30] Therefore, merging hydrogels with electronics and devices can perfectly bridge the gap between humans and machines in aspects of mechanical, electrical, and biochemical properties, and enable the development of next-generation soft bioelectronics. To date, a diversity of hydrogel-based soft bioelectronics, including sensors, displays, TENGs, and implantable electrodes, have been developed for both on-skin and implantable applications.

Despite the promising prospect of hydrogels in developing wearable and implantable bioelectronics, challenging issues still exist and need to be tackled before their clinical transition and practical applications. One crucial challenge is that hydrogel bioelectronics are prone to be damaged during their usage owing to the inherent low Young's modulus of hydrogels and the complex load-bearing and dynamic environment inside human bodies, which severely impede their long-term and reliable application. For instance, wearable electronics will inevitably suffer from various mechanical forces from the external environment, such as scratch, wear, tear, and puncture. Implantable bioelectronics may get disrupted by over-range stretching, stress fatigue, and stress-induced internal microcracks during the frequent and continuous movements of human organs and joints, such as the continuous contraction and expansion of hearts. Inspired by human skin, a complicated sensory system that can work for more than one hundred years because of its regeneration or repair nature when damaged, researchers are dedicated to imparting hydrogel bioelectronic with "self-regeneration" or "self-healing" capability to expand their durability, reliability, and longevity. The self-healing capability plays a significant role in soft bioelectronics because it can essentially overcome the inevitable structure fracture and function failure or degradation during their operation process. The underlying mechanism is that hydrogels with self-healing capacity are capable of reconstructing their broken


**Figure 1.** Schematic diagram of SHHs and their potential applications in soft bioelectronics. Wearable sensors: Reproduced with permission.[41] Copyright 2023, Elsevier. Supercapacitors: Reproduced with permission.[42] Copyright 2020, Elsevier. Display devices: Reproduced with permission.[43] Copyright 2016, American Association for the Advancement of Science. TENGs: Reproduced with permission.[44] Copyright 2020, American Chemical Society. Implantable bioelectronics: Reproduced with permission.[45] Copyright 2022, John Wiley & Sons. Reproduced with permission.[46] Copyright 2021, Elsevier.

bonds after damage and thus restoring their original mechanical, chemical, and electrical properties. This capability imparts hydrogel soft bioelectronics with several remarkable functions: 1) enabling soft bioelectronics to recover their original structures, functions, and performances after destruction; 2) improving the mechanical durability of devices through stress dissipation effects for long-term application (when subjected to load, the reversible dynamic bonds in self-healing hydrogels can act as sacrificial bonds to break and dissipate the accumulated stress and energy, thus alleviating the stress concentration and damage to the structure. When the load is removed, the broken reversible bonds can reform to recover the original structure and mechanical performances of the damaged hydrogel, thus resisting stress-induced cracks and stress fatigue, and enhancing the device's mechanical durability;[31,32] 3) endowing soft bioelectronics with shape adaptability, i.e., their structures can be adjusted to various tissue or organ shapes through the fracture and reformation of the reversible linkages in self-healing hydrogels.[33] Therefore, self-healing provides a promising and effective solution to the challenging issue existing in hydrogel-based soft bioelectronics, enabling their long-term application in personalized healthcare and therapy.

As of today, a diversity of self-healing hydrogels (SHHs) have been developed to reacquire their original structures, properties, and functions when damaged. The underlying principle is to exploit dynamic and reversible interactions to recross-link the polymer network. As illustrated in **Figure 1**, currently, self-healing mechanisms can be classified into three

categories: autonomous, external stimulus-triggered, and under harsh environments. Their applications in bioelectronics have spread to a variety of areas, such as self-healing sensors, bioactuators, optical display devices, supercapacitors, TENGs, implantable bioelectronics, etc. Diverse strategies have been constructed to simultaneously promote the self-healing ability and other properties of hydrogels, including mechanical strength, stretchability, conductivity, anti-freezing capacity, etc. Remarkable progress has been obtained in the rational design and synthesis of SHHs with excellent comprehensive performance for soft bioelectronics over the past few years. However, most of the previous reviews focus on SHHs and their biomedical usages, such as tissue engineering, wound dressing, and drug delivery.[34–40] A systematic review of SHHs from their self-healing mechanisms to applications in various soft bioelectronics, has rarely been reported.

Herein, we review SHHs and their derived self-healing bioelectronics, ranging from healing mechanisms, chemistries, and strategies for multifunction improvement to device design, fabrication, and applications. Firstly, the self-healing mechanisms, such as autonomous, external stimulus-triggered, and harsh environments, are elucidated in detail. After that, we summarize the advances in SHH-based bioelectronics, including wearable sensors, optical display devices, supercapacitors, TENGs, and implantable bioelectronics. In the last section, the perspective and persisting challenges hampering the development of SHH-based bioelectronics are presented, which indicate the future direction of soft bioelectronics and provide valuable insights for researchers.

## 2. Mechanisms of Self-Healing Hydrogels

According to their dependence on external healing agents, self-healing processes can mainly be categorized into two types: extrinsic and intrinsic. The extrinsic type commonly suffers from limited self-healing cycles and unrepeatable healing at the same location.[47–49] In contrast, intrinsic self-healing has drawn increasing attention because of its simple preparation strategy, repeated healing times,[50–52] and potentially tunable and controllable self-healing ability. Depending on whether extra stimuli (such as heat, pH, and light) are needed, the intrinsic processes can further be segmented into autonomous and external stimulus-triggered. This section presents a detailed discussion on the advancements in self-healing mechanisms utilized for hydrogels over the past several years. It includes autonomous and external stimulus-triggered self-healing, as well as self-healing strategies employed in hash environments, such as at low-temperature and underwater circumstances.

### 2.1. Autonomous Self-Healing Hydrogels

Autonomous self-healing is implemented through the interdiffusion and fluidity of polymer chains and the recombination of broken reversible bonds in hydrogel rupture interfaces.[53] It mainly involves two strategies: dynamic covalent and non-covalent bonding. Non-covalent bonding typically relies on the reversible physical interactions in cross-linked networks, including hydrogen bonds, metal coordination interaction, electrostatic/ionic interaction, host-guest interaction, and hydrophobic association.[47,48,54,55] Although non-covalent interactions can usually induce rapid self-healing, they suffer limited mechanical strength because of the weak bonding energy.[56] In contrast, SHHs through dynamic covalent bonding possess higher mechanical strength due to their stronger intermolecular forces.[57] Dynamic covalent bonds generally include imine, acylhydrazone, oxime, and borate ester bonds. In some cases, the combination of both non-covalent and covalent interactions is a feasible and typical strategy to address the tradeoff between self-healability and other properties. Following is a detailed discussion on the aforementioned autonomous self-healing mechanisms.

#### *2.1.1. Hydrogen Bonding*

Hydrogen bonding (H-bonding) is one common physical interaction that can generate dynamic and reversible binding force and has been broadly exploited to construct SHHs.[58,59] Generally, it is implemented through an attractive force between hydrogen atoms and electronegative atoms, e.g., oxygen (O), nitrogen (N), and fluorine (F).[55,60] The common protonated-polar functional groups that can result in H-bonding include hydroxyl groups (—OH), carboxyl groups (—COOH), and amino ($—NH_2$). As of today, a diversity of SHHs has been constructed using —OH, —COOH, and $—NH_2$-based H-bonds. For instance, polyvinyl alcohol (PVA) with abundant —OH can be cross-linked based on H-bonding. By freezing–thawing, the PVA hydrogel could autonomously self-healing at room temperature (RT, 25 °C).[61] Besides, the polyacrylamide (PAM)/graphene composite hydrogel was also able to self-repair with an 88% recovery in its tensile strength via the reformation of H-bonds between polymer chains and graphene sheets.

Although H-bonding is extensively utilized to construct SHHs, the bonding strength is relatively weaker (1–63 kJ $mol^{-1}$) than ionic and covalent bonds, leading to unmet mechanical properties in engineering applications.[62] Therefore, a variety of strategies have been dedicated to simultaneously improving mechanical strength and self-healing ability (**Figure 2**). Among them, designing proper network structures has been extensively utilized to enhance mechanical properties. Diverse polymer networks, including interpenetrating polymer networks (IPN)[63] and double networks (DN),[64,65] have been developed, which harness densely cross-linked networks and increased functional groups to balance the mechanical and self-healing properties. For instance, Zhao and co-workers presented a sodium alginate (SA)/PAM-based SHH with semi-IPN layered structures.[66] The SA molecules were self-assembled into the PAM matrix to form semi-IPN through H-bonds, which imparted the resultant hydrogel with a high tensile strength of ≈266 kPa. Meanwhile, the abundant functional groups (—OH and $—NH_2$) existing in SA and PAM chains contributed to numerous H-bonds (**Figure 3a**) and thus a high self-healing efficiency (SHE) of 99% at RT. The damaged hydrogel could restore its original mechanical properties without any external assistance. Feng et al. constructed a SHH with two noncovalent cross-linked networks based on agar, *N*-benzylacrylamide (NBAA), and acryloyl-glycinamide (NAGA) using the one-pot method.[67] The NAGA and

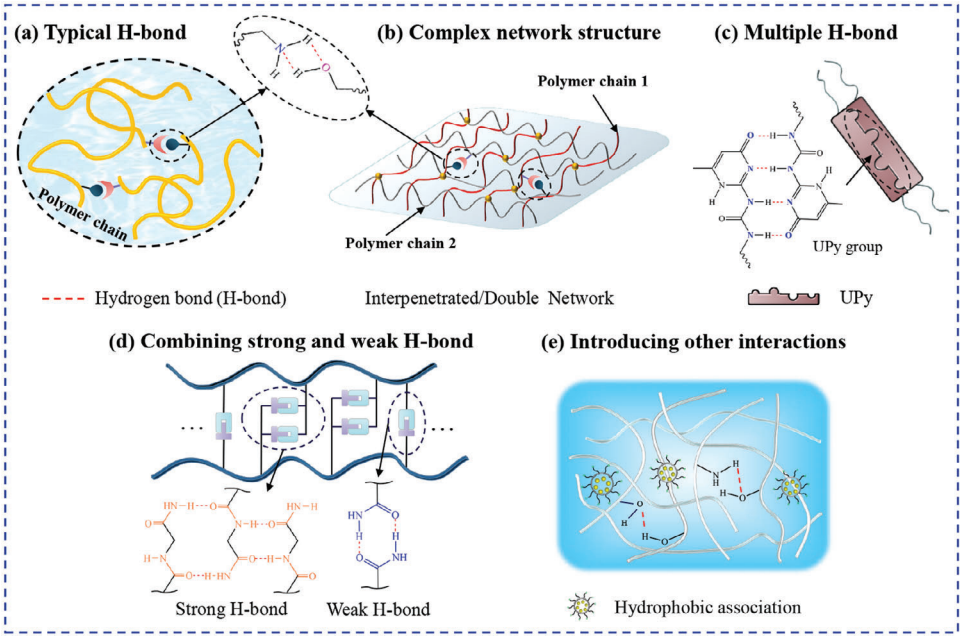


**Figure 2.** Mechanism of H-bonding interactions and strategies to improve the mechanical properties of H-bond-based SHHs. a) Schematic of typical H-bonding interactions. b–e) Strategies for mechanical properties improvement: b) Combining H-bond with complex network structures. c) Introducing multiple H-bonds (e.g., quadrupolar H-bond). d) Combining strong and weak H-bonds. e) Introducing other healing interactions (e.g., hydrophobic association).

NBAA monomers were co-polymerized into P(NAGA-*co*-NBAA) chains under ultraviolet (UV) light irradiation, which formed the first noncovalent network by intermolecular H-bonds between amide groups. The sol–gel phase transition of agars further generated a molecular entanglement network. The two types of networks were bound together by intramolecular H-bonding interactions between —OH from agars and —$NH_2$ from P(NAGA-*co*-NBAA) copolymer chains. The DN structure and large amounts of dynamic H-bonds enabled the hydrogel to have a mechanical strength of 1.1 MPa and a SHE of ≈95%. The DN strategy has been widely exploited to improve the mechanical properties of SHHs, such as those based on PVA and PAM polymers.[68–70]

Some researchers have been dedicated to designing multiple types of H-bonds in one hydrogel to enhance its mechanical properties. For instance, Fan et al. constructed a double-cross-linked SHH with high toughness and rapid self-healing capacity based on PVA and tannic acid (TA) using two types of H-bonds.[71] The hydrogel was formed by dipping PVA aerogels into TA solutions, in which both the strong H-bonds between PVA and TA and the weak H-bonds among PVA chains cross-linked the final network. Their combination significantly improved the mechanical properties of the resultant hydrogels, exhibiting a tensile stress of ≈9.5 MPa at ≈1000% strain, an elastic modulus of 1.7 MPa, and a SHE of 57.9% without external treatment. Liu and co-workers reported a rapid SHH at RT based on multiple H-bonds formed between the acylamino groups in poly(styrene-*co*-N, N-dimethylacrylamide) (P(St-*co*-DMAA)) and PAM chains (Figure 3b).[72] The mechanical SHE reached 99% within 2 h, and the conductivity could rapidly return to its initial value after ≈40 s. Zhang and co-workers constructed a hybrid conductive SHH composed of $\gamma$-polyglutamic acid (PGA) and poly(3,4-ethylenedioxythiophene): poly(styrene sulfonate) (PEDOT: PSS) based on multiple H-bonds between sulfonic groups (—$SO_3H$) of PSS and —COOH of PGA (Figure 3c).[73] The prepared hydrogel could be stretched over 300% without fracture, and its electrons transmission network and electro-conducting pathway could also be rebuilt once the damaged surfaces came into contact for 10 s. Moreover, the SHEs in elongation and strength at break were ≈90% and ≈65% after 24 h, respectively. With a fresh and free preparing method, Matteo and co-workers developed 3D-printed SHHs based on PVA and acrylic acid (AA) by utilizing poly(ethylene glycol) diacrylate (PEGDA) as the cross-linker and diphenyl (2,4,6-trimethylbenzoyl) phosphine oxide as the photoinitiator.[74] The carboxylic groups in the PAA chains formed the multiple H-bonds with the hydroxyl groups in PVA chains and thus improved the self-healing capacity. The healed hydrogel could bear deformation and restore 72% of its original strength within 12 h. Furthermore, it is demonstrated that the 3D-printed hydrogel had a better self-healing capacity than the bulk one because the 3D-printing enabled layer-by-layer photopolymerization could lead to higher homogeneous cross-linking density. Besides, multiple H-bonds were also formed by combining various copolymer chains containing rich functional groups (such as hydroxyl, amino, etc.) and macromolecular monomers (e.g., TA,[75,76] phytic acid (PA),[77] etc.).

Among diverse multiple H-bonding interactions, the ureidopyrimidinone (UPy) unit is a well-described hydrogen bonding motif, and has been broadly exploited in preparing SHHs with high toughness.[22,78,79] It features self-complementary quadruple H-bonding functionality and allows the building of reversible supramolecular networks. For instance, Jeon et al. devised an extremely stretchable and fast self-healing hydrogel by introducing

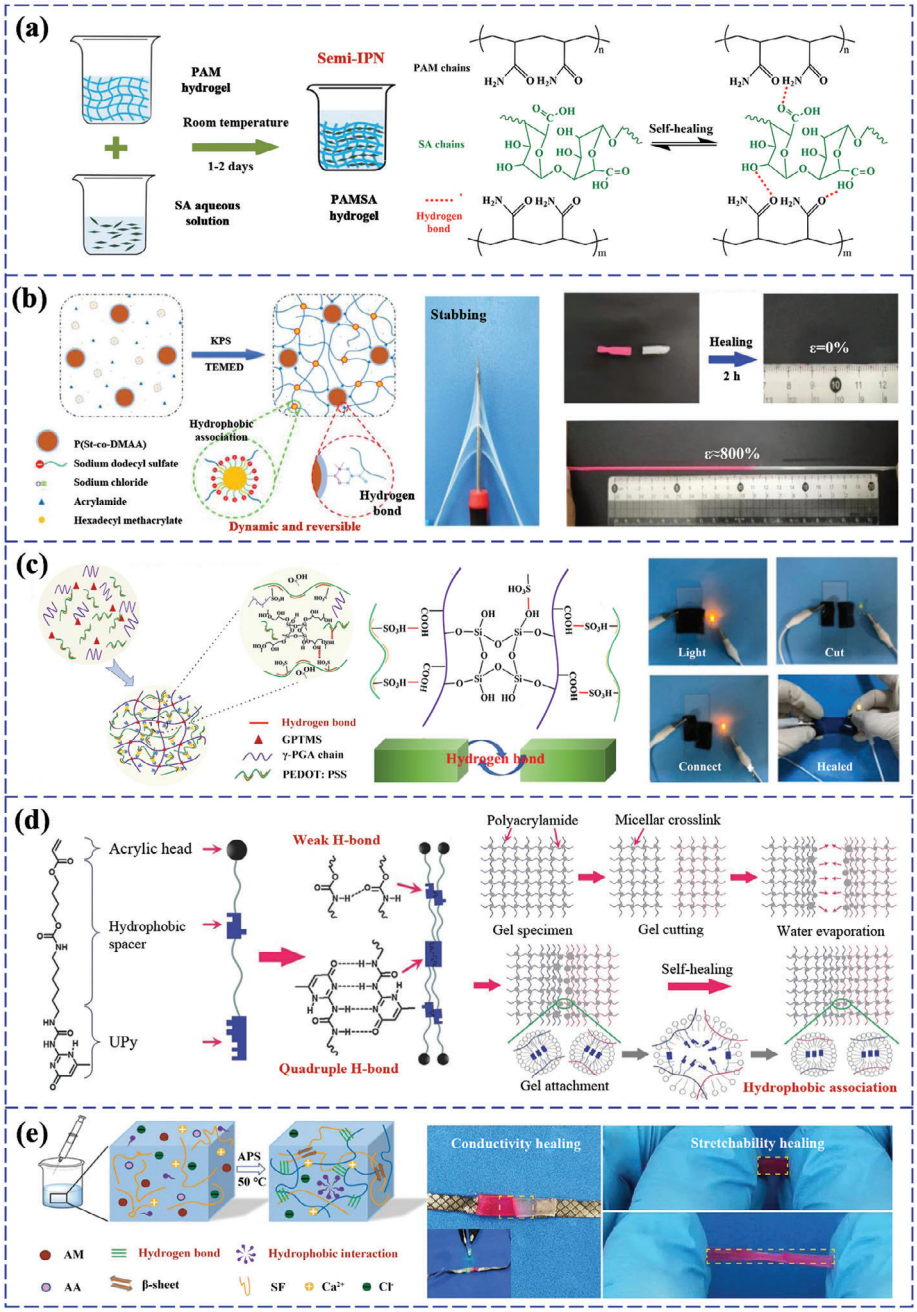


**Figure 3.** SHHs based on the H-bonding mechanism. a) Schematic of self-healing layered SA/PAM hydrogels with a semi-IPN structure and the reversible H-bonds between polymer chains. Reproduced with permission.[66] Copyright 2020, Elsevier. b) Schematic of the preparation and self-healing mechanism of the P(St-*co*-DMAA)-based SHH, the stabbing performance, and the self-healing property achieved by multiple H-bonds. Reproduced with permission.[72] Copyright 2020, Elsevier. c) Schematic of self-healing PGA/PEDOT: PSS hydrogels based on multiple H-bonds between —$SO_3H$ of PSS and —COOH of PGA, photographs of conductive self-healing property. Reproduced with permission.[73] Copyright 2022, Elsevier. d) Schematic of the component and healing mechanism of self-healing PAM/UPyHCBA hydrogel based on the UPy unit. Reproduced with permission.[22] Copyright 2016, John Wiley & Sons. e) Schematic of the preparation and internal interactions of self-healing P(AM-*co*-AA)/SF hydrogels, photographs of the conductive healing and stretchable healing properties. Reproduced with permission.[82] Copyright 2021, John Wiley & Sons.

the UPy unit into micellar polymerization of UPyHCBA and acrylamide (AAm) (Figure 3d).[22] Due to the strong interactions of the quadruple H-bond in UPy groups and its rapid reformation after fracture, the as-prepared hydrogel exhibited an ultrahigh fracture strain of 10000% and outright self-healing ability in 30 s without external stimuli. Chen et al. devised a stretchable conductive polymer-based SHH by introducing UPy groups into polyaniline (PANI)/PSS networks.[78] The prepared PANI/PSS hydrogel showed full and repeatable recovery in both its mechanical property and electrical conductivity in 30 s upon damage.

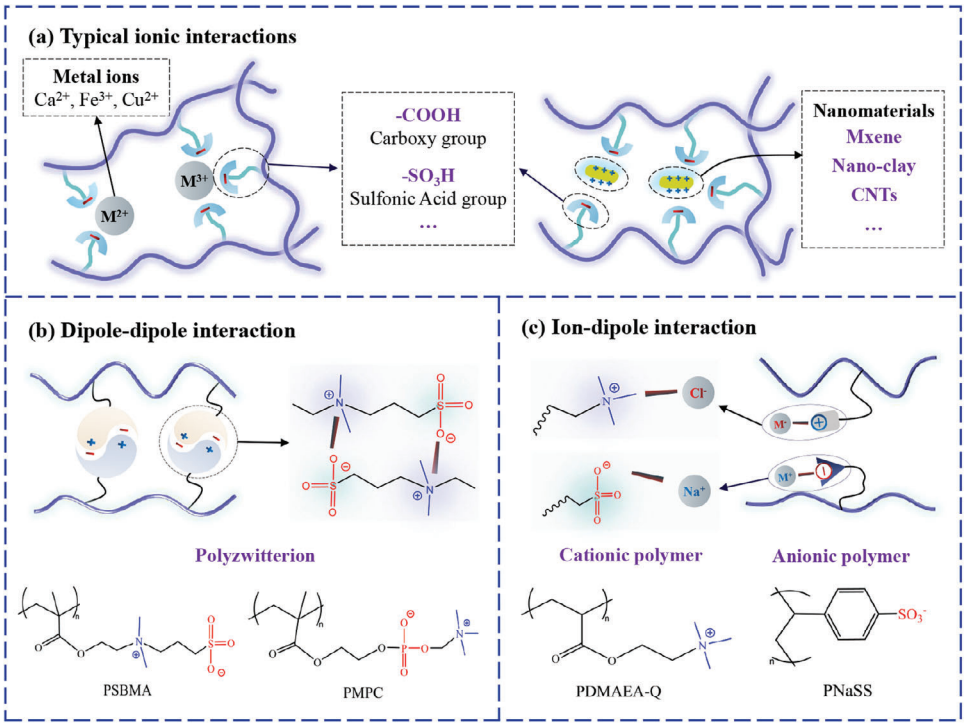


**Figure 4.** Mechanism schematic of SHHs based on ionic interactions. a) Schematic of the typical ionic interactions formed between metal ions or nanomaterials and the charged groups. b) Schematic of dipole-dipole interaction formed by polyzwitterion polymers and the typical polyzwitterion materials. c) Schematic of ion-dipole interaction formed between ions and cationic or anionic polymers.

Other examples can be seen in self-healing dextran/UPy hydrogels and Gel-UPy/dsCD hydrogel.[80,81]

Researchers have also explored the involvement of other dynamic and reversible crossed-linkages to strengthen the H-bonding interaction. For instance, Zhao et al. developed a multifunctional silk fibroin (SF)-doped hydrogel by chemically and physically cross-linking AAm, AA, and SF (Figure 3e).[82] The introduction of hydrophobic association (sodium dodecyl sulfate) shielded the effect of water molecules on amide H-bonds. The synergistic effect of H-bonding and hydrophobic association significantly elevated the mechanical property of the prepared hydrogel, enabling it to be stretched more than six times its original length. Zhang et al. reported a DN SHH based on PAM, octadecyl methacrylate, and polyurethane (PU), which was cross-linked through H-bonds and hydrophobic effect.[83] Both thermal stability and mechanical properties of the developed PAM-PU hydrogel were raised, and the SHE approached 88% after 60 min at RT. In addition, a highly stretchable (1600%) and self-healable (SHE of 95%) gelatin hydrogel was also constructed by combining the hydrophobic and H-bonding interactions.[84]

In all, H-bonds are widely present in various natural and synthetic hydrogels, and extensively utilized to construct SHHs. Owing to the relatively low energy required for their formation and breaking, H-bonds generally feature high reversibility, rapid cross-linking and de-cross-linking speeds (several seconds), and easy establishment at ambient conditions. However, on the other hand, H-bonds usually result in SHHs with relatively low mechanical strength and inferior stability, and are prone to be broken by external mechanical forces and environmental conditions (such as temperature, humidity, pH, etc.) because of their relatively low bonding energy (1–63 kJ $mol^{-1}$). Increasing the amount of H-bonds, introducing different types of H-bonds, and combining them with other self-healing mechanisms and multiple network structures are alternative methods to enhance both the self-healing ability and mechanical properties. In light of these characteristics, H-bonds-based SHHs can be used to develop soft bioelectronics for applications which has low requirement on mechanical strength, and work under mild environmental conditions.[85]

### 2.1.2. Ionic Interaction

Ionic interaction is another frequently used mechanism for the synthesis of SHHs. It's a type of molecular electrostatic interaction between ions with complementary charges, which can lead to the reformation of dynamic and reversible cross-links.[86,87] Generally, hydrogels obtained through ionic interaction can be implemented by cross-linking a charged polymer with oppositely charged materials, including charged polymers, nanoparticles, or ions.

The reversible ionic interaction in hydrogels is typically formed by the electrostatic interaction between metal ions (e.g., $Fe^{3+}$, $Ca^{2+}$, etc.) and oxyacid ions (e.g., sulfonic acid ion ($SO_3^-$)) or -COOH groups (**Figure** 4a). For instance, Wang et al. presented a gelatin-based conductive SHH by mixing ferric ions ($Fe^{3+}$) into polypyrrole (PPy) grafted gelatin solutions.[88] After adding $FeCl_3$ for only 30 s, the gelatin process occurred, forming the hydrogel.

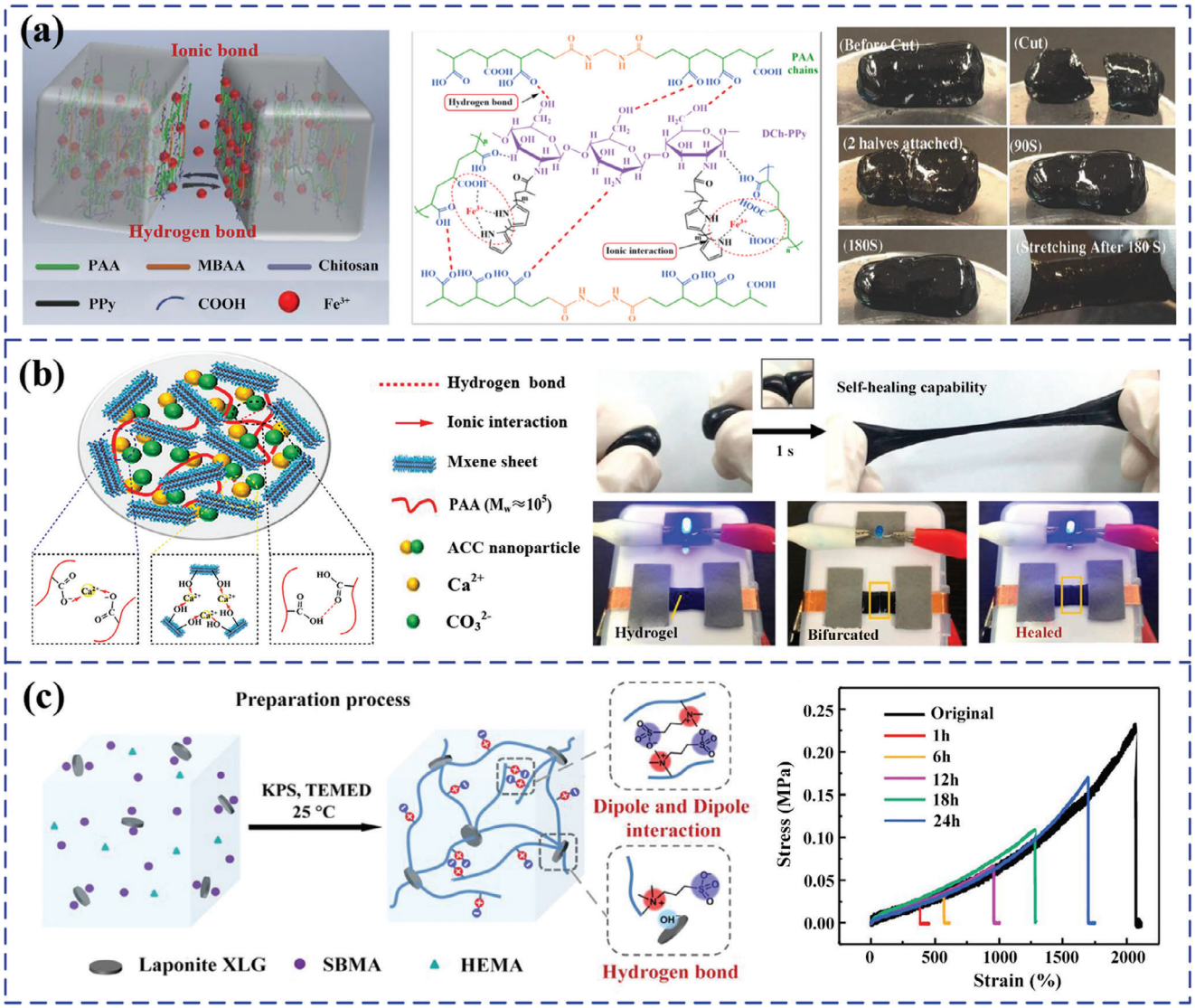


**Figure 5.** SHHs based on ionic interactions. a) Schematic of the internal networks and healing mechanisms of self-healable Chitosan/PAA/PPy/$Fe^{3+}$ hydrogel, photographs of the macro-mechanical healing process. Reproduced with permission.[89] Copyright 2017, John Wiley & Sons. b) Mechanism schematic of the self-healing MXene composite hydrogel, photographs of the bisected/healed hydrogel, and the LED light circuit on-off demonstration. Reproduced with permission.[95] Copyright 2021, American Chemical Society. c) The self-healing zwitterionic nanocomposite hydrogel constructed by dipole and dipole interaction, the mechanical properties before and after healing. Reproduced with permission.[100] Copyright 2019, American Chemical Society.

The formed dynamic and reversible ionic bonds between $Fe^{3+}$ and the —NH— of PPy and the —COOH of gelatin chains enabled a restoring ability of ≈70% in compressive strength after healing for 30 min. However, obtaining SHHs with high mechanical properties and SHE is difficult only through ionic interactions. Therefore, double networks and multiple types of dynamic bonding mechanisms were exploited to improve both the SHE and mechanical properties together with ionic interactions. For example, Darabi and co-workers proposed a self-healing DN hydrogel by combining dynamic ionic interaction with chemically cross-linking covalent networks (**Figure 5**a).[89] The covalently cross-linking networks between PAA and *N,N″*-methylenebisacrylamide (MBAA) strengthened the mechanical strength and improved the stretchability (≈1500%). Owing to the dynamic ionic interaction between —COOH and —NH— groups and $Fe^{3+}$, the prepared hydrogel exhibited a high self-healing capacity with 100% mechanical SHE in 2 min and 90% electrical SHE in 30 s. Additionally, a multicomponent SHH was fabricated by interpenetrating PANI and PAA networks using tannic acid-coated cellulose nanocrystals (TA@CNCs) as the reinforcing bridges.[90] The abundant intermolecular electrostatic interactions arose from the complementary charge between PANI and PAA chains. Combined with the introduced H-bonds between the TA@CNCs particles and polymer chains, the resultant hydrogel with reversible cross-links exhibited excellent and effective self-healing capability. After 24 h, the broken/healed hydrogel restored 98.2% and

92.6% of its initial tensile stress and strain, respectively. Even after undergoing ten cutting-healing cycles at the same position, the hydrogel could restore over 99% of its electrical conductivity.

Besides, the introduction of nanocomposites (e.g., nano clay,[91,92] MXene,[93,94] etc.) also provides another effective approach to form reversible ionic interactions. The ionic interactions between the contained ions or modified surface ligands of nanomaterials and polymer chains drove the reformation of nanocomposites-based SHHs. Nano-clays have been widely used as mechanical nano-reinforcer due to their ultrathin (ca. 1 nm) and high aspect ratio structural features (ca. 1000). The abundant −OH groups also make nano-clays easy to be modified, and enable them to cross-link with polymeric backbones to prepare SHHs.[36] Zhu et al. reported a self-healable ionic gelatin/PAM/clay hydrogel (GPNs gel) based on ionic interactions by introducing nano-clays.[91] The clay nanosheets, rich in $Na^+$, $Mg^{2+}$, and $Li^+$, dispersed in the networks of gelatin/PAM hydrogels and formed electrostatic interactions with —COOH and $—NH_2$ groups in PAM and gelatin. It significantly improved the SHE of the resultant hydrogels in comparison with gelatin/PAM DN hydrogel without the clay nanosheets. Specifically, the SHE increased from 53% (healing 40 h, ≈37 °C) to approximately 80% (healing 1 h, RT). Apart from nano-clays, MXene was also a star material for constructing self-healing conductive hydrogel. A MXene composite-based self-healable conductive hydrogel was constructed by introducing MXene into PAA/calcium ions ($Ca^{2+}$) networks (Figure 5b).[95] Due to the rapid reformation of ionic interactions between calcium ions and -OH from MXene sheets and -COOH from PAA chains, the hydrogel could rapidly self-repair after damage. It exhibited ≈100% conductive recovery and reproducible electrical self-healing ability of ≈100% even after five healing cycles.

Zwitterionic polymers are a kind of ionic polymers possessing both positively and negatively charged groups in one monomer unit,[96,97] such as poly(sulfobetaine methacrylate) (PSBMA)[98–100] and poly(2-methacryloyloxyethyl phosphorylcholine) (PMPC),[101–103] which have been recently used to assist SHHs via dipole–dipole interaction (Figure 4b). For instance, Wang et al. prepared a zwitterionic nanocomposite-based SHH (L4S90) by radically polymerizing PSBMA and 2-hydroxyethyl methacrylate (HEMA) under Laponite XLG (Figure 5c).[100] Due to the covalent networks and the dipole–dipole interaction between the positive and negative groups in the zwitterion polymer chains, the hydrogel exhibited a stretchability of ≈2000% and a fracture toughness of up to 2.45 MJ $m^{-3}$. Owing to the reversibility of dipole–dipole interaction, the resistance of the reconnected L4S90 hydrogel could recover to its original level within 11 s. The SHE of the fracture strength was ≈74% after 24 h. In another research, a self-healable polydopamine (PDA)/clay/PSBMA hydrogel with robust adhesion to human tissues was developed.[98] The recontacted interface was blurred after the broken hydrogel healed for 10 h at RT. The SHEs in fracture strength and electric resistance reached 80% in 24 h and 97.6% in 2 s, respectively. Zhang and co-workers proposed an injectable and self-healable RT-formed PEDOT: PSS hydrogel cross-linked by 4-dodecylbenzenesulfonic acid.[104] The reconnected hydrogel could heal within 5 min via the reformation of broken $\pi$–$\pi$ stacking and electrostatic interaction between $PEDOT^+$ and $PSS^-$. Furthermore, dynamic ion-dipole interaction as a kind of ionic interaction could also be used to prepare SHHs (Figure 4c). Ion–dipole interaction generally formed between cationic polymers (e.g., poly *N, N*-dimethylamino ethylacrylate (PDMAEA)[105,106]) or anionic polymers (e.g., poly sodium *p*-styrenesulfonate (PNaSS)[107,108]) and ions with opposite charges.

Overall, the ionic interactions-based self-healing mechanism essentially relies on the reversible electrostatic interactions of oppositely charged ions. Due to its higher bonding energy than that in H-bonds, it can contribute to SHHs with improved mechanical strength and performance stability. Compared to dynamic covalent bonds discussed in the following sections, this mechanism also possesses the advantages of facile cross-linking under ambient environment (such as room temperature), rapid self-healing speed (within seconds), and high dynamic reversibility. Furthermore, as ionic cross-links are generally formed by introducing various metal ions or conductive nanomaterials (such as MXene), ionic interaction-based SHHs usually have superior electronic or ionic conductivity or both, which can be widely employed in soft bioelectrodes, wearable sensors, supercapacitors, conductive circuits, as well as self-healing ionic skin.[109,110]

### 2.1.3. Metal Coordination Interaction

Metal coordination interaction stands for a promising mechanism for developing SHHs. It works by forming dynamic and reversible interactions among transition metal ions with vacant orbitals or functional groups with lone pairs of electrons as ligands (**Figure 6a**).[111] It exhibits multiple molecular parameters (e.g., metal ions, counterions, and ligands) and a vast range of accessibility with numerous applicable functional metal ions and ligands, and is prone to undergo spontaneously.[112] These unique advantages endow metal coordination interaction-based SHHs with a broadly tunable bond strength, diverse approaches to constitute, and an appealing capacity to self-heal without external stimuli. Metal coordination interaction exhibits bond energies in the range of 60–300 kJ $mol^{-1}$, which is much higher than those in noncovalent dynamic bonds such as H-bonds (1–63 kJ $mol^{-1}$), van der Waals force (typically 2–20 kJ $mol^{-1}$), and $\pi$–$\pi$ stacking (typically ≤ 10 kJ $mol^{-1}$).[62,113] Additionally, it is possible to control the strength of coordination bonds from 25% to 95% of a covalent bond by selecting different ligands and metal ions.[56,114]

To date, metal coordination interactions for SHHs include metal ions-carboxylate,[115–117] metal ions-catechol coordination, and metal ions coordination with other ligands, such as phosphonate, azolate, amine, pyridine, etc. Derived from —COOH groups in carboxylate and —OH groups in catechol, metal coordination is often accompanied by H-bonding to prepare SHHs. For instance, a nanocomposite-based SHH was developed by introducing TEMPO-oxidized cellulose nanofibers/carbon nanotubes (TOCNF/CNTs) into the PAA networks with $Fe^{3+}$ as ion cross-linkers and MBAA as the covalent cross-linkers.[118] The —COOH groups existing in TOCNFs and PAA chains formed dynamic and reversible coordination with $Fe^{3+}$. The mechanical and electrical SHEs of the resultant hydrogel reached 98.36% and 99.99% after 24 h of healing, respectively. The metal ions-carboxylate coordination interaction was also utilized to prepare chitosan (CS)/PAA/PPy-based SHHs.[117] The introduced $Fe^{3+}$ autonomously cross-linked the AA and CS polymers by

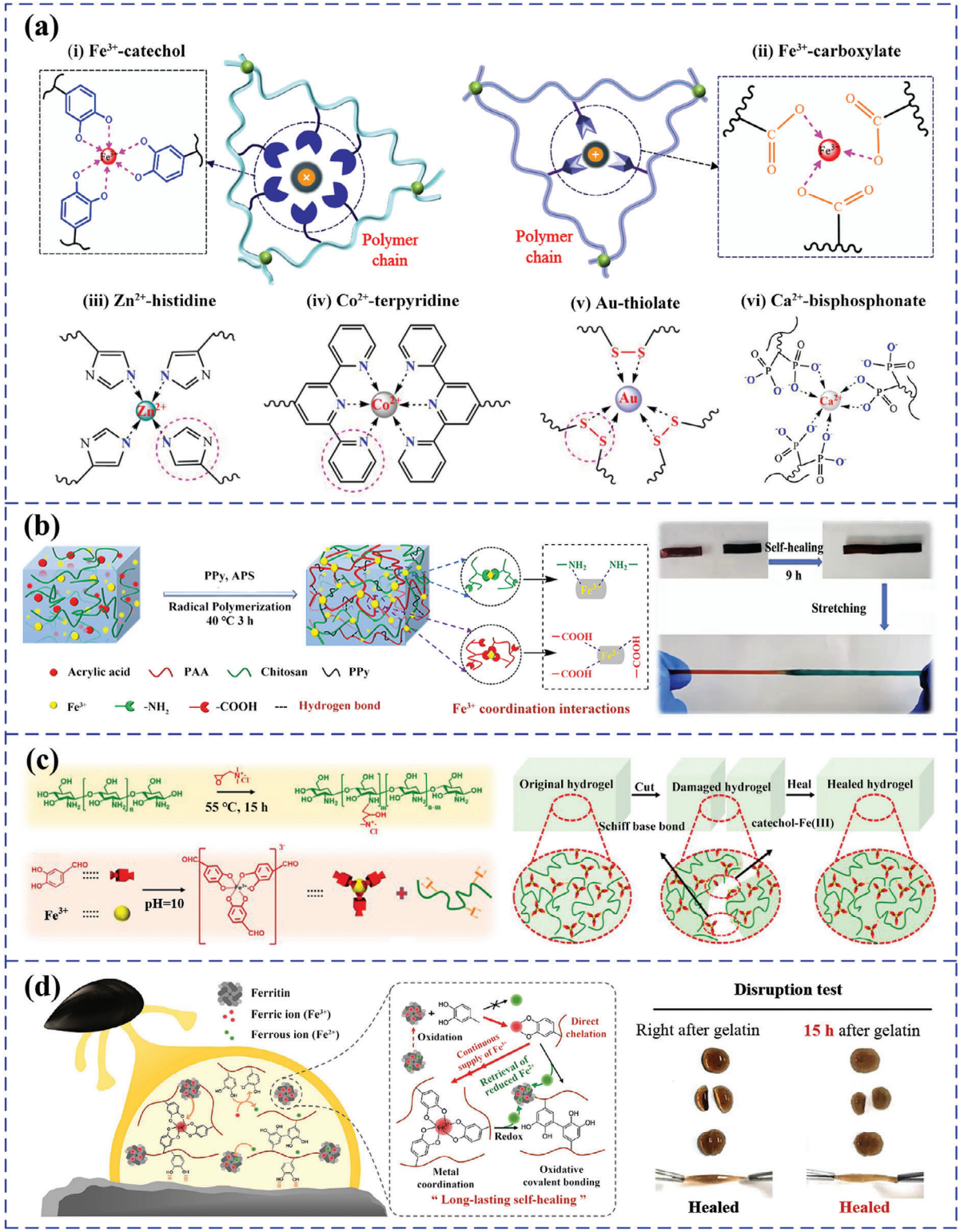


**Figure 6.** Mechanism schematic of SHHs based on metal coordination interactions and the prepared SHHs. a) Schematic illustration of the typical metal coordination interactions. b) Schematic of the preparation and internal interactions of the SHH formed by $Fe^{3+}$ coordination interaction and the photographs of the healed hydrogel. Reproduced with permission.[117] Copyright 2021, American Chemical Society. c) The SHH prepared by $Fe^{3+}$ and catechol coordination interaction. Reproduced with permission.[124] Copyright 2021, American Chemical Society. d) Schematic illustration of the roles of ferritin and long-lasting self-healing mechanism of the catechol-functionalized hydrogel by ferritin-catechol interactions, and the self-healing test of the HA-CA hydrogels produced by ferritin-mediated cross-linking. Reproduced with permission.[127] Copyright 2023, American Chemical Society.

forming coordination interactions with —COOH groups in PAA and —$NH_2$ in CS under RT (Figure 6b). The SHE of the hydrogel in tensile strength was 93% after 9 h of healing in the air. To study the contribution of metal coordination interaction in the self-healing property, a CS/PAA/PPy hydrogel without $Fe^{3+}$ was prepared for comparison and showed a SHE of 39.6%, which was much lower than that of the hydrogel containing $Fe^{3+}$. It was concluded that the coordination of $Fe^{3+}$-$NH_2$ and $Fe^{3+}$-COOH mainly determined the self-healing ability. Since the coordination interaction between $Fe^{3+}$ and -COOH groups is pH-insensitive, this strategy has been widely adopted for SHHs preparation.[119–121]

Metal ions-catechol coordination is also frequently used for synthesizing SHHs, typically forming stable bis- and tris-complexes under alkaline conditions.[122,123] Liang et al. designed an antibacterial SHH by harnessing dual-dynamic-bond cross-linking among $Fe^{3+}$, protocatechualdehyde (PA), and quaternized chitosan (QCS) (Figure 6c).[124] The self-healing capacity was derived from the metal coordination interactions among $Fe^{3+}$, catechol groups of PA, and the amino groups of QCS. The healed hydrogel showed no cracks within 2 h and could be stretched ≈200%. Jia and co-workers constructed a novel dual self-catalytic SHH with conductive, tough, and transparent properties composed of $Fe^{3+}$ and catechol-based molecules.[125] After 6 h healing, the recontacted hydrogel could restore 85% of its stretchability (0.6 wt% $Fe^{3+}$), 90% of its maximum tensile strength (0.8 wt% $Fe^{3+}$), and nearly 98% of its conductivity (1 wt% $Fe^{3+}$). The excellent SHE stemmed from the efficient reformation of dynamic metal coordination bonds among the $Fe^{3+}$, and —COOH groups in PAA and catechol groups in dopamine. Besides, benefiting from the good adhesive property of catechol groups, Jin et al. developed a tissue-adhesive and printable SHH consisting of TA, carboxymethyl cellulose, and metal ions (e.g., $Fe^{3+}$).[126] Owing to the metal ions-phenolic coordination and multiple H-bonds in the network, the broken hydrogel could be rapidly reconstructed. The rapid and in situ preparation of the hydrogel on the skin surface by 3D printing could further promote SHHs for engineering bioelectronics. Recently, Jin and co-workers proposed a novel strategy based on metal ions-catechol coordination for preparing long-lasting SHHs.[127] As illustrated in Figure 6d, by utilizing the ferritins' function of bidirectionally providing and retrieving $Fe^{3+}$, the lasting $Fe^{3+}$-catechol coordination was achieved. A comparison between the self-healing effects of directly $Fe^{3+}$-mediated and ferritin-mediated catechol-functionalized hydrogels verified that this strategy could prolong the lifetime of self-healing properties for phenolic-based hydrogels. Although the metal ions-catechol strategy has been widely exploited, key issues, such as controlling the degree of catechol oxidation under alkaline conditions in air and overcoming the low solubility of ferric ions that hinder the production of sufficient ions-catechol cross-links, still need to be addressed.[128] Apart from the two types of metal-ligand coordination mentioned above, other metal coordination interactions have also been developed for constructing SHHs, including $Zn^{2+}$-histidine coordination,[129] $Ni^{2+}$-pyridine coordination,[130] Au-thiolate coordination,[131] $Ag^{+}$-bisphosphonate coordination,[132] etc.[56,133]

In all, metal coordination interaction-based self-healing mechanisms are dependent on the proper selection of the metal ions and corresponding ligands, which generally exhibits a more stable bonding and thus results in much higher mechanical property than other mechanisms based on reversible non-covalent bonds.[85] Owing to their wide accessibility in the used metal ions and ligands, SHHs based on this mechanism feature a broad range of tunability in their mechanical strength, contributing to developing bioelectronics with a variety of softnesses and thus enabling initiate contact with different human tissues.[133] In addition, given that some introduced metal ions possess excellent biological activity, such as antibacterial properties (e.g., $Cu^{2+}$, $Ag^{+}$), metal coordination interaction-based SHHs hold significant potential for constructing soft electronics with therapeutic effects, such as anti-infection during wound healing or wearable sensing. Moreover, the incorporation of polyphenol groups in most metal coordination interaction-based SHHs can facilitate the development of self-adhesive bioelectronics.

#### 2.1.4. Host–Guest Interaction

Host–guest interactions are significantly important in constructing SHHs because they combine various noncovalent interactions among multiple complementary compounds, such as H-bonding, ionic, $\pi$–$\pi$ stacking, and hydrophobic interactions. This mechanism can form dynamic and reversible cross-links, and endow hydrogels with increased binding forces and complexation via fixed host-guest geometry and directionality.[134–136] Typically, the host is a kind of macrocyclic molecule that contains unique or specific cavities, and the guest molecules possess complementary shapes and physical or chemical properties.[137,138] Hydrophobic interactions induced self-assembly is the dominant driving force for most macrocyclic molecules to encapsulate the guest molecules. To date, a diversity of host molecules, including calixarenes (CAs), cyclodextrins (CDs), cucurbit[n]urils (CBs), cyclophanes, pillar[n]arenes, and crown ethers, have been proposed (**Figure 7a**). Among these, CDs[139,140] and CBs,[141] possessing hydrophobic cavities and hydrophilic surfaces, respectively, have been widely used to selectively encapsulate various guest molecules, such as ferrocene (Fc),[142] adamantane (Ad),[143] and azobenzene (Azo),[144] to prepare SHHs.[145]

The aforementioned host and guest molecules can be grafted on the branches of polymer chains (e.g., PAA chain, PAM chain, etc.) to impart hydrogels with the self-healing ability through the grafted-molecules induced host-guest interactions. For example, Nakahata and co-workers constructed a self-healable supramolecular hydrogel based on PAA by introducing $\beta$-cyclodextrins and ferrocene as the host and guest molecules, respectively (Figure 7b).[146] Its healing capacity stemmed from the host-guest interactions between the grafted $\beta$-CDs and ferrocene on PAA chains. After rejoining for 24 h at RT, the cracks in the fractured hydrogel disappeared, and its adhesion strength could recover 84% of its initial value. Similarly, a supramolecular $\beta$-CDs-Ad-Fc hydrogel capable of self-healing by utilizing two kinds of host-guest inclusion complexes was also developed.[147] Another strategy to develop host-guest interaction-based SHHs is to copolymerize host-guest supramolecules (HGSMs) with other polymers, monomers, or cross-linkers.[145] Based on this strategy, Wang et al. synthesized a rapidly self-healing HGSM hydrogel by utilizing the host-guest interaction between the

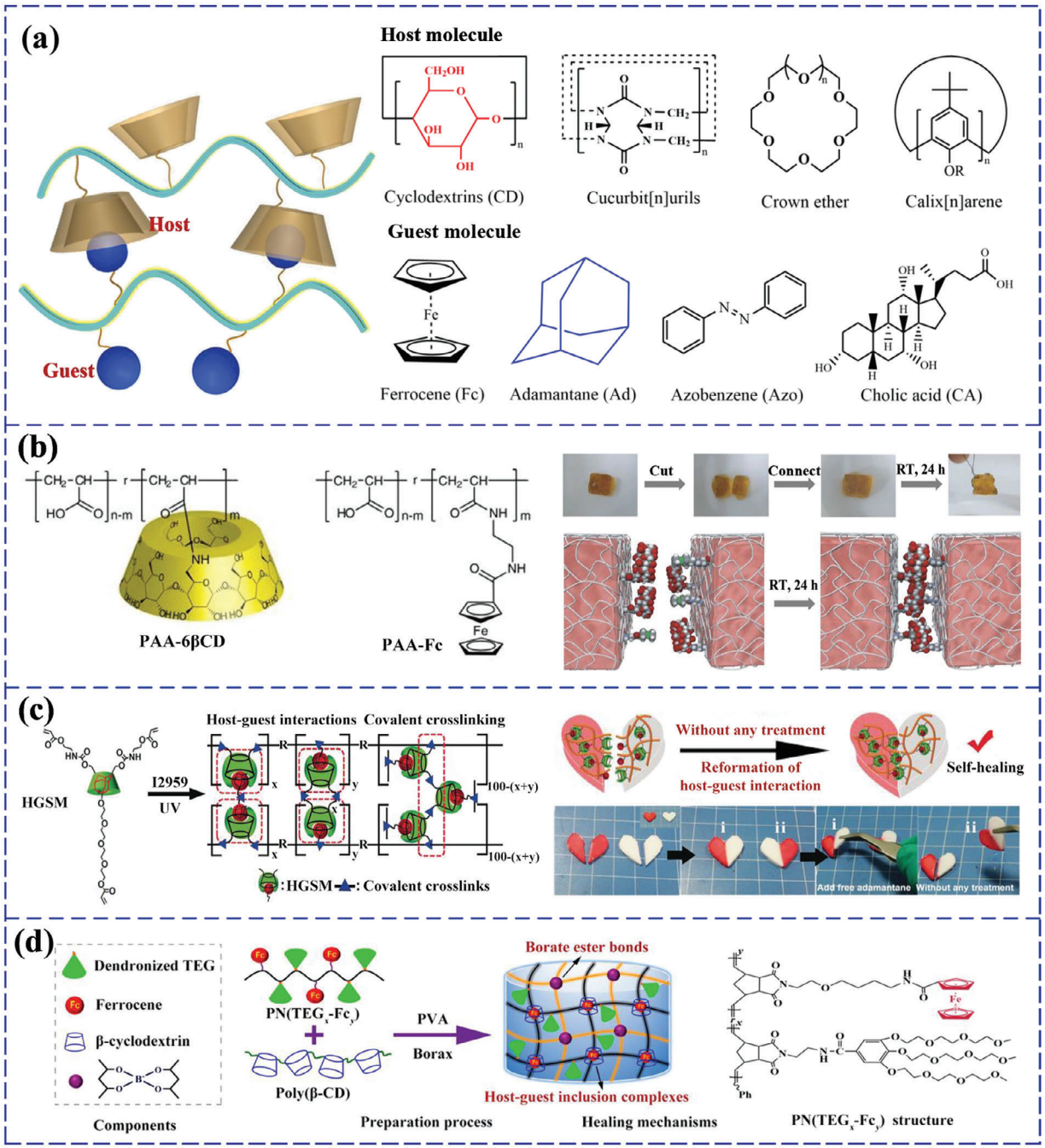


**Figure 7.** Mechanism schematic of SHHs based on the host-guest interactions and the prepared SHHs. a) Schematic of the host-guest interaction and typical host and guest molecules. b) Schematic of PAA chains grafted with $\beta$-CD and Fc groups, photographs of the healing process. Reproduced with permission.[146] Copyright 2011, Springer Nature. c) Schematic of the preparation and self-healing mechanism of HGSM hydrogel and photographs of the healing hydrogels. Reproduced with permission.[148] Copyright 2021, American Chemical Society. d) Schematic of the preparation and internal reversible interactions of the $\beta$-CD-based SHHs by combining host–guest interaction and borate ester bonds. Reproduced with permission.[142] Copyright 2021, American Chemical Society.

isocyanatoethyl acrylate modified $\beta$-CDs ($\beta$-CD-AOI$_2$) and 2-(2-(2-(2-(adamantyl-1-oxy)ethoxy)ethoxy)ethoxy)ethanol acrylate (A-TEG-Ad), and UV-initiated-radical polymerization (Figure 7c).[148] As a result, the prepared HGSM hydrogel was able to autonomously self-repair within 60 min. On this basis, a self-healing supramolecular hydrogel (HGGelMA) was further developed through the copolymerization between the arms of HGSMs and gelatin methacryloyl (GelMA).[149] The bisected hydrogel could be interconnected after 1 h of healing through reestablishing the host-gest interactions between the Ad and

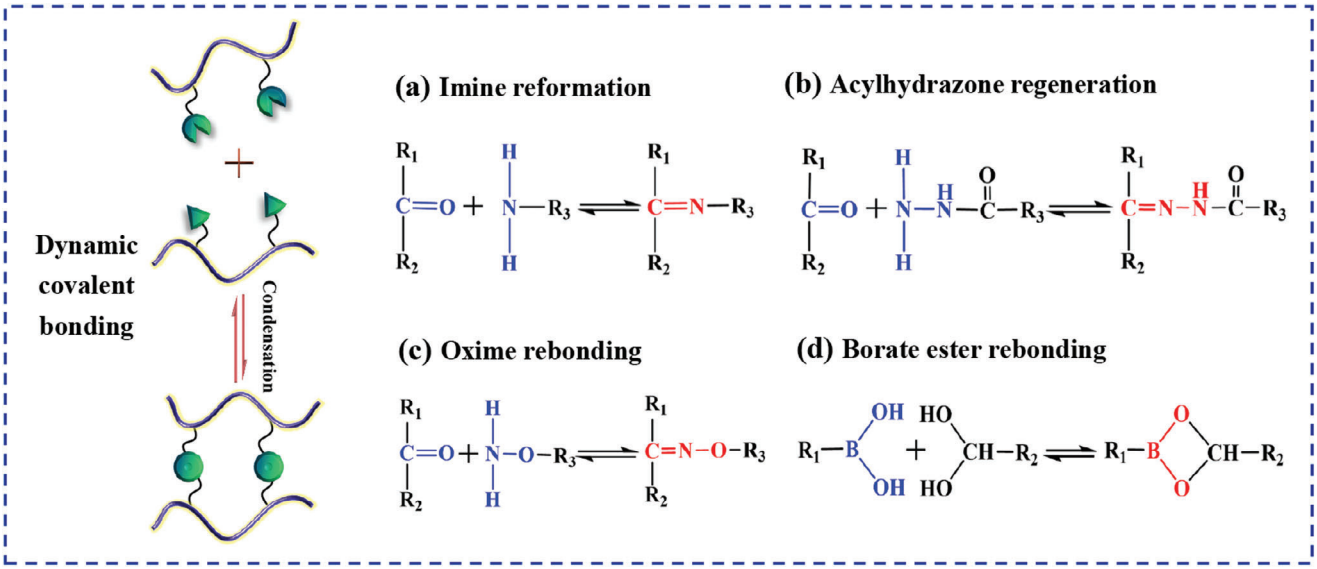


**Figure 8.** Designing strategies of SHHs based on dynamic covalent bonding interactions. a) Imine reformation. b) Acylhydrazone regeneration. c) Oxime rebonding. d) Borate ester rebonding.

$\beta$-CD molecules. The mechanical SHE could increased to ≈80% with the increase of the HGSMs concentration. Besides, SHHs utlizing host-guest interactions between host molecules (CDs, CBs, cyclophanes, etc.) and other guest molecules (cholic acid, carborane, azobenzene, etc.) have also been reported.[150–152]

The host-guest interactions were often combined with other interactions or network design strategies to obtain SHHs with improved multifunctional properties, mechanical strength, and conductive ability. Liu and co-workers constructed a multifunctional DN SHH through the host-guest interaction between $\beta$-CD and Fc combined with the dynamic borate ester bonds between PVA and borax (Figure 7d).[142] Owing to its DN structure, the hydrogel exhibited a stretchability of 436% and a fracture strength of 41 kPa. Importantly, it possessed a high mechanical SHE of 95% in 5 min because of the introduced multiple reversible interactions.

To summarize, host-guest interaction is formed by selective bonding between the host and guest molecules, which contains a variety of non-covalent interactions such as H-bonding, ionic, $\pi$-$\pi$ stacking, and hydrophobic interactions. This unique characteristic can be exploited to construct SHHs with good binding affinity, multifunctional bio-interfaces, stimuli-responsive ability, and specific molecular recognition capacity. In light of these features, host-guest interaction-based SHHs show great prospects in developing various biosensors and actuators for biochemical sensing and controllable drug delivery, as well as bioelectronics with shape memory ability. However, since the host-guest interaction is derived from several weak bonds, the resultant SHHs or bioelectronics show unmet mechanical properties.[150]

### *2.1.5. Dynamic Covalent Bonding*

Dynamic covalent bonding is a kind of chemical reaction where the covalent bonds can be destructed and reformed reversibly under mild conditions (**Figure 8**).[153,154] Its dynamic property is implemented by maintaining the chemical equilibrium status of the reversible reaction. Numerous covalent bonding cross-links are produced to compose a 3D network structure while the reversible reaction achieves its equilibrium.[155] Consequently, this kind of chemical cross-linking endows hydrogels with improved stability and mechanical strength compared with physical cross-linking (such as H-bonds, ionic interaction, and host-guest interaction). It shows great promise in constructing SHHs with tough mechanical properties. To date, diverse dynamic covalent bonding interactions have been devised for SSH synthesis, including dynamic imine bonds, acylhydrazone bonds, oxime bonds, and borate ester bonds (Figure 8).

Among different dynamic covalent bonds, the imine bond is one of the most used covalent bonding mechanisms because of its facile acquirement under common physical conditions and a broad range of sources for its functional groups. Generally, imine bonds are formed via the condensation reaction between electrophilic carbonyl compounds and amino groups, which are relatively abundant in natural polymer materials, such as chitosan, gelatin, and collagen.[156,157] For example, chitosan contains a large number of amino groups on its backbone, which can be well exploited to synthesize multifunctional SHHs by forming imine bonds with aldehyde groups. Chitosan derivatives with better water solubility and biological performance than chitosan are more attractive in developing SHHs, such as O-carboxymethyl chitosan (CMC), glycol chitosan, and quaternary ammoniumyl chitosan.[158,159] Liu et al. developed a CC-DP-based SHH by mixing CC and dibenzaldehyde-terminated telechelic PEG (DP).[160] The rejoined hydrogel could form an integrated gel and withstand a certain stretchability, and its storage modulus could recover close to 100% at the low strain sweep of 1% even after repeated healing cycles. Similarly, a dynamic SHH cross-linked by benzaldehyde-terminated four-arm PEG and carboxymethyl chitosan was reported for the potential hemostatic material.[161]

Despite the wide use of dynamic imine bonds between amine-containing and aldehyde-functionalized natural polymers to

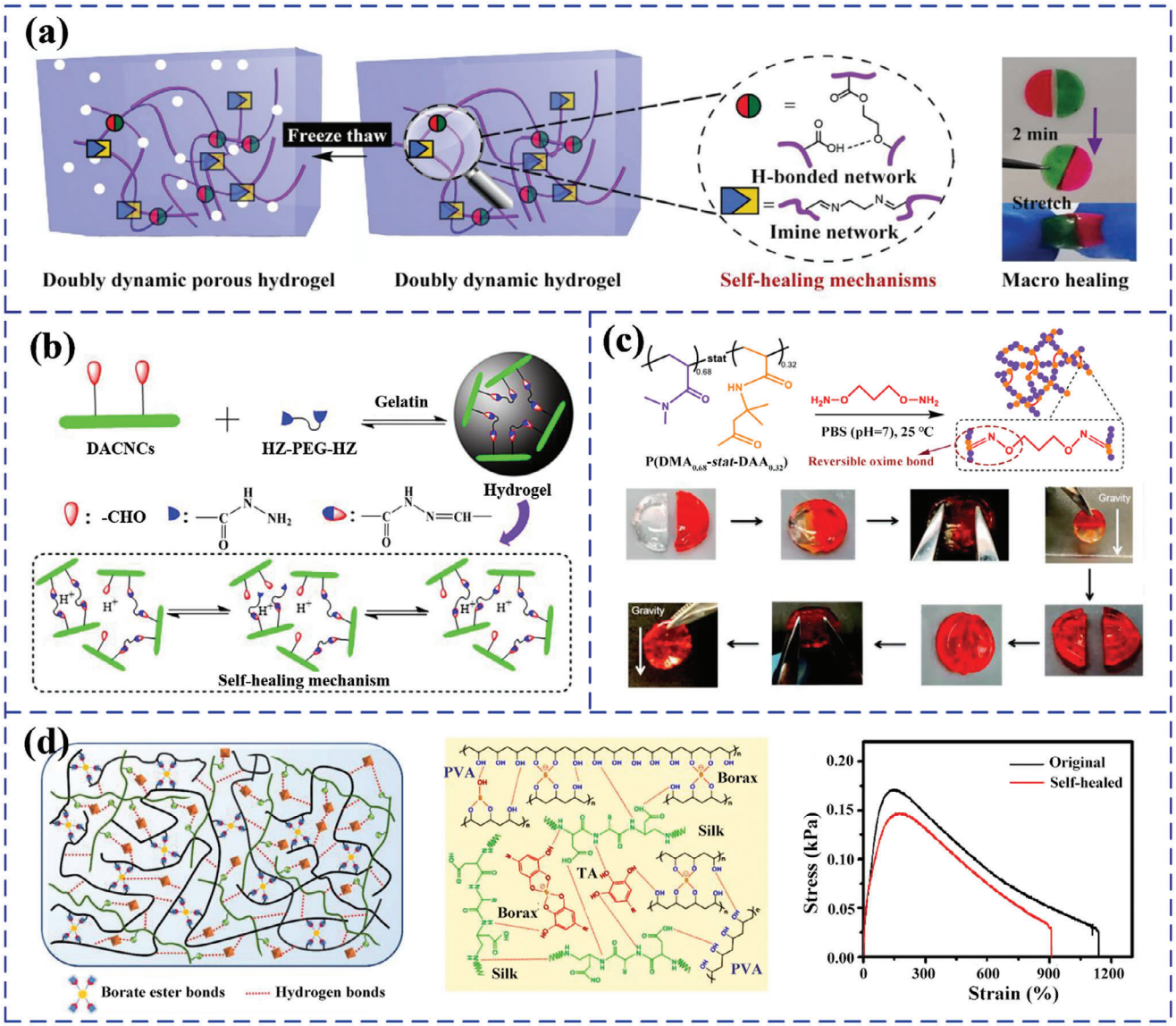


**Figure 9.** SHHs based on dynamic covalent bonding interactions. a) Schematic of the dynamic interactions in self-healing copolymer hydrogel formed by imine bonds, photographs of the self-healed hydrogel. Reproduced with permission.[162] Copyright 2019, John Wiley & Sons. b) Mechanism schematic of self-healing biomass-based nanocomposite hydrogel formed by acylhydrazone bonds. Reproduced with permission.[164] Copyright 2019, Elsevier. c) The self-healing mechanism of P(DMA-stat-DAA) hydrogels based on oxime bonds, photographs of the cutting-healing processes of SHHs. Reproduced with permission.[173] Copyright 2015, Royal Society of Chemistry. d) Schematic of components and internal interactions of self-healing PVA/SF/TA/Borax hydrogel, the healing mechanism based on borate ester bonds and H-bonds, and the mechanical self-healing property. Reproduced with permission.[177] Copyright 2021, American Chemical Society.

prepare SHHs, the functionality of natural polymer hydrogels cannot be easily adjusted to the required extent, such as the weak mechanical strength. Therefore, imine bonds-based synthetic SHHs with controllable mechanical properties were exploited and investigated in-depth in their mechanisms. For example, Jiang and co-workers proposed a rapidly self-healing freeze-thawed DN hydrogel consisting of H-bonds and imine bonds.[162] It was obtained by designing a copolymer based on oligo(ethyleneglycol) methacrylate (OEGMA), poly(methacrylic acid) (PMMA), and 4-hydroxybenzaldehyde (poly($MAA_{116}$-*co*-$BA_{39}$-*co*-$OEGMA_{45}$)), and further cross-linking with ethylenediamine (EDA) (**Figure 9**a). Dynamic imine bonds formed by aldehyde groups (-CHO) and EDA imparted the prepared hydrogel with a fast self-healing speed. The reconnected hydrogel could withstand stretching without breakage after 2 min healing because of the rapid exchanging kinetics of both imine and H-bonds in its cracked surfaces. Its tensile strength could restore 84% of its initial value after 50 min healing at RT, manifesting a fast and effective self-healing behavior. Furthermore, the SHE of freeze–thawed hydrogels can be improved by increasing the healing time and imine cross-linking densities within a certain range. Besides, Wang et al. developed an injectable

SHH by mixing a multifunctional triblock copolymer (PFMNMF) and polyethyleneimine (PEI).[163] With the reformation of imine bonds between -CHO from PFMNMF and -$NH_2$ from PEI, the jointed surface of hydrogels completely disappeared after 30 min healing at RT. The self-healing mechanisms at the molecular scale were investigated by quantitatively probing the interaction forces between PFMNMF and PEI in phosphate buffer saline solution at pH 7.4 with a surface force apparatus. It was demonstrated that the adhesion force between PFMNMF and PEI mainly stemmed from the formed dynamic imine bonds. The adhesion force increased from 9.8 to 14.0 mN $m^{-1}$ with the contact time increasing from 5 to 30 min, which was ascribed to the increased imine bonds under the long contact time. The adhesive force leveled off at 30 min, suggesting that the reaction between the benzaldehyde and amine groups reached an equilibrium state across the two surfaces. This work provided insight into the self-healing mechanism at the nanoscale.

Acylhydrazone bonds have also been considered as an efficient and reliable approach to constructing SHHs, which form via reversible condensation between hydrazine or hydrazide and aldehyde/ketone. Notably, the acylhydrazone bond is much more stable than the imine bond and prone to achieve chemical equilibrium in ambient circumstances. For instance, Xiao and coworkers prepared a biomass-based SHH by cross-linking dialdehyde CNCs (DACNCs) with acylhydrazine-terminated polyethylene glycol (HZ-PEG-HZ) (Figure 9b).[164] The introduced acylhydrazone bonds endowed the hydrogel with the self-healing property under an acid catalyst. Its self-healing ability could be flexibly controlled via the concentrations of the gelator (DACNCs, HZ-PEG-HZ), catalyst, pH value, as well as healing time. Specifically, the SHE of hydrogels with 20.1% and 14.4% gelator concentrations could approach 92.0% and 97.5%,respectively, under a certain healing time at pH 2.5. The hydrogel with a gelator concentration of 20.1% exhibited higher mechanical strength but required a longer time to recover. This could be ascribed to the weakening of polymer chain fluidity and the hindrance of the tighter network structure cross-linked by the acylhydrazone bond exchange reaction. Zhu et al. prepared a kind of oxidized alginate (OSA)-PAM-$Fe_3O_4$-CNCs ionic hydrogel by combining metal coordination interaction with acylhydrazone bonds.[165] This ionic gel could rapidly self-heal within only several seconds, and the healing efficiency of tensile stress could reach up to 93.54%. Analogously, plenty of polymers containing hydrazine groups on their own or after modification were developed to fabricate multifunctional SHHs by harnessing acylhydrazone bonds.[166–169] With the further introduction of adipic acid dihydrazide, SHHs based on imine and acylhydrazone bonds with stronger mechanical performances were reported.[170–172]

Oxime bonds with a linkage similar to imines are another promising option for constructing SHHs. They are produced through the reaction between hydroxylamine (R-O-$NH_2$) and aldehyde/ketone, which exhibit enhanced hydrolytic stability and breaking strength in comparison with imine and acylhydrazone bonds.[154] Mukherjee and co-workers proposed an oxime-functional SHH by chemically cross-linking copolymers (P(DMA-stat-DAA)) formed by polymerizing DMAA and diacetone acrylamide (DAA) with difunctional alkoxyamines via oxime bonds (Figure 9c).[173] The reconnected hydrogels could self-heal within 2 h and withstand a certain stretching and weight. Besides, Nadgorny et al. cross-linked poly(*n*-hydroxyethyl acrylamide-*co*-methyl vinyl ketone) with bifunctional hydroxylamines and developed a 3D-printable macro-porous hydrogel, which could fully and rapidly self-heal without any additional stimuli.[174]

Recently, borate ester bonds were highly concerned for preparing SHHs, which were produced through the transesterification reaction of boronic acids or their derivatives with *cis*-diols (1,2-diols or 1,3-diols),[175] featuring fast and multiple self-repair capacities. For instance, Shin et al. proposed a novel self-healing multifunctional Alg-BA/OEGCG/NaCl hydrogel based on the borate ester bonds between boronic acid-modified alginate (Alg-BA) and oligomerized epigallocatechin-gallate (OEGCG).[176] The rejoined hydrogel could perfectly blend into a whole without obvious fracture cracks. The consistent storage and loss modulus again exhibited its splendid healing capability. Furthermore, the SHH displayed its function in EMG signal recording as an implantable electrode. Besides, Zheng et al. designed a conductive SHH by cross-linking PVA, SF, borax, and TA based on the synergistic effects of borate ester bonds and H-bonds (Figure 9d).[177] The borate ester linkage between borate ions and the hydroxyl groups from TA and PVA imparted the prepared hydrogel with remarkable self-healing capacity and stretchability (≥1000%). The rejoined hydrogel could withstand tension by hand after contacting for 30 s, and its mechanical SHE reached 82.26% after healing for 60 s. After several cutting-healing cycles, its resistance could recover to its initial value in 1.3 s, indicating rapid self-healing capability. Based on the excellent self-healing ability of borate ester bonds formed between the PVA chain and borax, numerous PVA-based composite SHHs have been developed.[178–181]

Although dynamic borate ester bonds have demonstrated their effectiveness in constructing SHHs, their reformation requires specific pH conditions (generally pH range from 7 to 9) and thus additional alkaline regulators.[182,183] Therefore, researchers were devoted to developing dynamic borate ester bond-based SHHs without additional alkaline regulators. For instance, Ji et al. created a SHH based on dynamic borate ester bonds by directly mixing *N*-methylol acrylamide (NAM) and 1,4-benzene diborane acid (BDBA) with dimethylaminoethyl methacrylate (DMAEMA).[184] Specifically, the DMAEMA was utilized as an alkaline monomer to promote the borate ester bond formation, which could avoid using an additional alkaline regulator. The influences of DMAEMA, BDBA, and NAM concentrations on self-healing properties were explored in detail. All of them contributed to increased SHE within certain concentration ranges, but produced the opposite effects above the given ranges. In addition, the SHE enhanced with the contact time but descended with increasing separation time. The optimal hydrogel successfully achieved a fracture stress recovery of 91% within 1 h and a fracture strain of 100% after 24 h.

In all, compared to non-covalent bonds, dynamic covalent bonds generally have higher bonding energy, which can contribute to SHHs with stronger mechanical strength. However, their dynamic and reversible cross-linking has a high dependence on environmental conditions (such as pH condition and temperature), resulting in decreased SHE and self-healing speed. In particular, imine bonds exhibit moderate chemical stability but are vulnerable to hydrolysis, and can be easily attacked in acidic conditions. This characteristic makes the imine bonds-based SHHs suitable for developing soft bioelectronics

involving degradability and pH-responsibility, such as bioabsorbable smart bandages, degradable cardiac patches, and electronic epineurium.[153] Acylhydrazone networks generally feature a higher reactivity and better stability than imines.[50] However, they are sensitive to temperature and pH. Therefore, acyhydrazone bonds-based SHHs are commonly used as injectable hydrogel carriers in living organisms, microactuators for drug delivery, and conductive electrodes for adjuvant therapy. Since the lone pair of electrons in the oxygen adjacent to the C=N bond increases the stability of the oxime bonds, oximes-based SHHs generally exhibited less swelling effect, slower degradation kinetics, and tunable mechanical properties, making them attractive for long-term implantable bioelectronic applications.[50,185] Borate ester bond-based SHHs offer advantages such as rapid gelatin, and superior mechanical properties, while they are highly sensitive to the environment, such as acid, reductive agent, and glucose.[186] Therefore, they have promising applications in stimuli-responsive bioelectronics for drug delivery and reversible glues.[185] In addition, due to the presence of catechol, they are also desirable to develop various electronic skins, wearable sensors, and implantable patches with self-adhesive capacities. Therefore, SHHs based on different dynamic covalent bonds exhibit distinct characteristics in specific circumstances. The rational design of SHHs at the molecular level is crucial to achieving optimal performance for suitable bioelectronic applications.

#### 2.1.6. Multiple Synergistic Interactions

To promote practical applications of SHHs in biological, sensing, and actuation or robotic fields, both excellent self-healing and mechanical properties are required. However, as mentioned in previous sections, SHHs based on a single self-healing mechanism have obvious limitations, such as limited SHE, limited healing cycles, and difficulty in compromising self-healing ability and mechanical strength. For instance, H-bonding can endow hydrogels with high dynamic and reversible cross-linking ability; nevertheless, they suffer structural instability and poor mechanical properties. SHHs based on dynamic covalent bonds generally possess improved mechanical strength and stability while lower SHE, healing speed, and longer healing time. The combination of multiple synergistic interactions provides a feasible solution to these issues. This makes it possible to merge the advantages of different interaction mechanisms and achieve synergistic improvement in self-healing, mechanical, conductive performances, etc.[187]

For example, Das and co-workers prepared a novel DN SHH (PSUGF-2) composed of poly(4-styrene sulfonate-*co*-methyluracil-imidazolium) chloride (PSS-MUI), gelatin, and $Fe^{3+}$ by simultaneously involving H-bonding, ionic and metal coordination interactions (**Figure 10a**).[188] The prepared hydrogel exhibited excellent healing ability, strength, and stretchability. Its tensile strength reached 97% of the original value after 2 h of healing, showing almost completely restored mechanical properties. Its conductivity slightly decreased after 3 cutting-healing cycles. These results proved that multiple synergistic interactions could significantly improve the self-healable, mechanical, and electrical properties. Besides, Pan et al. fabricated an antibacterial SHH based on triple physical interactions (H-bonding, ionic, and coordination interactions) by cross-linking $Al^{3+}$ and CMCS nanoparticles (NPs) with PAA chains (Figure 10b).[189] Due to the strong triple-cross-linked network and dynamic interactions, the hydrogel exhibited a fracture elongation of 1930% and an excellent self-healing capability of 92.9% and 98.8% in stress and strain within 24 h, respectively. Differently, Mo and co-workers designed a SHH with high stretchability and adhesive performance by mixing TA with AA, (3-Acrylamidophenyl) boronic acid (AAPBA), and $Ca^{2+}$.[190] With abundant catechol groups, TA served as a key mediator molecule to form H-bonds, borate ester bonds, and coordination bonds with $Ca^{2+}$. Due to the introduction of multiple energy dissipation mechanisms, the hydrogel exhibited an ultrastretchability of 7300% and a robust interfacial performance (50 kPa adhesion on porcine skin). The tensile strength could restore 60.98% after 24 h of healing, and the conductivity could rapidly recover in 0.88 s upon damage. In addition, disulfide, hydrogen, and $Fe^{3+}$-carboxylate coordination bonds were also simultaneously utilized to enhance the overall performances of SHHs.[191]

In particular, incorporating nanomaterials has been proven to be an appealing approach to enhancing the comprehensive performance of SHHs. The abundant functional groups, conductive ions, large aspect ratio, and remarkable reinforcement effect of nanomaterials can potentially introduce multiple dynamic bonds (e.g., H-bonds), improving both the conductivity and mechanical properties. Huang et al. constructed a multi-component SHH based on TA, poly(allylamine hydrochloride) (PAH), PAA, poly-(N-isopropyl-acrylamide) (PNIPAM), and graphene by combining multiple dynamic intermolecular interactions (Figure 10c).[192] These interactions included multiple H-bonds, ionic interactions between PAH and PAA chains, $\pi$–$\pi$ stacking interactions between graphene and TA, and cation-$\pi$ interactions between PAH and aromatic benzene rings. Among them, graphene assisted in improving mechanical and electrical properties because of the introduction of H-bonds and $\pi$–$\pi$ stacking interactions and a compact conductive network. The resultant hydrogel exhibited a tremendous fracture strain of 1420%, an impressive mechanical SHE of 87%, and a fast recovery speed of 201 ms in the electrical conductivity after 3 healing cycles. Besides, Wu et al. devised a conductive SHH via one-pot polymerization of AAm and 2-aminoethyl acrylamide hydrochloride (AEAM) and incorporation of carboxyl-functionalized multiwall CNTs (MWCNTs), LiCl, and aldehyde-modified Pluronic F-127 (F127-CHO) (Figure 10d).[193] The self-healing ability was obtained by combining the H-bonds between polymer chains, the imine bonds between -$NH_2$ from P(AM-*co*-AEAM) copolymer chains and F127-CHO micelles, and the ionic interactions between AEAM and -COOH on the surfaces of MWCNTs. The multiple internal interactions, further combined with nanofiller reinforcement and micelle cross-linking, endowed the resultant hydrogel with a broad spectrum of performances, including a stretchability of 1200%, an exceptional elasticity (recovery from 1000% strain), a SHE of 53%, and a conductivity of 3.96 S $m^{-1}$. The superior mechanical property could be ascribed to the nanocomposite network constructed by MWCNTs, which exhibited an advanced reinforcement effect on the hydrogel system. Various other nanomaterials, such as clay nanosheets,[194] were also widely employed for tough and conductive SHH synthesis. The mechanisms and main performances of typical autonomous SHHs are summarized in **Table 1**.

**Table 1.** A summary on the mechanisms, materials, and mechanical and healing performances of autonomous SHHs.

| Self-healing mechanism | Hydrogel materials | Stretchability | Maximum stress [MPa] | Self-healing properties | Self-healing efficiency | Refs. |
|---|---|---|---|---|---|---|
| Hydrogen bond | PAM/SA | – | ≈0.266 | Tensile strain | 99%, 12 h | [66] |
| | SF/P(AM-*co*-AA) | ≈1000% | ≈9.5 | Tensile strain; conductivity | ≈50%, 12 h; ≈100%, 2 min | [82] |
| | PVA/TA | 3060% | 1.365 | Tensile strain | 57.9%, 12 h | [71] |
| | PAM-*co*-PHMA/P (St-*co*-DMAA) | ≈650% | 0.38 | Tensile stress; conductivity | 99%, 12 h; ≈100%, 40 s | [72] |
| | $\gamma$-PGA/PEDOT: PSS | ≈540% | ≈0.11 | Tensile strain; conductivity | ≈90%, 24 h; ≈100%, 10 s | [73] |
| | PVA/PAA/PEGDA | ≈2000% | – | Tensile stress | 72%, 12 h | [74] |
| Ionic interaction | PPy/GelMA/$Fe^{3+}$ | – | 0.05 | Compressive stress | 70%, 0.5 h | [88] |
| | TA@CNCs/PAA/PANI | ≈700% | 0.384 | Tensile stress; conductivity | ≈98.2%, 24 h; 99%, 0.3 s | [90] |
| | Gelatin/PAM/Clay | ≈2400% | ≈0.06 | Tensile stress | 85%, 1 h | [91] |
| | PSBMA/HEMA/Laponite XLG | ≈1100% | ≈0.09 | Tensile stress | 74%, 24 h | [100] |
| | PDA/Clay/PSBMA | ≈2000% | ≈0.225 | Tensile stress; conductivity | 80%, 24 h; 97.6%, 2 s | [98] |
| Metal coordination | TOCNF-CNTs/PAA | 628% | 0.33 | Tensile strain | 98.36%, 24 h | [118] |
| | CS/PAA/PPy/$Fe^{3+}$ | ≈850% | 0.059 | Tensile stress | 93%, 9 h; | [117] |
| | DA/TA/TP/$Fe^{3+}$ | ≈1900% | ≈0.013 | Tensile strain; tensile stress; conductivity | 85%, 6 h ≈90%, 6 h; ≈98%, 6 h | [125] |
| Host-guest interaction | A-TEG-Ad/$\beta$-CD-AOI$_2$/GelMA | 70% | ≈0.225 | Tensile strain and stress | 80%, 1 h | [149] |
| | $\beta$-CD/Fc/PVA/borax | 436% | 0.041 | Tensile stress and strain | 95%, 5 min | [142] |
| | PAA-$\beta$-CDs/PAA-Fc | – | – | Interface adhesive strength | 84%, 24 h | [146] |
| Imine bond | P(MAA-*co*-BA-*co*-OEGMA) | ≈520% | ≈3.0 | Tensile stress | 87%, 40 min | [162] |
| | CMCS/OCMC/GOx | – | – | Macroscopic | the incision nearly disappeared, 5 h | [195] |
| Acylhydrazone bond | DACNCs/HZ-PEG-HZ | 45% | ≈0.15 | Tensile stress | ≈100%, 24 h | [164] |
| | DCMC/DTP/CNFs | – | ≈0.108 | Compressive stress | 89.8%, 1 h | [196] |
| | OSA/PAM/$Fe_3O_4$/CNCs | ≈1100% | ≈0.026 | Tensile stress | 93.54%, 10 min | [165] |
| Oxime bond | P(DMA-stat-DAA) | – | – | Macroscopic | withstand its weight, 2 h | [173] |
| Borate ester bond | BDBA/DMAEMA/NAM | 542% | 0.368 | Tensile stress; Tensile strain | 91%, 1 h; 100%, 24 h | [184] |
| | PVA/Borax/SF/TA | ≈1100% | ≈0.017 | Tensile stress; conductivity | 82.26%, 60 s; ≈100%, 1.3 s | [177] |
| | PVA/Borax/SA/TA | ≈780% | ≈0.022 | Tensile stress | 93.56%, 10 min | [197] |
| Hydrogen bond, Ionic interaction, and Metal coordination | PSS-MUI/Gelatin/$Fe^{3+}$ | ≈1500% | 0.02 | Tensile stress; conductivity | ≈97%, 4 h; ≈100% | [188] |
| Hydrogen bond, Metal coordination, and Borate ester bond | AA/AAPBA/TA/$CaCl_2$ | ≈7300% | ≈0.05 | Tensile strength conductivity | 60.98%, 24 h; ≈100%, 0.88 s | [190] |
| Hydrogen bond Metal coordination, and Imine bond | Gelatin/DATNFC/$Fe^3$ | ≈70% | ≈1.3 | Tensile modulus; conductivity | 45.3%, 10 min; ≈100%, 0.1 s | [198] |
| Hydrogen bond, Ionic interaction, and Imine bond | Poly (AM-*co*-AEAM)/F127-CHO/MWCNTs/LiCl | 1200% | ≈0.15 | Tensile strain; compressive strain | 97%, 1 min; 100%, 1 min | [193] |

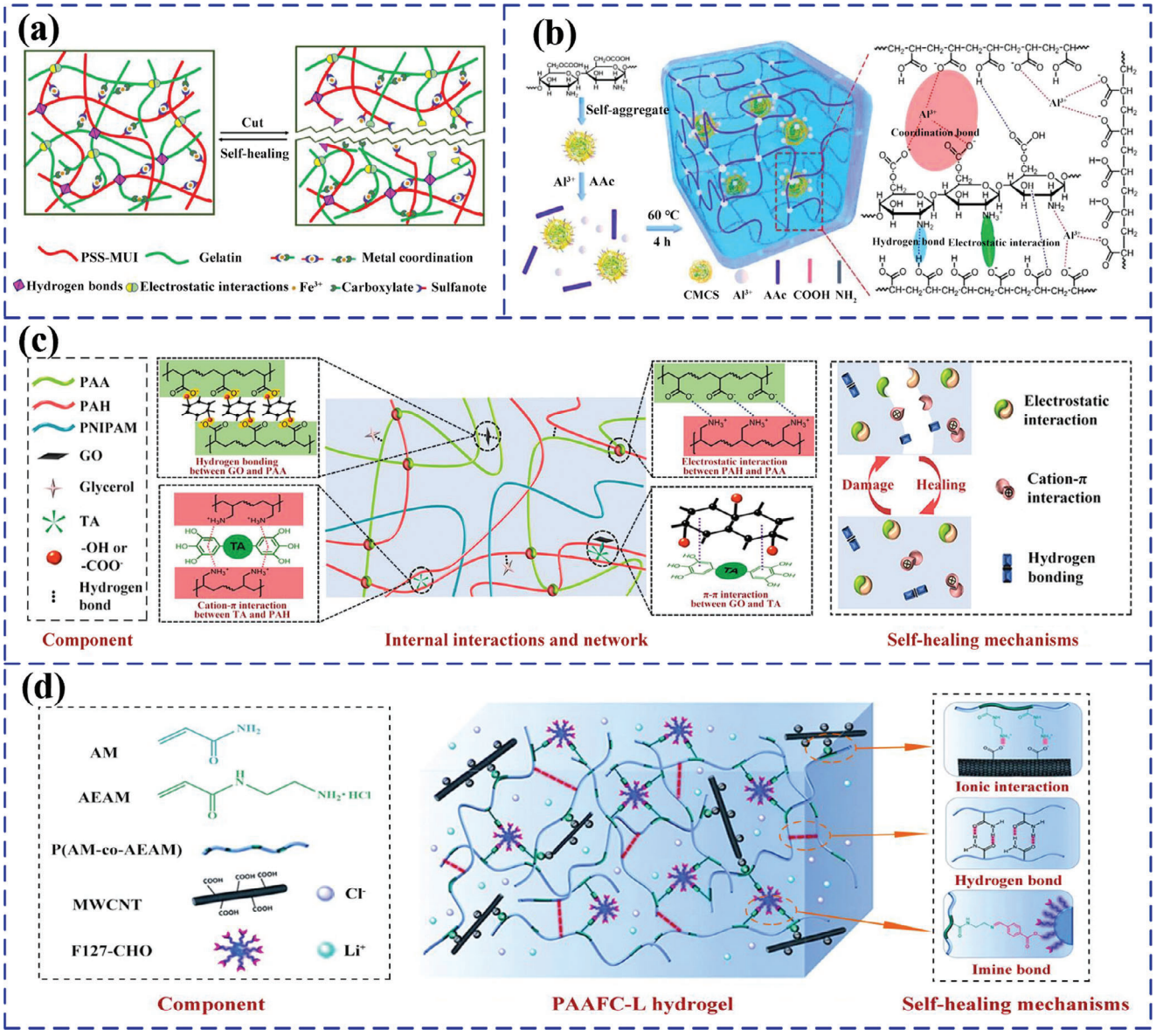


**Figure 10.** SHHs based on multiple interactions synergistically. a) Schematic of the self-healing mechanism of gelatin/PSS-MUI/$Fe^{3+}$ hydrogels formed by H-bonds, ionic and metal coordination interactions. Reproduced with permission.[188] Copyright 2020, American Chemical Society. b) Schematic of the internal interactions of the self-healing CMCS/PAA/$Al^{3+}$ hydrogel based on H-bonds, ionic, and coordination interactions. Reproduced with permission.[189] Copyright 2019, Elsevier. c) Schematic of the internal interactions of self-healing PNIPAM/PAA/PAH/TA/Graphene hydrogels constructed by H-bonds, $\pi$–$\pi$ stacking interactions, and electrostatic interactions. Reproduced with permission.[192] Copyright 2022, Elsevier. d) Schematic of the internal interactions of self-healing PAAFC-L hydrogel formed by H-bonds, ionic interactions, and imine bonds. Reproduced with permission.[193] Copyright 2020, Royal Society of Chemistry.

### 2.2. Stimulus-Triggered Self-Healing Hydrogels

Apart from autonomous self-healing, stimulus-triggered self-healing is another category widely used in SHH preparation. This SHH is not able to conduct a self-repair process under ambient or mild conditions (such as RT ). The self-healing process generally starts under a certain external stimulus, such as heating, pH, light irradiation, or healing agents. The underlying reason is that their broken bonds require more energy to reform than those of autonomous SHHs. Nevertheless, stimulus-triggered self-healing mechanisms also exhibit a lot of specific merits. First, the increased energy required for dynamic cross-linking can lead to high bond strength and thus a sufficiently high mechanical property and stability. Second, since external stimuli supply the energy needed for bonding formation, the SHE and speed can be well-tuned through external conditions, showing decent controllability.[199–201] For instance, the self-healing process can be triggered on or off by varying the pH or temperature conditions.[86,202] Additionally, damaged surfaces with long-term exposure to air can also be healed by controlling the external

stimulus, which can not be realized in autonomous self-healing processes, showing a robust self-repair ability.[203] Currently, external stimuli used for SHHs include heat, light, pH, and healing agents. Besides, magnetic and electrochemical stimuli are also promising trigger sources for the non-autonomous self-healing process.[204–206]

### 2.2.1. Heat-Triggered Self-Healing Hydrogels

Among various external stimuli, heating is one of the most effective strategies to trigger the self-healing process. Heat-triggered SHHs mainly originate from thermally reversible chemical bonds or thermo-reversible covalent chemistries, which can be broken and reformed by setting appropriate temperature conditions. The absorption of heat can increase the potential and kinetic energy of damaged chains, thus forming thermo dynamically and kinetically favorable recoupling conditions and enabling the self-repairing of networks.[207] To date, various thermo-reversible covalent bonds have been constructed, including Diels-Alder (DA) reactions,[208,209] disulfide bonds,[183,210] alkoxyamine exchanges,[211,212] and diaryl-bibenzofuranone[213] (**Figure 11a**). Among these, the DA reaction holds the greatest promise in practical application because of its high specificity, high healing efficiency, simplicity, and repeated healing capacity. As a [4+2] cycloaddition between an enriched diene and an electron-deficient dienophile, it can be reversed through a dissociative retro-Diels-Alder (rDA) reaction at elevated temperatures. Composites containing moieties like furan, anthracene, and cyclopentadiene with the s-cis structure are typical dienes to participate in DA reactions.[214] For instance, the furan-maleimide pair is one of the most prominent DA reaction systems. Shao et al. fabricated a CNC/PEG nanocomposite-based SHH by utilizing reversible DA reactions formed between furyl groups incorporated in CNC and maleimide groups grafted in PEG (Figure 11b).[215] The broken hydrogel could well be repaired under 90 °C within 24 h, demonstrating a SHE of 78% in the fracture stress. It was also verified that the degree of substitution of furyl and the furyl-to-maleimide molar ratio could significantly affect the healing efficiency. Besides, a dextran-based SHH was presented by using fulvene-decorated dextran as the main polymer chains and dichloromaleic-acid-decorated PEG as the cross-linker.[209] The cut hydrogel could easily merge into an integral and bear its weight when incubated at 37 °C for 12 h. By analyzing the scratch depth before and after healing, its ultimate SHE was estimated as 98.7% after 7 h of healing. More recently, Zhang et al. designed a gelatin-based DN SHH based on dynamic imine bonds and DA reactions.[216] Owing to the synergetic effect of the autonomous imine bond, the hydrogel exhibited an enhanced mechanical strength and a remarkable self-healing capacity at 37 °C. Similarly, a pectin/chitosan-based SHH was fabricated via DA reaction and electrostatic interaction, which could self-repair after damage at 37 °C within 5 h.[217] Detailed mechanisms for the aforementioned thermally reversible covalent reactions can refer to Refs. [153,207,213].

In some cases, heating is also helpful to promote the self-healing speed and improve the SHE by increasing the fluidity and molecular kinetics of polymer chains. A heat-triggered self-healable PNAGA hydrogel with excellent mechanical strength and stability was prepared by introducing glycinamide (amidated glycine).[218] Due to the stable dual amide H-bonds in the networks, a high-temperature stimulus was needed to reform the broken bond (Figure 11c). The broken PNAGA hydrogel could self-repair with an indistinguishable interface after healing for 3 h at 90 °C, and its mechanical strength was up to 1 MPa with a SHE of 84%. Yang and co-workers fabricated a self-healable and multitasking PVA/PNAGA DN hydrogel containing hard PVA crystalline micro-domains and soft PNAGA regions (Figure 11d).[219] Although the cut PVA/PNAGA hydrogel could slightly merge into a single one, its tensile strength and fracture strain were significantly reduced in comparison with its original values. However, after heat treatment at 90 °C, the healed hydrogel exhibited higher toughness and elongation, demonstrating an increased SHE. This was because the reconstruction of the H-bonds in the PNAGA network at high temperatures was much stronger than at RT. Besides, by exploiting the thermally reversible nature of $\kappa$-carrageenan, self-healing $\kappa$-carrageenan/PNAGA DN hydrogel was also developed.[220]

Although significant progress has been achieved in heat-triggered SHHs, challenging issues remain to be solved. One of them is that some thermally reversible reactions require a temperature of more than 100 °C, which may not be directly applied in physiological environments and is difficult to control in practical applications. In addition, the structure and performance of undamaged regions of hydrogels may suffer injuries during the heat-triggered healing process. Thus, the applications of SHHs that heal under high-temperature conditions in soft bioelectronics need further research, and their trigger temperatures can be tuned through invovations in network structures and cross-linking mechanisms. Anyway, heat-triggered SHHs within the physiological temperature range can be used in epidermal sensing devices, such as soft temperature sensors, moisture sensors, as well as bioactuators for drug delivery and object manipulation.[221–223]

### 2.2.2. Light-Triggered Self-Healing Hydrogels

Light is a promising external stimulus for non-autonomous SHHs because it features high reaction rates and allows spatial and temporal control of the healing over damaged areas in a non-contact approach.[224,225] Light-triggered self-healing process can proceed based on three main categories of chemistries: reversible photo-cross-linking reactions between photo-reactive moieties, photo-induced metathesis reactions, and photo-thermal effects. The photo-cross-linking reactions involve the reversible photodimerization and photocleavage of chromophores, such as cinnamoyl, coumarin, and anthracene.[224] That is, upon damage, the reversible cross-links in polymer networks will first undergo photocleavage under UV light irradiation of higher energy (wavelength $\leq$ 300 nm) to increase the photoreactive moieties and polymer chain mobility and subsequently rebuild to heal via photodimerization (such as [2+2] cycloaddition or [4+4] cycloaddition reactions) by exposing to light with a longer wavelength (>300 nm). For instance, two coumarin moieties can form cyclobutane-linked dimers under long-wave UV light through [2+2] cycloaddition (**Figure 12a**), and then the dimer

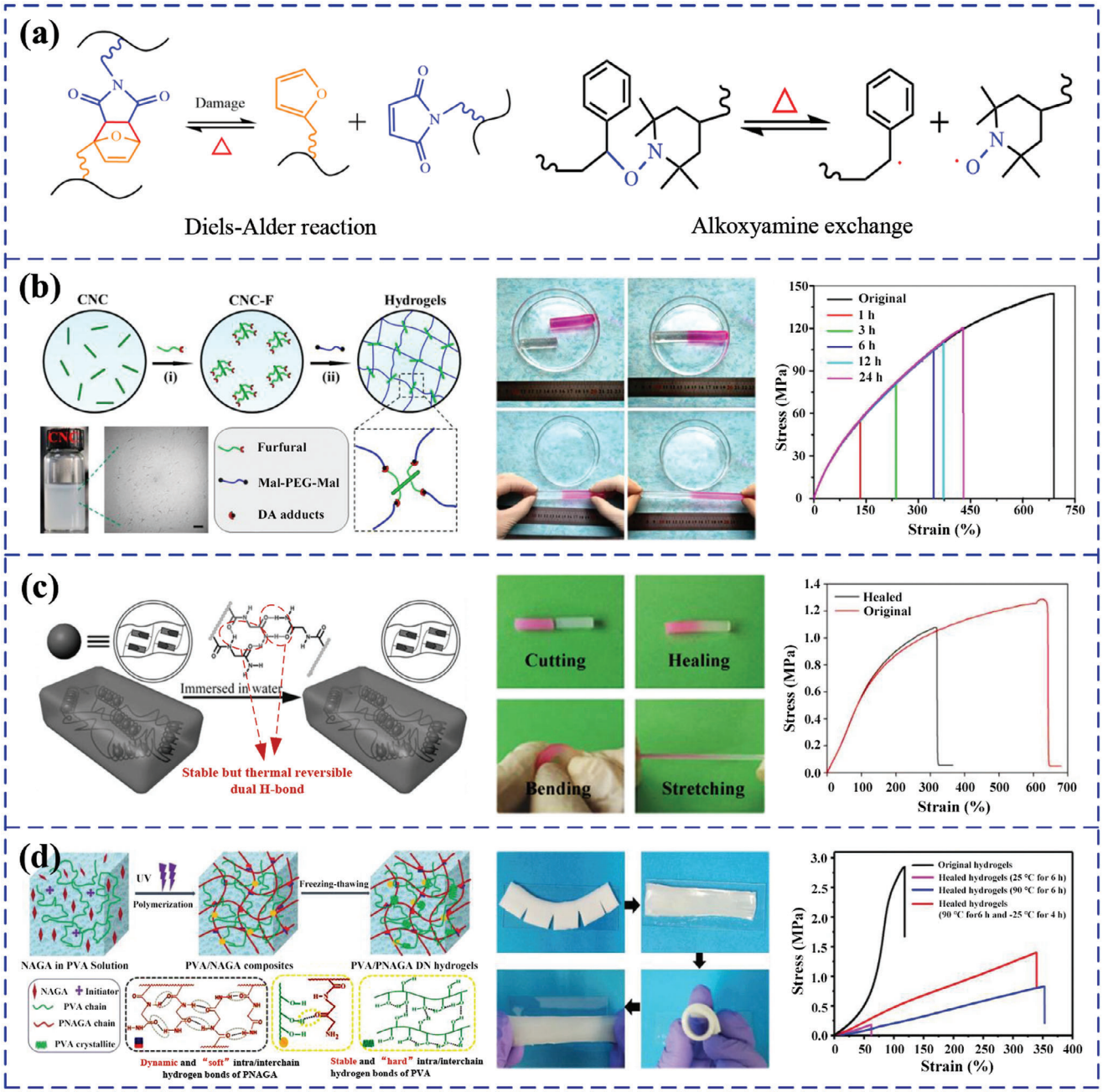


**Figure 11.** Schematic of heat-triggered self-healing mechanisms and the prepared SHHs. a) Typical heat-triggered reversible reactions: Diels–Alder and alkoxyamine exchange. b) Schematic of the preparation and internal interaction of SHHs formed by DA reaction, photographs of the cutting-healing hydrogel, and the mechanical self-healing property. Reproduced with permission.[215] Copyright 2017, American Chemical Society. c) The internal interactions of PNAGA hydrogel, photographs of the cutting-healing hydrogel, and the mechanical self-healing properties. Reproduced with permission.[218] Copyright 2015, John Wiley & Sons. d) Schematic of self-healing PVA/PNAGA DN hydrogel preparation and internal interactions, photographs of the healing process, and tensile self-healing property. Reproduced with permission.[219] Copyright 2021, John Wiley & Sons.

de-cross-links to release two original coumarin groups under short-wave UV light.[226] Based on this reversible process, coumarin-contained monomers or polymers could be used to prepare photo-reversible SHHs. By introducing coumarin methacrylate cross-linkers, Yu et al. proposed a light-triggered SHH based on poly(amidoamine) (PADA).[227] The cut hydrogels can be healed under light with wavelengths at 280 and 365 nm based on [2+2] cyclo-addition of coumarin moieties (Figure 12b). A further study on the effects of irradiation showed that both the tensile modulus and breaking prolongation increased with the irradiation time. The highest SHE of 88.6% was observed by exposing it to 365 nm UV light for 60 min. Besides, UV-triggered self-healable polyurethane and PEG were also synthesized using the same mechanism.[228,229]

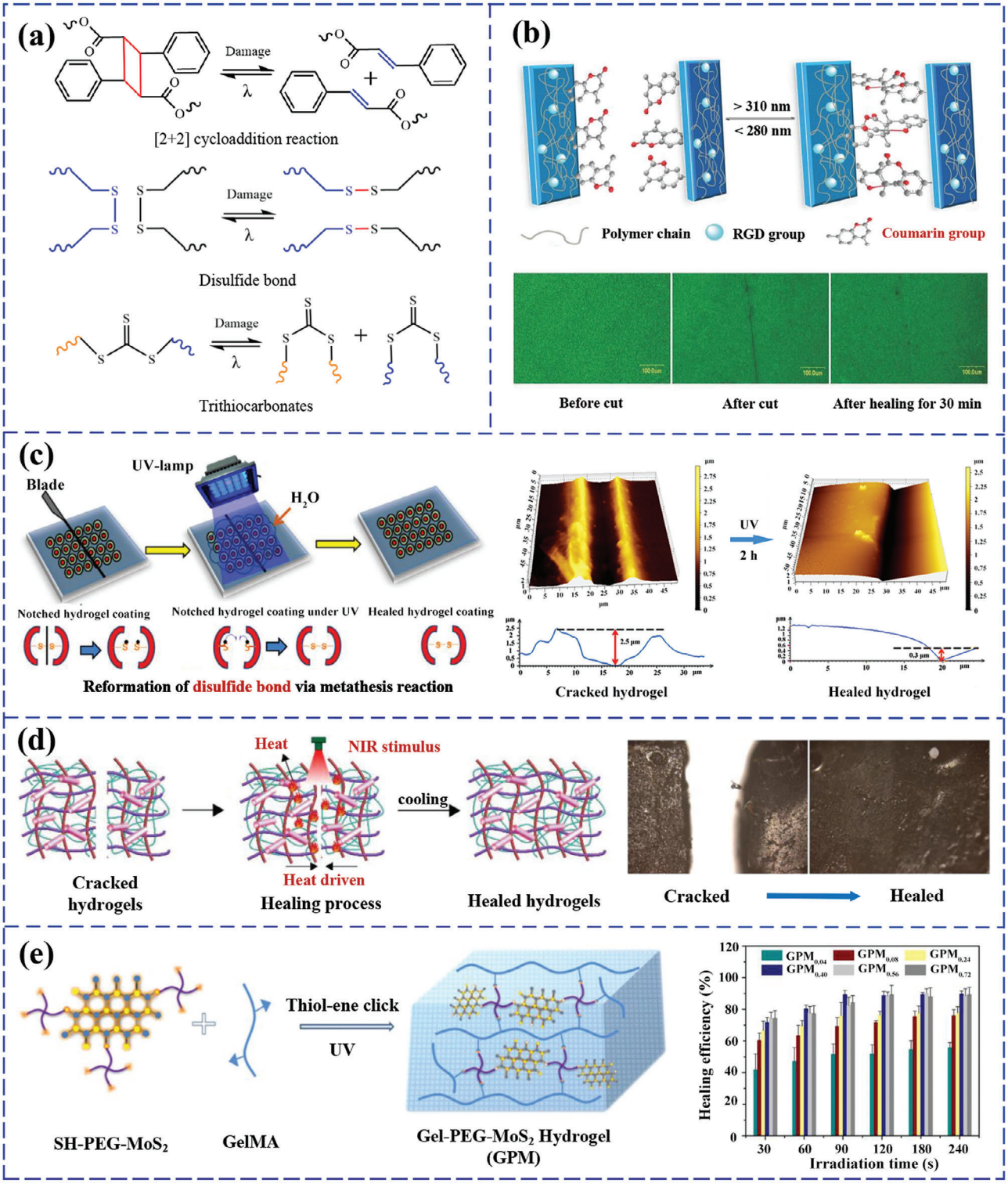


**Figure 12.** Schematic of light-triggered self-healing mechanisms and the prepared SHHs. a) Typical light-triggered reversible reaction: [2+2] cycloaddition reaction, disulfide bond, and trithiocarbonates. b) Schematic of the internal interactions of self-healing PADA hydrogel formed by [2+2] cyclo-addition of coumarin moieties and SEM images of the healing process. Reproduced with permission.[227] Copyright 2016, John Wiley & Sons. c) Schematic of the healing process of the UV light-triggered self-healable hydrogel based on disulfide bond, the images of the depth height variation of hydrogel film before and after healing. Reproduced with permission.[232] Copyright 2018, American Chemical Society. d) Schematic of the healing process of the cracked HNTs/PDA/PAM/Gelatin hydrogel under NIR light irradiation and photographs of the broken and healed hydrogel. Reproduced with permission.[237] Copyright 2020, Elsevier. e) Schematic of the preparation of self-healing GPM hydrogels and the healing property. Reproduced with permission.[236] Copyright 2020, Elsevier.

Photo-induced metathesis reactions are another type of applicable mechanism for light-triggered SHHs, which function by reshuffling dynamic photo-reversible covalent bonds, such as disulfide and trithiocarbonates (Figure 12a).[224,230] Typically, sulfur anion or sulfur-free radical can be easily triggered by sunlight or UV light for further disulfide exchange or aromatic-disulfide exchange reaction, which are highly adopted in photo-healable hydrogels.[231] Banerjee and co-workers constructed an antifouling zwitterion-based SHH by combining a photo-induced disulfide metathesis reaction with ionic interactions between the zwitterionic segments (Figure 12c).[232] The influence of the disulfide metathesis reaction on self-healing was studied by coating as-prepared hydrogel films on glass slides and observing via optical instruments. The disulfide bonds were homolytically cleaved to generate sulfenyl radicals under UV light irradiation in the beginning, and consequently the generated sulfenyl radicals were exchanged with uncleaved disulfide bonds to implement the healing process. The cut hydrogel coatings exhibited the highest SHE of 88%, evaluated in terms of film depth height variation before and after healing. Besides, Dong et al. reported an ionic cross-linked hydrogel constructed by the reshuffling reaction of the trithiocarbonate (TTC) moiety.[233] UV (365 nm) irradiation could stimulate the homolysis of the C-S bond of TTC and further result in the exchange reaction with neighboring TTC moieties to realize self-repair. The broken hydrogel could restore its original network structure within 1 h.

Although reversible photo-cross-linking and photo-induced metathesis reactions have shown wide applicability in developing light-triggered SHHs, the limited penetration depth (typically $\leq$ 200 μm) and high dependence on material transparency constrain their applications in thin films or translucent structures.[213] Photo-thermal effect opens new perspectives for developing light-triggered SHHs, which have been extensively explored in recent years. The underlying mechanism is that it can convert light into local heat and utilize the heat-based healing features to increase the healing depth and eliminate the limitation on the light transmission of materials. The photo-thermal effect-based SHHs were synthesized by incorporating photo-thermal materials (such as graphene oxide (GO),[234,235] molybdenum disulfide ($MoS_2$) nanosheet,[236] gold NPs, polydopamine (PDA), PPy, etc.) into the hydrogel network. Yang et al. devised a near-infrared (NIR) light-triggered SHH by introducing PDA particles into PVA hydrogels.[225] The composite hydrogel exhibited reinforced mechanical and self-healing capacity because of the superior photo-thermal effect of PDA and the reversible formation of H-bonds. Its SHE reached 92% in terms of the tensile test under NIR irradiation of 0.75 W $cm^{-2}$ in 30 s. A comparison with the healed hydrogel under 37 °C for 36 h (a SHE of ≈24%) without NIR irradiation indicated that the PDA particles contributed much to the self-healing property. This was because the PDA particles converted light into heat, raised the local temperature of the broken region, and promoted the PVA chain mobility and H-bond reestablishment. More recently, Cao et al. reported a halloysite nanotubes (HNTs)/PDA-reinforced PAM/Gelatin composite hydrogel with NIR-triggered self-healing capacity (Figure 12d).[237] The prepared hydrogel showed a favorable photo-thermal effect and water dispersion ability, assuring light-to-heat conversion and uniform heat distribution. The fracture interface of the broken hydrogel could be well healed under NIR light of 2 W $cm^{-2}$ for 180 s, exhibiting a SHE of 76%. The temperature of the exposed region under constant irradiation could reach above 100 °C, which promoted the free movement and mutual diffusion of the PAM and gelatin polymer chains at the fracture interface. Afterward, Wu et al. exploited $MoS_2$ nanosheet as a photo-thermal conversion agent and synthesized an NIR-triggered SHH based on gelatin and PEG (Figure 12e).[236] The cracked areas of the resultant hydrogels started to heal upon exposure to NIR light. The SHE improved from 41.7% to 91.3% while the exposure time increased from 30 s to 240 s. The underlying mechanism was based on the photo-thermal effect of $MoS_2$ upon NIR irradiation, which resulted in the diffusion and re-entangling of the thermal-sensitive GelMA to heal the cracks. Similarly, a light-triggered hybrid PVA/$MoS_2$ nanosheet SHH was erected, which demonstrated a high SHE of 91.8% under NIR light irradiation within 3 min.[238] In addition, various light-triggered SHHs, such as supramolecular polymer/MWCNTs composite hydrogels[239] and graphene-hectorite-clay/PDMAA hybrid hydrogels,[235] have also been constructed for device applications.

The trigger lights for the aforementioned SHHs are UV or NIR, both of which require additional devices for light generation, complicating the self-healing system design and process. One interesting direction started in recent years was to develop sunlight or visible light-triggered SHHs, which could eliminate the dependence on specific light sources and extend their practical usage. For instance, Wang et al. constructed a visible light-triggered SHH consisting of a PEG-grafted poly(ethyl methacrylate) (PEMA) derivative and a disulfide linkage by exploiting thiol-disulfide exchange.[240] The as-prepared hydrogel coatings could self-heal under ambient conditions within 10 min (visible light irradiation from sunlight), enabling their application in a natural environment. Based on a similar strategy, sunlight-triggered PU-2, 20-hydroxyethyl disulfide (HEDS), liquid crystalline gels, and C/P(AM-*co*-AA)/$Fe^{3+}$ SHHs were also proposed.[241–243]

In summary, light-triggered SHHs feature the advantages of rapid healing speed, high healing efficiency, photo-responsive characteristics, and accurate controllability in the healing areas with a contactless approach. These merits enable SHHs to be advantageous for various light-sensitive biodevices, such as intelligent photo-controlled electronic switches, intelligent soft displays (such as smart windows), wound dressing for therapeutic applications, soft electronics for controlled drug delivery, photothermal effect-based self-power supply, etc.[235,236,244,245] However, since the light can penetrate the limited depth of the material, light-triggered SHHs feature shortages in constructing bioelectronics with a thick thickness or without optical transmittance.

### 2.2.3. Catalyst/pH-Triggered Self-Healing Hydrogels

Catalyst or pH-triggered self-healing mechanisms are facile access to preparing SHHs, which, in essence, chemically adjust the bonding and deboning processes of hydrogel networks via changing pH conditions or adding proper catalysts. The pH-triggered self-healing refers to dynamic reversible relations under strong acid (pH < 5) or alkaline (pH > 9) conditions, which has

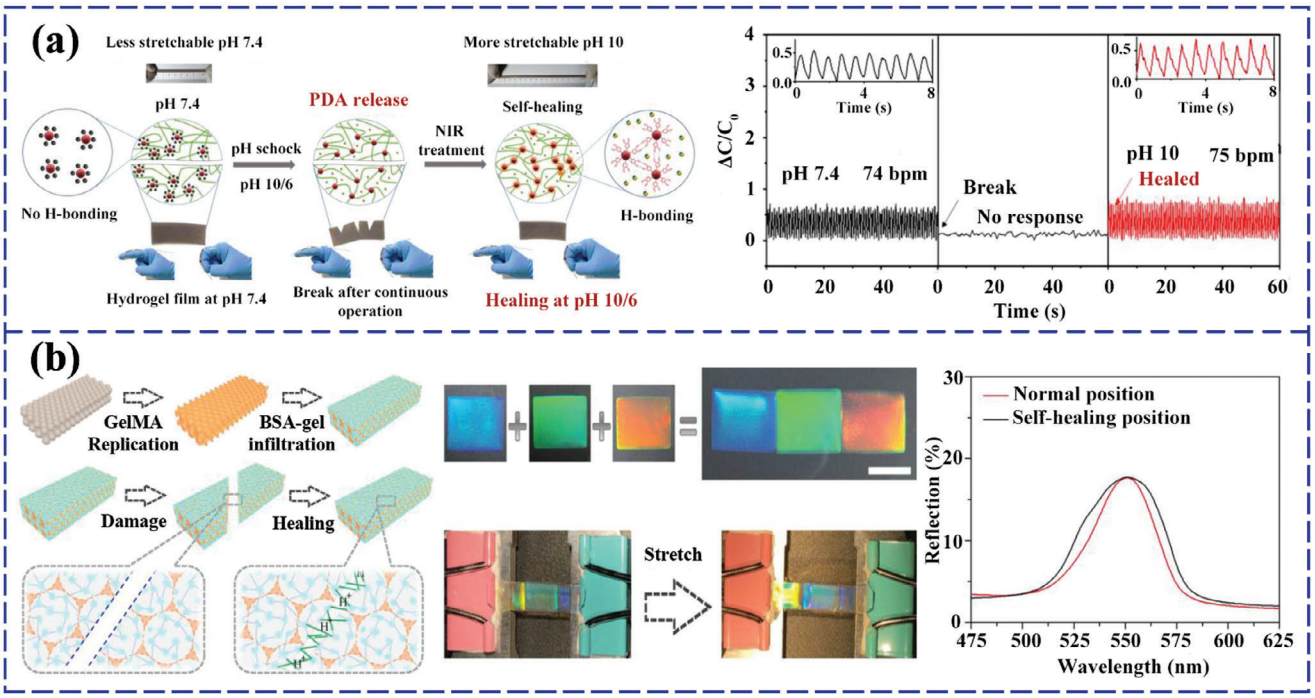


**Figure 13.** SHHs based on the pH/Catalyst-triggered mechanism. a) Schematic of the healing process of the self-healing P(NIPAM-*co*-AMPS)/cPDA@ZPD hydrogel triggered by pH conditions under NIR light induction and the electrical healing property. Reproduced with permission.[248] Copyright 2021, Elsevier. b) Schematic of the preparation and healing process of the self-healing nano-structural color hydrogel triggered by enzyme additives and catalysts, photographs of the healed hydrogel, and the optical performance after healing. Reproduced with permission.[249] Copyright 2017, National Academy of Sciences.

distinctive differences from dynamic covalent bonds based on autonomous self-healing under mild conditions. For instance, pH-triggered self-healing D-hydrogels with tough strength and shape memory were fabricated by exploiting both self-complementary quadruple H-bonds between UPy dimers and $Fe^{3+}$-COOH coordination bonds.[246] The cut hydrogel samples could be treated to heal by dropping several drops of alkaline solution (pH 14) at its broken interface, soaking in a 0.06 M $Fe(NO_3)_3$ solution, and then in deionized water for 5 h and 24 h, respectively. The underlying mechanism was that the high alkaline condition promoted the mobility of polymer chains and led to closer proximity between functional groups, and thus contributed to the re-establishment of the multiple interactions ($Fe^{3+}$-COOH coordination) after soaking in $Fe(NO_3)_3$ solution. These interactions finally resulted in the welding of the broken surfaces (55% in SHE). The repaired hydrogel could be bent and twisted, exhibiting a tensile strength of ≈7.7 Mpa. By taking advantage of a dual physical cross-linking strategy, Guo et al. developed a pH-triggered high-strength SHH by combining PVA and poly-acrylamidohexanoic acid (PAACA).[247] The presence of protonated and deprotonated -COOH groups on the PAACA chains endowed the prepared hydrogel with a pH-triggered self-healing capacity. The bisected hydrogel sample healed when immersed in hydrogen chloride (HCl) solution (pH < 3) and separated when exposed to NaOH solution. The healed hydrogel showed a tensile strength of 0.2 MPa and a stretchability of 310%. Shit and co-workers developed a NIR-induced pH-triggered SHH reinforced by zwitterionic polymer dot (cPDA@ZPD) (**Figure 13a**).[248] When exposed to acidic or alkaline pH (pH 10) conditions, the hydrophobic association was broken along with the release of cPDA because of the generation of ionic interaction in the ZPD. Consequently, the photo-thermal effect of PDA was activated under NIR irradiation, leading to the rearrangement of H-bonds between released cPDA and promoting the self-healing of hydrogels. Although pH-triggered self-healing mechanisms can enhance the controlling capability of the healing process, their SHEs and speed need further improvement. Meanwhile, the influences of pH on the structure, morphology, and performance of hydrogels should also be considered.

Apart from pH-triggered SHHs, various catalyst-triggered SHHs have also been constructed recently. For instance, Fu et al. proposed a glucose-triggered SHH with nano-structural color based on GelMA inverse opal scaffold and glutaraldehyde cross-linked BSA by incorporating glucose oxidase and catalase (Figure 13b).[249] When adding extra glucose on the damaged interface of the hybrid hydrogel, the glucose oxidase oxidized the glucose into gluconolactone and then formed gluconic acid by further hydrolysis. The resultant gluconic acid could adjust the pH environment and assist the reformation of imine bonds between -CHO from the glutaraldehyde and lysine residues from glucose oxidase, BSA, and catalase. The catalase further decomposed the by-product $H_2O_2$ to avoid oxidizing the imine bond, enabling the cyclic reaction of glucose oxidation. Eventually, the broken hydrogel was repaired and could maintain its initial structural color, demonstrating excellent self-healing properties. Besides, another enzyme-triggered self-healing DN hydrogel was synthesized based on AAm and allylglycine-terminated

Leu-Pro-Glu-Thr-Gly (LPETGGG) peptides by using Sortase A (SrtA), a peptide ligase, to transform the covalent peptide linkages to reversible covalent bonds.[250] Two pieces of the resultant hydrogels could merge into an integral under the existence of SrtA solution and pressure of 2–5 kPa, demonstrating a certain self-healing ability. Nevertheless, in the absence of a SrtA solution, no obvious self-healing phenomenon was discovered. The mechanism was that the SrtA could lower the activation barrier and result in reversible cleavage and the formation of cross-linkers. More research about enzyme-regulated/triggered SHHs can be seen in Ref. [251].

In all, pH or catalysts-triggered self-healing mechanisms essentially harness the pH conditions or proper solvents to regulate the cross-linking and de-cross-linking process. This makes the resultant SHHs naturally sensitive to the corresponding pH or catalysts. Therefore, pH or catalysts-triggered SHHs can be widely in developing soft biochemical sensors for pH or chemical molecules monitoring of in vivo or in vitro environment, controllable actuators for drug delivery, and soft bioelectronics with shape memory capacity.[245,246,252] Although pH or catalysts-triggered SHHs bioelectronics possess facile and simple controllability on their healing process, pH conditions or catalysts may destroy the structure and morphology of the other components of the device, and thus degrade the whole performance.

#### 2.2.4. Other Emerging Stimuli-Triggered Self-Healing Hydrogels

Aside from the aforementioned stimuli, other stimuli, such as magnetism, ultrasound, and electricity also hold great potential in developing stimuli-triggered SHHs, since they enable remote, wireless, and localized control over the self-healing process. These stimuli are particularly useful in real applications where damaged parts need to be repaired in situ. Among them, ultrasound can accurately steer the acoustic energy into the damaged areas with minimum side-effect and penetrate larger depths than light because of its unique penetrability. Lu et al. first demonstrated the concept of using high-intensity focused ultrasound (HIFU) to trigger the healing of dynamic cross-linked shape memory polymers.[253] After treating with the HIFU for 60 min at a power of 3 W, damaged samples could recover ≈92% of their original elongation at break. In comparison, conventional heating-triggered healing (90 °C for 60 min) only yielded around 56% recovery. This demonstrated the feasibility and prospect of ultrasound-triggered self-healing.

Magnetism-triggered self-healing strategies were also developed for constructing SHHs, which harnessed the magnetothermal effect and the ability of remotely magnet-actuating contact. Shibaev and co-workers developed a SHH by assembling cobalt ferrite $CoFe_2O_4$ NPs into carboxymethyl hydroxypropyl guar/borax hydrogel.[254] The abundant H-bonds and borate ester bonds enabled the hydrogel to achieve a 100% SHE within 10 min. Intriguingly, two bisected hydrogels could be brought together remotely under magnetic force acting on the NPs in the hydrogel network, successfully achieving self-healing without manual intervention. Based on the strategy of magnet-actuating contact, a conductive, stretchable SHH based on GaInSn/Ni-based composite was developed, further verifying the effect of magnetic-triggered self-healing behavior.[255] Qin et al. developed a multi-stimuli-triggered healable $Fe_3O4$@Au/PAM (MFP) hydrogel by combining the magneto-thermal effect of $Fe_3O_4$ and the photo-thermal effect of Au NPs.[256] The as-prepared hydrogel could be triggered to self-heal by both magnet and NIR irradiation through the reformation of Au-SR coordination bonds. The hydrogel with an incision could recover 86.3% of its initial tensile strain under NIR irradiation and withstand stretchability without cracking under alternating magnetic fields.

Besides, electricity-triggered self-healing mechanisms exploit the electrothermal effect of materials (e.g., CNTs) to reform dynamic bonds in hydrogel networks.[257–260] For instance, Chen et al. prepared a self-healable PPy-incorporated Au NPs/CNT/PAM (GCP@PPy) hydrogel with abundant dynamic Au-thiolate (Au-SR) bonds within the network, which could reconstruct and lead to healing of the prepared hydrogel under electricity stimulus.[261] After healing for 15 min under a current of 50 mA, the cutting-healing hydrogel could restore its original tensile strain and conductivity of 86% and 96%, respectively.

In all, ultrasound, magnetism, and electricity initiated new mechanisms for devising stimuli-triggered SHHs and endowed the self-healing process with excellent controllability. For instance, ultrasound-triggered SHHs can be widely utilized in constructing implantable bioelectronics for controlled drug release based on their penetration ability, and bioelectronics with shape memory effects based on their thermal or mechanical effects.[262] Similarly, magnetism-triggered SHHs can be used in biomedical devices, actuators, and soft robots for cell manipulation and foreign body removal.[263] Although various SHHs have been developed using the aforementioned trigger sources, their deep understanding and further applications in bioelectronics are still ongoing. The key performances of the aforementioned stimulus-triggered SHHs are presented in **Table 2**.

### 2.3. Self-Healing Hydrogels in Harsh Environments

The aforementioned SHHs mainly apply to common ambient environments, such as at RT or in the air. However, in nature, a great number of devices are applied in harsh environments, such as low-temperature conditions in winter or high-latitude regions and underwater circumstances. In these cases, the self-healing capacity will lose or be inhibited by the extremely harsh conditions. For instance, in winter or high-latitude environments, the subzero temperature will make the water embedded in hydrogel networks solidify into crystals, inhibiting the polymer chain fluidity and dynamic bond reformation at broken interfaces. In high-humidity or even underwater circumstances, water molecules can act as donors and acceptors of H-bonds, ligands, polar solvents, etc. These inhibit the reformation of dynamic bonds by saturating the H-bonds, coordinating with the metal cation, and solvating the ions, significantly destroying the self-healing capacity.[266] Besides, the majority of hydrogels composed of hydrophilic polymers inevitably swell in water, disabling the self-healed hydrogels. The loss of self-healing behavior in aforementioned harsh environments greatly narrows the practical applications of SHHs. Therefore, developing SHHs that can resist the influences of harsh conditions has drawn increasing attention.

**Table 2.** A summary of mechanisms, materials, mechanical and healing performances of stimulus-triggered self-healing hydrogels.

| Self-healing mechanism | Hydrogel materials | Stretchability | Maximum Stress/MPa | Healing condition | Self-healing property | SHE | Refs. |
|---|---|---|---|---|---|---|---|
| Heat triggered | CNC/PEG | 690% | 0.16 | 90 °C | Tensile stress | ≈78%, 24 h | [215] |
| | PNAGA | 1400% | 1.1 | 90 °C | Tensile stress | 84%, 3 h | [218] |
| | PVA/PNAGA | ≈125% | ≈2.8 | 90 °C | Tensile stress | 50%, 6 h | [219] |
| | κ-Carrageenan/PNAGA | ≈250% | 1.7 | 90 °C | Tensile stress | ≈26.4%, 3 h | [220] |
| | P(NAGA-co-AAm)/LiCl | ≈900% | 2.27 | 60 °C | Tensile strength | 85%, 10 min | [264] |
| | Gelatin/Chondroitin sulfate | ≈310% | ≈0.04 | 37 °C | Tensile strain | ≈85%, 2 h | [265] |
| Light triggered | PAM/c47/PADA | ≈120% | ≈0.225 | UV | Tensile modulus | 88.6%, 1 h | [227] |
| | HNTs@PDA/PAM/Gelatin | ≈250% | 0.133 | NIR | Tensile stress | ≈76%, 3 min | [237] |
| | GelMA/PEG/$MoS_2$ | – | ≈0.283 | NIR | Tensile modulus | 91.3%, 4 min | [236] |
| | PVA/$MoS_2$-DTT | – | ≈0.217 | NIR | Tensile stress | 91.6%, 3 min | [238] |
| | Supramolecular polymer/MWCNTs | ≈50% | ≈0.8 | NIR | Conductivity | ≈100%, 1 min | [239] |
| pH triggered | P(AM-*co*-AA)/UPyMA/$Fe^3$ | 541% | 7.9 | pH (14) | Tensile stress | 55%, 5 min | [246] |
| Electricity triggered | PAM/CNT/Au NPs@PPy | 2380% | 1.25 | Current (50 mA) | Tensile strain | 86%, 15 min | [261] |
| Magnetism triggered | $Fe_3O_4$@Au/PAM | 2250% | 3.1 | Magnetic filed | Tensile strain | 52%, 10 min | [256] |

### *2.3.1. Anti-Freezing Self-Healing Hydrogels*

One effective strategy to achieve SHHs in freezing environments is to suppress the H-bonding with water molecules and decrease the freezing point.[267–269] For this, a large number of researchers introduced organic solvents into hydrogel matrices and exploited the stronger H-bonds formed between the solvent and water molecules to weaken the formation of the crystal lattice of ice and simultaneously hinder water vapor pressure.[268,270] For example, Liao and co-workers developed an anti-freezing and conductive SHH by using ethylene glycol (EG) to substitute a part of water molecules in MXene nanocomposite-based hydrogels (MNH) (**Figure 14a**).[271] The MNH could withstand large stretching and arbitrary twisting after storing at -40 °C for 6 h, exhibiting an excellent low-temperature tolerance. This was because the abundant H-bonds generated between the water and EG disrupted the process of crystal lattice formation at subzero temperatures. The abundant H-bonds also imparted the hydrogel with a long-lasting water retention capacity (keeping ≈90% of its initial weight after storing at 20 °C for 8 days) by hindering the water evaporation. Owing to the borate ester bonds between the -OH groups of PVA and tetra-hydroxyl borate ions, as well as the H-bonding interactions among EG, PVA, and MXene, the fractured hydrogel could be healed at 20 °C and 50% humidity, demonstrating excellent SHE in both mechanical (an efficiency of ≥85% after 12 h of healing) and electrical properties. Wang et al. developed an anti-freezing and conductive SHH by directly doping glycerol into PVA/SA hydrogel.[272] The resultant hydrogel could be stretched and twisted after storing at −20 °C for 24 h, and also normally light an LED lamp. The mechanical test at −20 °C showed that the tensile strain was almost identical to that at RT. It was also proved that the freezing temperature of the prepared hydrogel decreased as the concentration of glycerin increased. With the synergistic effect of H-bonds and borate ester bonds, the prepared hydrogel exhibited a high SHE of 95% after 4 h healing. Zheng and co-authors constructed an anti-freezing and moisturizing SHH by incorporating EG and CNTs into TA/PVA/Borax.[269] It exhibited an anti-freezing temperature of −60 °C, a long-term moisturizing property of 30 days, and mechanical SHE of more than 98% in tensile and compressive strain testing. Based on a similar strategy, many other anti-freezing SHHs, such as PAM-clay hydrogel with the incorporation of glycerol,[273] PVA/starch/tea polyphenol-based composite organohydrogel,[274] and poly(acrylic acid-*co*-maleic acid)/glycerol/boron nitride nanosheet composite hydrogels,[275] were also constructed for soft electronics applications in a low-temperature environment.

Introducing zwitterion materials into hydrogels is an emerging and appealing approach to developing anti-freezing SHHs. With abundant negative and positive charges in one unit, the zwitterion can destroy the H-bonds within water molecules to prevent their binding, thus lowering the freezing point.[276] Zhang et al. invented an anti-freezing SHH with a skin-like mechanoresponsive performance by introducing a kind of zwitterion, betaine, into PAA networks.[277] The DN network structure consisted of the covalent PAA chains and fugitive supramolecular betaine chains imparted the developed hydrogel with a high stretchability of 1600% and an immense strain-stiffening property (24-fold modulus enhancement). Owing to the function of betaine in preventing water crystallization and adjusting water stress in subzero and water-deficit circumstances, the resultant hydrogel could preserve water content with almost no changes for 7 days at a relative humidity (RH) of 60% and maintain prominent elasticity at -40 °C. Moreover, the scratched hydrogel could completely self-heal and withstand bending and stretching after 12 h of healing at RT and 80% RH, in which the movable water promoted the reformation of all physical bonds. Guo et al. demonstrated an anti-freezing zwitterionic SHH by

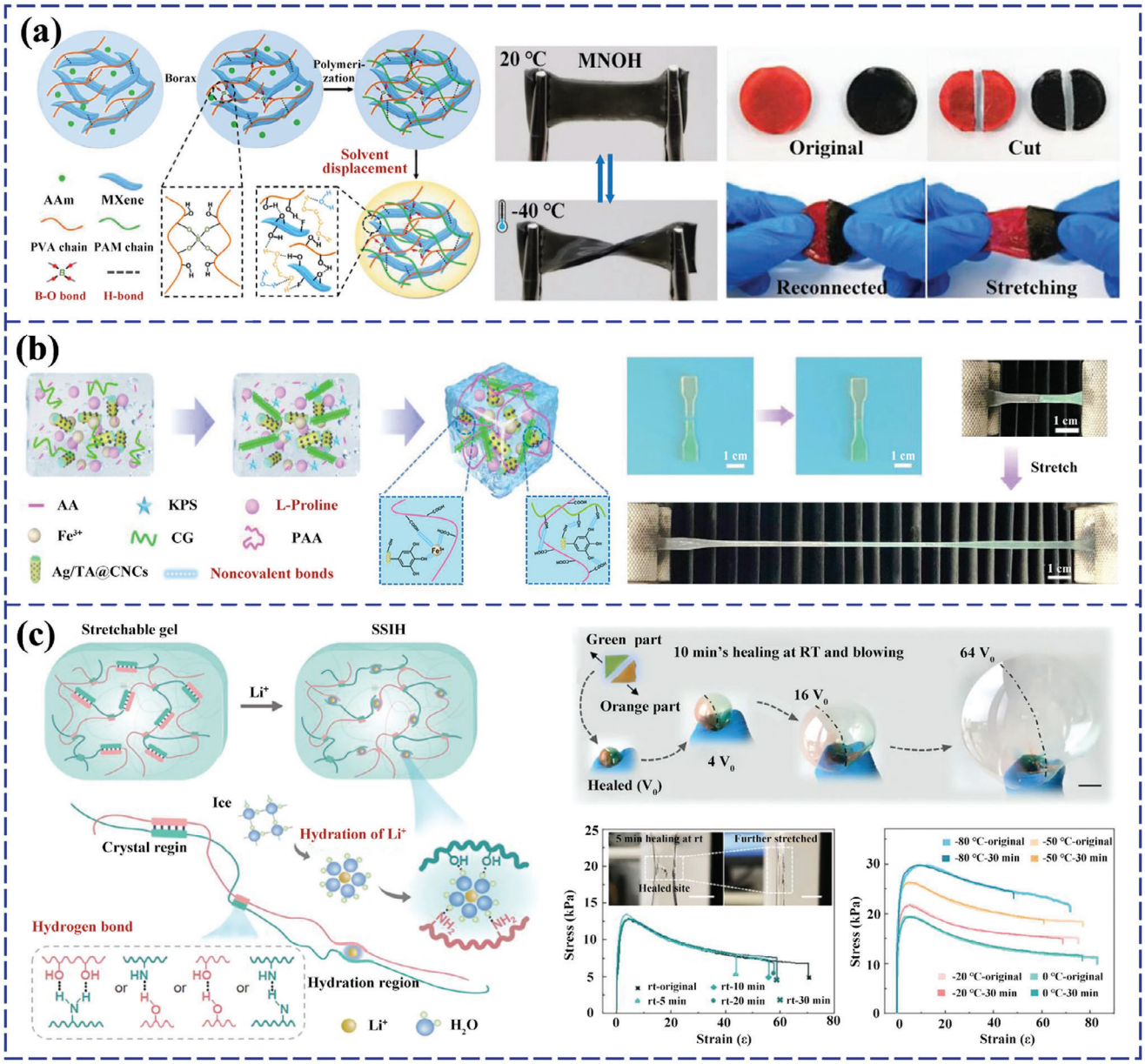


**Figure 14.** SHHs in low-temperature environments. a) Schematic of the synthesis process of cold-resistant PAM/PVA/MXene hydrogel based on EG solvent replacement, photographs of the hydrogel at RT and −40 °C, and the healing process of the hydrogel. Reproduced with permission.[271] Copyright 2019, John Wiley & Sons. b) Schematic of the internal interactions of the anti-freezing SHH based on hydration effects of zwitterion materials and photographs of the self-healing process. Reproduced with permission.[279] Copyright 2022, American Chemical Society. c) Schematic of the anti-freezing mechanism of SSIH by utilizing the strong hydration of inorganic salt and the self-healing properties at ultra-low temperatures. Reproduced with permission.[266] Copyright 2022, John Wiley & Sons.

polymerizing [3-(methacryloylamino) propyl] dimethyl (3-sulfopropyl) ammonium hydroxide inner salt, HEMA, AA, and LiCl particles in a glycerol-water hybrid solution.[278] The resultant hydrogel could keep its original morphology and elasticity after storing at −20 °C for 10 h. This was because the colligative property of LiCl (decreasing the vapor pressure and then the freezing point) and the strong H-bonds formed between glycerol and water molecules. The original hydrogel showed a stretchability of up to 10 891% and a toughness of up to 11.32 MJ $m^{-3}$. The cut hydrogel could self-repair within 3 days, exhibiting a SHE of 94.7% in fracture strain. Besides, Fan et al. presented an SHH with anti-freezing properties by introducing Ag/TA@CNCs and L-proline into a GG/PAA hybrid network (Figure 14b).[279] Ag/TA@CNCs served as the key media, which could improve the self-healing ability by forming reversible $Fe^{3+}$ coordination and H-bonds with other functional groups. L-Proline could induce hydration effects by producing H-bonding and electrostatic interactions with water, which endowed the hydrogel with a SHE of 80.8% when stored at −15 °C for 6 h. Moreover, zwitterionic nanochannels composed of zwitterionic

liquid and methacrylate lysine[276] and zwitterionic poly(ionic liquid)[280] were also employed to synthesize various self-healing polymers to be used at subzero temperatures.

Apart from the organic solvent and zwitterion materials, inorganic salts were also employed to extend the temperature tolerance of SHHs. Wang et al. developed a versatile LiCl-incorporated hydrogel with stable and fast self-healing properties at an ultralow temperature (−80 °C) (Figure 14c).[266] The self-healing capacity originated from the H-bonding and electrostatic interactions between hydroxyl-rich PVA and amino-rich PEI in the ternary hydrogel system. The strong hydration of $Li^+$ could inhibit the directional arrangement of H-bonds at cold conditions, enabling the continuous activation of dynamic interaction reconstruction and polymer chain diffusion to promote self-healing. The cracked interface of the resultant hydrogel could entirely disappear at RT within 10 min. The self-healing ability could well maintain under decreasing temperature, exhibiting a SHE of 71.57% after healing for 30 min at −80 °C. Similarly, Zhang et al. integrated $ZnCl_2$/$CaCl_2$ into cellulose hydrogel networks to improve their anti-freezing ability.[281] They demonstrated a moderate anti-freezing property at a low temperature of −70 °C and a fast healing capacity at 60 °C for less than 30 s.

#### 2.3.2. Underwater Self-Healing Hydrogels

To achieve SHHs for underwater applications, one possible mechanism is to weaken the influence of water molecules on the dynamic cross-linking behavior, such as H-bonding, dissolution of ions, coordination with metal irons, and combined dynamic covalent bonds.[282] In recent years, Chen et al. presented a self-healing DN agarose/PVA hydrogel for both air and underwater applications based on H-bonding and borate ester bonds (**Figure 15a**).[283] The prepared hydrogels with different concentrations of agarose consistently exhibited fast and high self-healing capabilities (almost 100% recovery in their strength and elongation within 10 s) at RT in the air. The healed hydrogel with 1.0 wt% agarose could recover 70% of the original tensile stress after 60 s in the underwater environment. The underlying reason was that boron ions could freely and quickly travel through the water to form borate ester bonds with the abundant —OH groups in PVA chains. Based on the same mechanism, an ultrafast self-healing starch/PVA/borax hydrogel was fabricated with reusable and conductive properties for underwater application.[284] Its mechanical and electrical properties could recover within 10 s and 90 ms in air, respectively. In the underwater environment, the SHE in terms of tensile stress reached up to 93.5% after 120 s healing, implying the ultrafast self-healing capacity underwater (Figure 15b). Besides, the HPMC/SiW-PDMAEMA hydrogel[285] and PAA-$Al^{3+}$-CHI-TA hydrogel[286] also exhibited superior self-healing ability underwater.

Another effective approach to achieving SHHs for underwater applications is to facilitate dynamic interactions or bonds rebuilding by restraining the aggregation or removing water molecules on the fractured interfaces. Fu and co-workers devised a tough underwater SHH based on acrylonitrile (AN), AAm, and MMA by exploiting the synergism of multiple H-bonds and strong AN–AN dipole–dipole interaction (Figure 15c).[287] The cut pieces of the resultant hydrogel could be entirely merged underwater within 60 min with no breakage traces. Its tensile strength and stretchability in an underwater environment approached those of the original hydrogel, showing a high underwater SHE of 98%. The underlying mechanism relied on the high dipole moment and strong electrostatic property of the cyan groups, which could effectively prevent water molecules from intervening in the reformation of the aforementioned multiple interactions. In addition, the strong ion–dipole or dipole–dipole interaction has also been widely employed for developing self-healing elastomers[288] and ionogels[289] in underwater environments. The main performances of the state-of-the-art SHHs in harsh environments are summarized in **Table 3**. In addition to low temperatures and underwater environments, research on SHHs has also been extensively concerned with other harsh or corrosive environments, such as strong acids and alkalis and high concentrations of salt solutions.[290,291]

## 3. Applications of Self-Healing Hydrogels in Soft Bioelectronics

### 3.1. Self-Healing Hydrogel Wearable Sensors

One primary application of SHHs is to develop self-healing wearable sensors, which can conformably integrate with human skin to implement real-time and continuous detection of vital physiological signals. The SHHs, combining self-healing ability with their skin-mimic mechanical and chemical properties, can endow wearable sensors with appealing comprehensive performances, such as excellent biocompatibility, superior conformability, remarkable reliability, and a long-time life span, encouraging the development of next-generation wearable sensors. Therefore, increasing research interests have focused on SHH-based wearable sensors recently. Various self-healing wearable sensors have been constructed by taking advantage of the piezoresistive property, conductivity, elasticity, and tunable mechanical and chemical properties of SHHs. Their functions have spanned from physical sensings, such as strain, pressure, temperature, etc., to biochemical signal detection, such as humidity, gas, sweat, glucose, etc.

#### 3.1.1. Self-Healing Hydrogel Strain and Pressure Sensors

SHH-based strain and pressure sensors were intensively investigated because they can monitor a diversity of physiological signals (such as heart rate, blood pressure, pulse wave velocity, ECG, respiration rate, etc.) through monitoring human life activities (e.g., arterial pulsation, vocal cord vibration, joint motion, breathing, etc.) induced strain or pressure variations.[23,294–297] Their sensing principles can be mainly divided into two categories: piezoresistive and capacitive.

*Piezoresistive Strain and Pressure Sensors*: For SHH-based strain and pressure sensors based on resistance variations, the key challenge is how to impart hydrogels with both excellent self-healing ability and piezoresistivity. For this, carbon-based materials, MXene, metals, conductive polymers, and ionic materials have been widely utilized as building blocks of piezoresistive

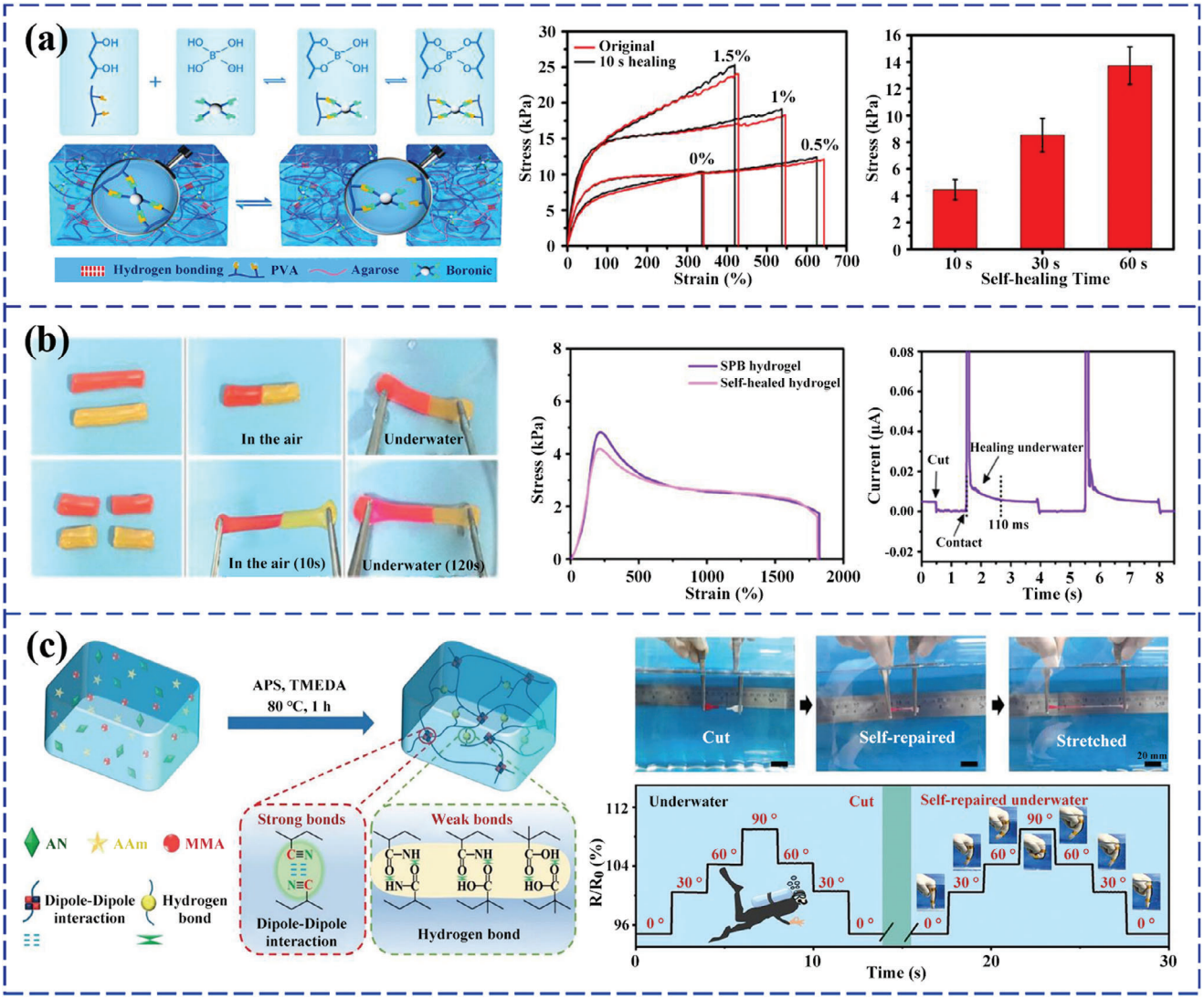


**Figure 15.** SHHs in wet or underwater environments. a) Schematic of the internal interactions of underwater self-healing agarose/PVA DN hydrogels and their mechanical self-healing properties. Reproduced with permission.[283] Copyright 2018, American Chemical Society. b) Photographs of the healed starch/PVA/borax hydrogel in the air and underwater, the mechanical and electrical self-healing properties in underwater conditions. Reproduced with permission.[284] Copyright 2020, American Chemical Society. c) Schematic of the preparation process of underwater self-healing supramolecular hydrogel constructed by dipole–dipole interaction and the underwater self-healing properties. Reproduced with permission.[287] Copyright 2022, John Wiley & Sons.

SHHs. For instance, Liu et al. fabricated an ultrasensitive self-healing strain sensor based on self-healing PVA/PVP/CNC/$Fe^{3+}$ hydrogels (**Figure 16a**).[298] The "hard" $Fe^{3+}$ cross-linked CNC networks with the reversible CNCs-$Fe^{3+}$ coordination interactions as the self-healing domain were introduced to the "soft" polymer networks composed of PVA and PVP, forming synergistic "soft and hard" hierarchical and porous network structures, and enabling the resultant hydrogel with a mechanical strength of 2.1 MPa, a high stretchability of 830%, a fast self-healing capability within 5 min. The self-healing strain sensor was constructed by wrapping two copper electrodes on a SHH strip. It could effectively monitor finger joint movements, breathing, and blood pulses in different motion states, exhibiting a strain sensitivity of 0.478 in a strain of 0–200% and a reliable resistance variation within 200 tensile cycles under 100% strain. Cai and co-workers developed a piezoresistive strain sensor with ultra stretchability by assembling a self-healing conductive PVA/Borax/SWCNT hydrogel between two VHB elastomer substrates.[5] The SWCNT wrapped in the 3D hydrogel network built the electronically conductive channel and meanwhile enhanced the stretchability (up to 1000%) and elastic response. During 5 cutting-healing processes, the resistance remained unchanged, and a high SHE of up to 98% was achieved in ≈3.2 s. The self-healing strain sensor could effectively monitor diverse motions of human bodies, showing a gauge factor (GF) of 1.51 at 1000% strain and a durability of 1000 cycles under 700% strain. Li et al. proposed a degradable self-healing strain sensor based on a conductive MXene nanocomposite

**Table 3.** A summary of self-healing mechanisms, hydrogel materials, mechanical and healing performances of SHHs in harsh environments.

| Self-healing mechanism | Hydrogel materials | Stretchability | Maximum stress/MPa | Healing environments | Self-healing properties | Self-healing efficiency | Refs. |
|---|---|---|---|---|---|---|---|
| H-bond<br>Metal coordination | GG/PAA/Ag/TA@CNCs/L-proline | 550% | 0.69 | −15 °C | tensile strain | 80.8%, 6 h | [279] |
| H-bond | PVA/PEI/LiCl | >7000% | ≈0.03 | −80 °C | tensile strain | 71.75%, 30 min | [266] |
| H-bond | PAM/Clay/Glycerol | 3360% | 0.25 | −30 °C | conductivity | > 90%, 0.8 s | [273] |
| H-bond<br>Metal coordination | P(AA-*co*-MA)/Glycerol/BNNS/$Fe^{3+}$ | 400% | ≈0.05 | −15 °C | tensile stress | ≈70%, 24 h | [275] |
| Borate ester bond | Agarose/PVA | 625% | ≈0.012 | Underwater | tensile stress | 70%, 1 min | [283] |
| H-bond<br>Borate ester bond | Starch/PVA/Borax | ≈1500% | ≈0.005 | Underwater | tensile stress;<br>conductivity | 93.5%, 2 min;<br>≈100%, 0.11 s | [284] |
| H-bond<br>Dipole interaction | AN/PAM/PMMA | ≈600% | ≈1.5 | Underwater | tensile strain | 98%, 1 h | [287] |
| H-bond<br>Metal coordination<br>Ionic interaction | PAA/CS/DCMC/$Al^{3+}$ | 900% | 0.14 | Underwater | tensile stress | 90%, 10 min | [292] |
| H-bond<br>Borate ester bond | PEO/PVA/Borax | 566% | 0.009 | Underwater | tensile strain | 86%, 2 min | [293] |

hydrogel by incorporating the MXene nanosheet into PAA and amorphous calcium carbonate (ACC) hybrid networks.[299] The fabricated sensor displayed a quick resistance recovery ability of less than 0.2 s and a stretchability of 450%, which enabled it to detect various body movements with a high GF of 10.79. Additionally, self-healing strain or pressure sensors composed of other stretchable, self-healable, and conductive hydrogels were also developed, such as PVA/MXene/PEDOT: PSS/PDA,[300] TOCNF/PAA/Graphene,[301] and DA/Talc/PAM.[302]

To increase the sensitivity at large strains and device transparency, many researchers were devoted to constructing ionic conductive SHH strain and pressure sensors by introducing ionic liquids, electrolytes, etc.[303] For instance, Yao and co-workers constructed a super-stretchable and adhesive self-healing strain sensor by constructing a PAM/phenylboronic acid-ionic liquid (PBA-IL)/CNF-based ionic conductive hydrogel.[304] The introduction of the PBA-IL and CNFs endowed the as-prepared hydrogel with semi-IPN polymer network structures, multiple dynamic interactions (involving borate ester bonds, H-bonds, and ionic interaction), and enhanced ion mobility and self-adhesive ability. These contributed to a good tradeoff among multifunctional properties, such as a super stretchability of 1810%, a high mechanical strength of 349 kPa, and a SHE of 92%. The developed sensor was used to monitor diverse human physiological movements, including wrist, finger, elbow bending, and swallowing, showing a high GF of 8.36 in a broad strain range of 1000%. Li et al. devised an ultra-durable and self-healable ionic strain and pressure sensor by blending ILs into PU networks.[305] The resultant sensor exhibited a high strain sensitivity of 1.23 within 50% strain range and a pressure sensitivity of 0.37 $kPa^{-1}$ under pressure less than 20 kPa, as well as a durability of 10 000 stretching cycles. Furthermore, it could completely heal at 65 °C and maintain its original performance after storing for 200 days in the air.

Furthermore, some researchers have developed ionic and electronic conductive self-healing piezoresistive strain and pressure sensors by introducing conductive polymers (such as PANI, PPy, PEDOT, and polythiophene) into SHHs. For instance, Su et al. presented wearable strain/pressure sensors by constructing a self-healing conductive hydrophobic association PAA (HA-PAA)/PANI hydrogel.[306] The conductive nature of PANI polymers and their dynamic interfacial interactions with self-healable HAPAAs balanced the tradeoff among the mechanical, conductive, and self-healing performances. The developed sensors could implement various strain or pressure detections, exhibiting a high GF of 17.9, a low limit of detection (LOD) of 0.05%, a fast response time of 80 ms, and nearly identical electrical signals between their healed and original samples. Yang et al. developed stretchable and adhesive SHH strain and pressure sensors by introducing polyfunctional trypan blue (TB) and PPy into PAA networks.[307] The combination of TB and PPy components maintained the structure strength and enhanced the conductivity by facilitating the conductive pathway, resulting in a conductivity of 15 S $m^{-1}$ and a stretchability of 750%. The developed sensors could firmly adhere to various surfaces and reliably detect repetitive large strains and subtle pressure. Additionally, a CD topological nanoparticles-cross-linked SHH was also reported.[308]

In addition, SHH piezoresistive strain/pressure sensors combined with other diverse functions were also developed. Inspired by the adhesion mechanisms in mussel and zwitterionic, Pei and co-workers reported a zwitterionic SHH-based strain sensor with a tissue-adhesive capacity (an adhesion strength of 19.4 kPa), which could reversibly and robustly adhere to human organs to monitor vital organ motions for remote diagnostics.[98] Xu et al. reported a self-healable ionogel-based strain sensor possessing multifunctions, such as high transparency, stretchability, recyclability, resistance to solvent and temperature, and underwater self-healing capacity and adhesiveness.[309] Besides, SHH strain sensors with the anti-freezing ability and electromagnetic interference shielding performance were also invented.[310,95]

*Capacitive Strain and Pressure Sensors*: Self-healing capacitive strain and pressure sensors are another appealing application of SHHs because of their simple transduction mechanism and relatively high-temperature stability. In these sensors,

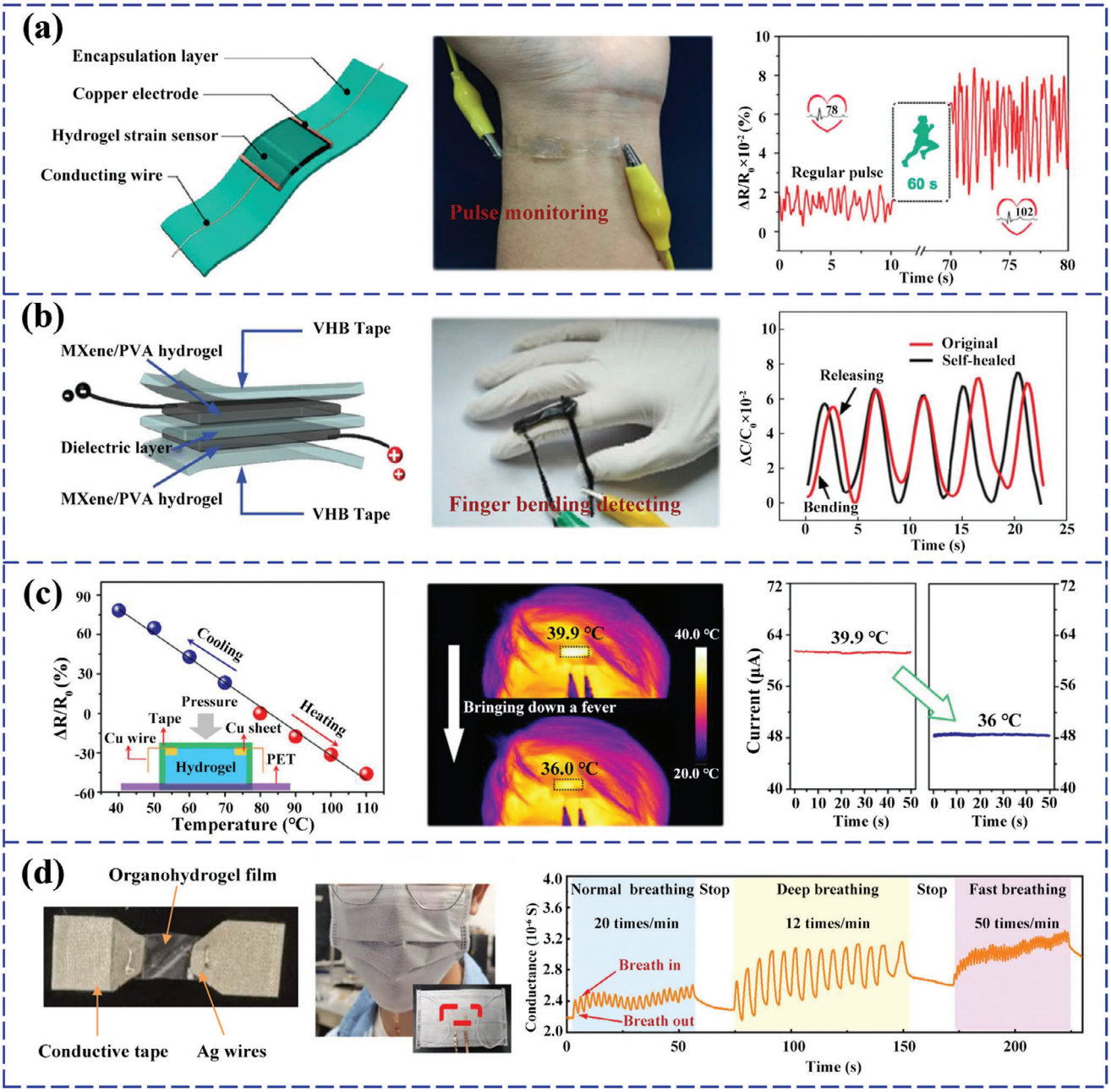


**Figure 16.** SHH-based physical sensors. a) Structure schematic of SHH strain/pressure sensor based on resistance variations, the prepared sensor sample, and pulse monitoring. Reproduced with permission.[298] Copyright 2017, American Chemical Society. b) Structure schematic of SHH strain/pressure sensor based on capacitive variations, the prepared sensor sample, and finger bending monitoring using the original and healed sensors. Reproduced with permission.[311] Copyright 2019, John Wiley & Sons. c) Structure schematic of the SHH-based temperature sensor and experimental results of temperature testing, its application as a human forehead "fever indicator," and stability testing. Reproduced with permission.[319] Copyright 2020, American Chemical Society. d) Structure schematic of the SHH-based humidity sensor and its application as a wireless mask-style breath monitor for real-time testing. Reproduced with permission.[323] Copyright 2022, John Wiley & Sons.

SHHs are employed as conductive electrodes or dielectric elastomers. The key challenge is to balance the self-healing capacity, conductivity, and mechanical elasticity. For this, Zhang et al. constructed a self-healable capacitive strain sensor by adopting MXene/PVA-based SHHs as the electrodes and VHB as the dielectric layer (Figure 16b).[311] The hydrogel electrode could recover its original conductivity within 0.15 s, exhibiting an electrical healing efficiency of 97.4% even after five cutting–healing cycles. The healed sensor could reach up to 97.5% of its original capacitance under a strain of 80%. Besides, the device also exhibited high-performance stability, i.e., with only a 5.8% decrease in its capacitance after 10 000 cycle tests. Similarly, a

self-healing capacitive pressure/strain sensor was developed by utilizing the VHB tape as the dielectric layer and self-healable calcium carbonate/PAA/SA hydrogel as the electrodes.[312] Zhang and co-workers used an adhesive DA-triggered gelation (DTG) hydrogel as the electrodes and developed self-healing and adhesive capacitive pressure and strain sensors.[313] The DA served as both the polymerization initiator and dynamic mediator to cross-link hydrogel networks, resulting in remarkable adhesion, excellent elasticity, and self-healing capacity. The flexible capacitor could detect strains from 5% to 200% with a GF of 0.71 and pressures from 0.16 kPa to 4.0 kPa with a pressure sensitivity of 0.096 $kPa^{-1}$. The healed sensors could restore their original capacitance even though the DTG hydrogel electrode suffered several severe damages. Similar examples can be seen in self-healing PAA/SA/CNTs/$Ca^{2+}$ hydrogel[314] and PVA/CNF hydrogels[315] based strain and pressure sensors.

Apart from being used as conductive electrodes, SHHs can also function as the dielectric layers of capacitive strain/pressure sensors by taking advantage of their soft and elastic properties. For instance, Rao et al. devised a high-sensitive capacitive strain sensor for physiological motion monitoring by exploiting a self-healing polydiacetylene/PAA/$Cr^{3+}$ hydrogel as the intermediate layer and two silver layers as the outer electrodes.[316] The dielectric hydrogel maintained a high mechanical elasticity and sensing sensitivity because of the introduction of PDA and $Cr(H_2O)_6^{3+}$ complexes. The prepared sensors exhibited a high GF within a broad range, i.e., a GF of 4.8 and 33.4 in strains of 100% and 500%, respectively. Zhang and co-workers constructed a capacitive pressure sensor with a liquid metal-created sponge-inspired porous SHH as the dielectric layer.[317] The porous structure could effectively enhance the compressive ability and response of the dielectric hydrogel, contributing to a sensitivity of 0.85 $kPa^{-1}$. Further, to increase the sensitivity, an iontronic pressure sensor based on the electrical double layer (EDL) principle was constructed by using a self-healing ionic hydrogel as the iontronic layer and two electronically conductive fabrics as the electrodes.[277] To overcome the conflict between mechanical elasticity and self-healing capacity, supramolecular zwitterionic reorganizable networks driven by entropy were introduced to the H-bond cross-linked PAA networks. Consequently, the hydrogel iontronic layer exhibited an excellent stretchability of 1600%, a SHE of almost 100%, an excellent elasticity of 97.9%, and a high transparency of 99.7%. The developed pressure sensor exhibited an ultrahigh pressure sensitivity of 200 $MPa^{-1}$ within 0.5 kPa, and 3.5 $MPa^{-1}$ in a higher range of 3–7 kPa, and could sensitively monitor various finger movements.

The aforementioned self-healing capacitive strain or pressure sensors generally could not realize device-level self-healing because some components of the multilayer structures were made of materials without self-healing ability. To tackle this challenge, Jiang and co-workers constructed omni-healable capacitive strain sensors by assembling two self-healing silver nanowires (AgNWs)/rGO aerogel-PAM (ARAP) electrodes with a self-healable oleophilic gel dielectric.[318] The self-healing ARAP hydrogel was synthesized based on a strategy combining hard and soft dynamic networks strategy, i.e., associating conductive AgNWs with wrinkled rGO nanosheets and Ag-S coordination-aided PAM hydrogel networks. This resulted in excellent versatile performances, such as a stretchability of 3250%, a resistance change of 223% at 2000% strain, and fast optical and electrical-triggered self-healing in 4 min. The self-healing oleophilic gel dielectric could elongate to 1085% with a SHE of 90% within 1 min. The resultant strain sensor showed a device-level stretchability of 1080% and almost no decrease in capacitive response within 400% to 1000% strain over 1000 cyclic stretchings. Notably, owing to the reversible metal-thiolate (Ag, Au-SR) bonds in both the electrodes and dielectrics, the strain sensor exhibited omni-healability. The healed strain sensor could produce nearly consistent signals with the pristine one in monitoring human movements.

#### 3.1.2. Self-Healing Hydrogel Temperature Sensors

SHH-based temperature sensors also gained considerable interest recently owing to their thermal-response nature. Most SHH-based temperature sensors can be developed by integrating ionic or electronic conductive hydrogels, using their thermally activated mobility-induced resistance changes to realize temperature measurement. For instance, Ge et al. constructed a self-healing dual-sensory sensor for strain and temperature detection using a stretchable and self-healable PAA-PANI binary network hydrogel (Figure 16c).[319] The PANI nanofibers endowed the hydrogel with excellent mechanical elasticity and thermosensation. The resultant temperature sensor demonstrated a SHE of 90.8%, a temperature coefficient of resistance (TCR) of −0.016 °C, and a temperature resolution of 2.7 °C. SHH-based temperature sensors utilizing both conductive fillers and polymers have also been extensively studied. Zhu et al. developed a self-adhesive PVA/PDA-CNT SHH-based temperature sensor for real-time temperature measurement of the human wrist.[320] The device exhibited a rapid thermosensitive response with increasing ionic mobility, which could match the skin temperature in 10 s. The temperature sensor was further integrated into an alarm circuit for high-temperature signal warnings. Taking a similar strategy, many other SHH-based temperature sensors based on various thermo-responsive hydrogels have also been reported.[192,223,321,322] However, the response and other performances of hydrogel temperature sensors after healing were rarely studied.

#### 3.1.3. Self-Healing Hydrogel Humidity Sensors

Humidity reflects the environment's comfort level and plays a significant role in typical biosignal monitoring, such as respiratory rate and skin wetness. Recently, Ding et al. devised a breathable SHH humidity sensor for wireless respiration monitoring using a PVA-CNF organohydrogel (Figure 16d).[323] The sensing mechanism was based on the change of conductance induced by its ionic mobility, dielectric constant, and interfacial charge transport variations after water adsorption. Owing to the abundant H-bonds, the humidity sensor could self-heal the incisions without obvious cracks under 80 °C within 1 min. The healed device responded consistently with the original one towards different humidities, indicating excellent repairing performance. By integrating with a printed circuit board, the monitoring system demonstrated a reliable recognition of different degrees of breathing. Wu et al. devised an ultra-stretchable, self-healable, and lucent humidity sensor based on ionic carrageenan/PAM DN hydrogels modified by glycerol.[324] Incorporating glycerol effectively

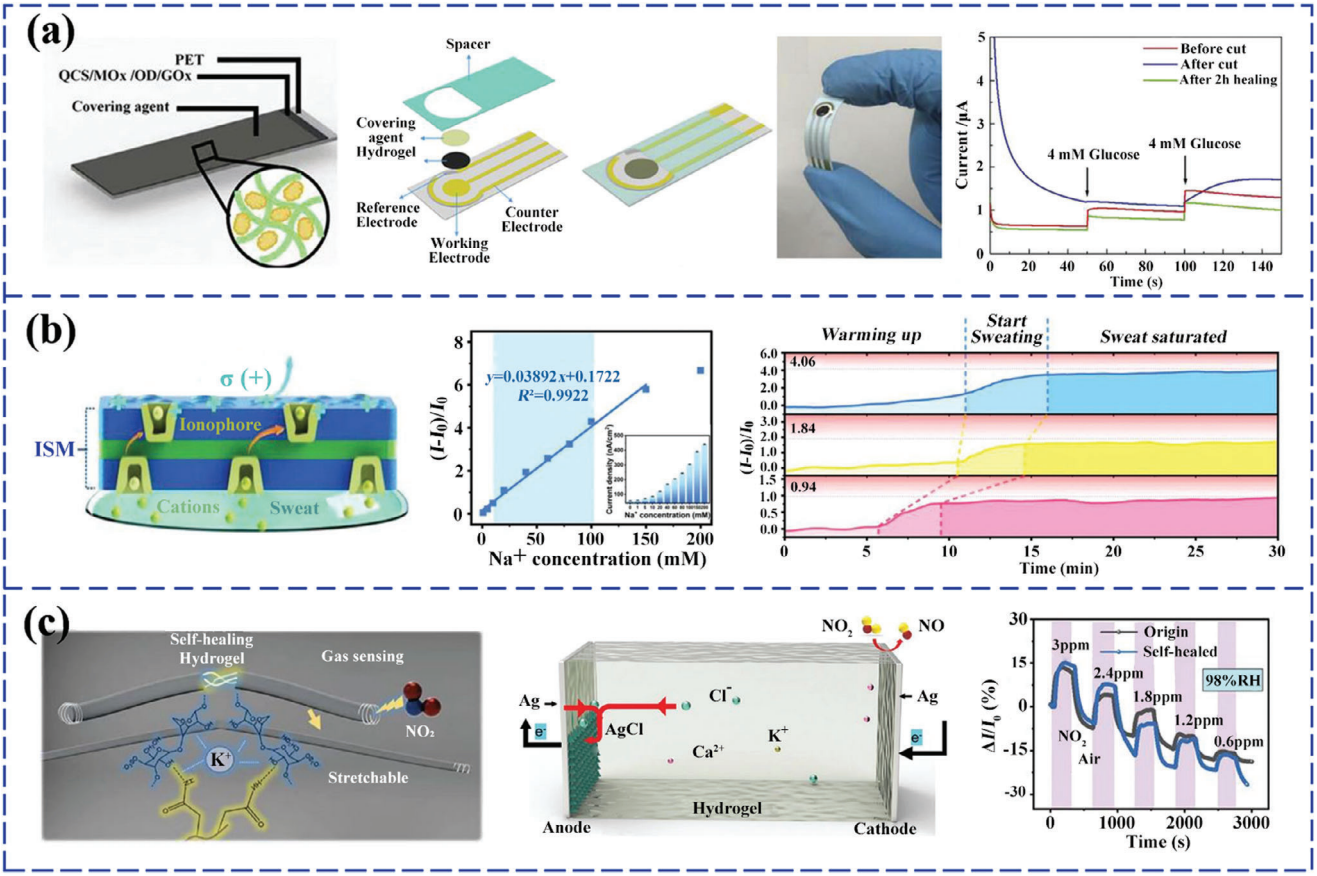


**Figure 17.** SHH-based biochemical sensors. a) Structure schematic of the SHH-based glucose sensor, the prepared sensor sample, and glucose testing curves. Reproduced with permission.[327] Copyright 2020, Elsevier. b) Principle schematic of self-healing self-powered CPPH sweat sensor, the relative current variation with to $Na^+$ concentration, real-time detection of $Na^+$, $K^+$, $Ca^{2+}$. Reproduced with permission.[328] Copyright 2022, John Wiley & Sons. c) Structure schematic of SHH-based $NO_2$ gas sensor, sensing mechanism for $NO_2$ under an external electric field and dynamic responses to 3–0.6 ppm $NO_2$ at original and healed states. Reproduced with permission.[329] Copyright 2021, John Wiley & Sons.

enhanced the humidity-sensing capability by facilitating the generation of numerous H-bonds with water molecules. The developed sensor could sensitively and repeatedly detect human respiration, showing a response time of 0.27 s and a RH detection range of 4–90%.

### *3.1.4. Self-Healing Hydrogel Biochemical Sensors*

Wearable biochemical sensors can provide a relatively deep and broad assessment of health status (e.g., dehydration, physical fatigue, mental stress, and diseases) by monitoring biomarkers in human biofluids, such as saliva, sweat, tears, and interstitial fluids.[325,326] Recently, SHH biochemical sensors have been particularly attractive because they integrate multi-desirable functions into one device, such as biocompatibility, mechanical matching with skin, self-healing ability, and biochemical signal sensing performances. The SHH biochemical sensors are primarily developed by integrating electrochemical or optical biosensing strategies into functional hydrogel systems. Liang and co-workers fabricated an SHH glucose sensor by constructing the self-healable composite hydrogel on a PET electrode (**Figure 17a**).[327] $CeO_2/MnO_2$ hollow nanospheres were covalently cross-linked in the QCS/oxidized dextran hydrogel network, facilitating the immobilization of glucose oxidase and increasing specific surface area. The prepared sensor demonstrated a broad linear detection range of 1–111 mM with a response time of less than 3 s and a sensitivity of 176 μA $mM^{-1}$ $cm^{-2}$. After healing for 2 h without any stimuli, the repaired sensor could produce a nearly original electrochemical output toward 4 mM glucose. Besides, Qin et al. invented a self-powered SHH-based sweat sensor by assembling a hydrophobic ion-selective membrane with self-healing TOCNF/PANI-PVA hydrogel electrodes encapsulated with PDMS (Figure 17b).[328] The TOCNF nanocomposites endowed the sweat sensor with an excellent stretchability of 1530%, an electrical conductivity of 0.6 S $m^{-1}$, and mechanical and electrical SHEs over 96% within 10 s in ambient conditions. The as-prepared sweat sensor could realize real-time sensing of $Na^+$, $K^+$, and $Ca^{2+}$ in human perspiration via triboelectric effect with a high sensitivity of 0.082 $mmol^{-1}$ for $K^+$ and transmit the results to a user interface wirelessly.

Besides biomarkers detection in human biofluids, some researchers pioneered SHH-based gas sensors for environmental or breathing gaseous molecule monitoring. For example, a

**Table 4.** Comprehensive performances comparison of various SHH wearable sensors.

| Sensing mechanism | Hydrogel material | Monitoring signal | Responsivity/GF | Self-healing property | Self-healing efficiency | Refs. |
|---|---|---|---|---|---|---|
| Piezoresistance | PVA/PVP/CNCs/$Fe^{3+}$ | Strain | 0.478 (0–200%) | Electrical | ≈100%, 5 min | [298] |
| Piezoresistance | PVA/SWCNT/Borax | Strain | 1.51 (0–1000%) | Electrical | 98 ± 0.8%, 3.2 s | [5] |
| Piezoresistance | PAA/MXene/ACC | Strain | 1.51 (0.3–30%); 10.79 (30–450%) | Electrical | ≈100%, 0.2 s | [299] |
| Piezoresistance | PAM/PBA-IL/CNF | Strain | 3.41 (0–300%); 8.36 (300–1000%) | Mechanical | 91.98 ± 2%, 2.5 h | [304] |
| Capacitance change | PVA/MXene/Borax | Strain | ≈0.4 (0–200%) | Functional | 97.5%, 0.15 s | [311] |
| Capacitance change | PSBMA/DA/PEGDA | Strain; pressure | 0.71 (5–200%); 0.096 $kPa^{-1}$ (0.16–4 kPa) | Functional | ≈100% | [313] |
| Resistance change | PAA/PANI/$Fe^{3+}$ | Temperature; strain | TCR = -0.016 $°C^{-1}$ (40–110 °C); 19.28 (169.04–268.9%) | Mechanical | 90.8%, 6 h | [319] |
| Resistance change | TA/Graphene/PAH/PAA/PNIPAM | Temperature; strain | TCR ≈ 0.012 $°C^{-1}$ (20–80 °C); GF = 1.3 (0–300%) | Mechanical | 87%, 6 h | [192] |
| Conductance change | PVA/CNF/Glycerol | Humidity | 250 (11–98% RH) | Mechanical | 60.4%, 1 min | [323] |
| Amperometry and cyclic voltammetry | QCS/MOx/OD/GOx | Glucose | Sensitivity: 176 μA $mM^{-1}$ $cm^{-2}$ | Functional | > 75%, 2 h | [327] |
| Resistance change under gas exposure | PAM/Carr/$CaCl_2$ | $NO_2$ | Sensitivity: 1.199 $ppm^{-1}$ | Electrical | ≈100%, 4.5 s | [329] |
| Current change under gas exposure | PAM/CS | $O_2$ | Sensitivity: 0.002 $ppm^{-1}$ | Functional | ≈100% | [330] |

SHH-based $NO_2$ gas sensor was created using two Ag wire electrodes to enwound a multifunctional $CaCl_2$-infiltrated ion-conductive hydrogel (Figure 17c).[329] By making use of the redox reactions generated at the hydrogel-electrode interfaces, the sensor exhibited a rapid electrical response to $NO_2$ gas, demonstrating a sensitivity of ≈120% $ppm^{-1}$ and a low LOD of 86 part per trillion (ppt). Furthermore, the original and healed sensors produced almost consistent responses to 3–0.6 ppm $NO_2$ in a humid environment (98% RH) due to the reconstruction of ion transport channels at the healing interface with the reformation of H-bonds. Similarly, a self-healable, stretchable, and self-adhesive organohydrogel-based $O_2$ sensor was constructed based on a two-electrode chemiresistor structure by using PAM/CS DN organohydrogel as a transduction material.[330] The redox reaction generated at the hydrogel-electrode interface and the induced current change responded to the $O_2$ concentration variation. The sensor exhibited a concentration detection range of 0–100%, a LOD of 5.7 ppm, a sensitivity of 0.2% $ppm^{-1}$, as well as good linearity and excellent repeatability. Notably, the prepared hydrogel gas sensor could produce almost the same response before and after healing, proving a robust restoring capacity. Various other self-healing gas sensors, such as diol oligomer functionalized self-healing graphene hydrogel-based $NH_3$ sensors, have also been constructed.[331] **Table 4** systematically compares the performances of various SHH-based wearable sensors.

### 3.2. Self-Healing Hydrogel Supercapacitors

Soft supercapacitors are an indispensable electronic component for wearable electronics, sensors, and bioactuators, which can satisfy the demanded power and enable the true wearability of flexible electronic systems.[332–334] Typically, one supercapacitor comprises two outer electrodes and one intermediate electrolyte. The used materials for the electrode and electrolyte essentially determine the device's flexibility and electrochemical performance. There has been tremendous interest in SHH-based supercapacitors in recent years because of their capacity to combine multiple appealing functions into one device, including biocompatibility, stretchability, flexibility, self-healing capacity, and widely tunable physicochemical properties. These merits originate from the versatile nature of hydrogels, such as excellent biocompatibility, superior stretchability, tunable physical and chemical properties. Remarkably, unlike conventional solid or liquid materials, hydrogels possess not only liquid-like ionic conductivity but also solid-like dimensional stability, which is desirable for the development of flexible supercapacitors.[335–337] Furthermore, the self-healing capacity could further expand the reusability of soft supercapacitors after damage and thus lifetime. Therefore, numerous efforts have been put into the investigation of flexible supercapacitors, and their advances are discussed in the following sections.

In most developed self-healing supercapacitors, SHHs are employed as the electrolyte material. The research focused on improving their overall properties, including their ionic conductivity, mechanical stretchability, power density, self-healing ability, etc. Typically, hydrogel electrolytes consist of host polymer matrices, copolymers, inorganic ionogen salts (such as acids, alkalis, salts, or ionic liquids), plasticizers, and in some cases, inorganic fillers.[338] Liu et al. designed a stretchable and self-healable supercapacitor composed of a SHH electrolyte sandwiched between two MWCNTs electrodes.[339] The hydrogel

electrolyte was formed by incorporating LiCl into PEI, PVA, and 4-formylphenylboronic acid (Bn) based hydrogels. The resultant hydrogel exhibited a high stretchability of 1223%, a SHE of 94.3% in 120 s, and a conductivity of 2.149 S $m^{-1}$. The supercapacitor demonstrated an operating potential range of 1.4 V, a specific capacitance of 16.7 mF $cm^{-2}$, an energy density of 3.13 μWh $cm^{-2}$, and a high stability of 10 000 charging/discharging cycles with 86% capacitance retention. Kim et al. demonstrated a self-healable supercapacitor with degradable properties (**Figure 18a**).[152] The hydrogel electrolyte was synthesized by cross-linking Azo-PAM and water-soluble α-CD-grafted-epichlorohydrin (α-CDP) with LiCl incorporated. The healed hydrogel electrolyte exhibited near conductivity with its original one (43.25 mS $cm^{-1}$) and 98% of its original electrochemical property during 10 cutting-healing cycles. Owing to the superior performance of the hydrogel electrolyte, the supercapacitor could maintain over 90% of its original capacitance after 5 healing cycles,and be stretched to 50% for more than 500 times without significant performance reduction. Besides, the developed supercapacitor could degrade and dissolve in water under UV light irradiation. Similarly, self-healing and adhesive supercapacitors based on ionic liquid hydrogel electrolytes were also developed.[340]

To decrease the contact resistance at electrolyte-electrode interfaces and address issues such as the delamination, interlayer slippage, and crease formation of the multilayer configuration under twisting, bending, and stretching, a large number of researchers were devoted to constructing fully integrated or all-in-one SHH-based supercapacitors. For example, a fully self-healing and shape-editable wearable supercapacitor by sandwiching a SHH electrolyte between two PEDOT: PSS-rGO electrodes was designed by Zhao and co-workers (Figure 18b).[341] The hydrogel electrolyte involved UPy and lauryl groups, contributing to superior self-healing capacity and stretchability (>12 000%). The PEDOT: PSS-rGO nanocomposite electrodes enhanced the device capacitance and self-healing ability after stream treatment (80 °C). Additionally, the polyurethane-polycaprolactone (PU-PCL)-based substrate also afforded self-healing and shape editability. Consequently, the fabricated supercapacitor demonstrated fully self-healing ability, repeatable shape editability, and superior electrochemical performance, i.e., 95% and 95.8% capacitance retention after 5 cutting-healing cycles and after 10 000 charging/discharging cycles, respectively. It also showed negligible capacitance loss during different shape editing, like "U", "spiral", and "ring" shapes. Guo et al. developed a self-healable all-in-one supercapacitor by in situ polymerizing and depositing SWCNT-PANI nanocomposites on the surfaces of a PVA-$H_2SO_4$-based SHH electrolyte (Figure 18c).[342] The assembled capacitor avoided delamination of the structure under deformation and exhibited improved capacitance (15.8 mF $cm^{-2}$), good cycling stability, and a restoring capability with 80% capacitance retention after 5 healing cycles. Based on the same strategy, self-healable all-in-one supercapacitors based on PAA/PSBMA/$H_2SO_4$ and PAA/PSBMA/$Fe^{3+}$/$H_2SO_4$ were also developed.[343,344] By introducing chemical bonds between interlayer interfaces, Mo and co-workers fabricated an all-in-one supercapacitor based on SHH electrolyte composed of SF conjugated with β-CD (SF-CD) and PAA conjugated with β-CD (PAA-β-CD) and PPy-supramolecular hydrogel-based electrodes (Figure 18d).[345] Multiple interactions formed between hydrogel layers as well as inside hydrogels, including host-guest interactions, imine bonds, and H-bonds, are introduced. No delamination was discovered during the bending and twisting process of the prepared supercapacitor, exhibiting stable electrochemical performance and excellent self-healing ability (≈95.8% of the original capacitance after cutting and healing for 30 cycles). Similarly, Chen et al. constructed a highly stretchable and omni-healable supercapacitor by assembling a GP/$Na_2SO_4$ hydrogel electrolyte between two GCP@PPy hydrogel electrodes.[261] Owing to the nearly similar components and the same chemical bonds, every layer could be bonded tightly together and assembled into integrity without visible cracks. Other self-healable super-capacitors consisting of multi-stimuli healable $Fe_3O_4$@Au/PAM hydrogel electrolyte[256] and PVA/CPBA/$Ca^{2+}$ hydrogel electrolyte,[346] were also fabricated.

Some other researchers were devoted to exploiting self-healing supercapacitors under harsh conditions, such as for application in wide temperature ranges or underwater circumstances. For instance, Tao et al. proposed a self-healable and anti-freezing supercapacitor by assembling a DA-grafted SA/potassium chloride (SA-g-DA/KCl) hydrogel electrolyte between two activated carbon (AC) electrodes (Figure 18e).[347] Owing to the tolerance of alginate networks to KCl and the regeneration of catechol-borate ester bonds, the hydrogel electrolyte presented excellent ionic conductivity at low temperatures and superior self-healing capability without extra stimuli. As a result, the healed capacitor could reach 95.9% of the original specific capacitance (97 F $g^{-1}$ at 1.0 A $g^{-1}$) within 10 min. It could also retain a solution and charge-transfer resistance approaching its original state even after 10 healing cycles. The capacitor also had a good cold-resistant ability between −10 °C and 0 °C, with 18% decrease in specific capacitance at −10 °C compared with that at 25 °C. Similarly, Wang et al. constructed a low-temperature self-healing and renewable supercapacitor based on a self-healable P(*N*-vinylimidazole-*co*-hydroxypropyl acrylate)/$NaNO_3$ hydrogel electrolyte demonstrating a superior electrochemical self-healing capacity at temperatures varying from 25 to −15 °C.[348] Besides, Peng and co-workers also prepared a wide-temperature tolerant self-healable supercapacitor by introducing ionic liquid ($EMIMBF_4$) into PVA/Agar/$Li_2SO_4$ hydrogel electrolyte.[349] The as-prepared supercapacitor delivered high capacities (28.8 F $g^{-1}$ at 0.3 A $g^{-1}$) at a broad operating temperature ranging from −30 to 80 °C and could recover over 80% of the original electrochemical performances after five cutting–healing cycles. The main performances of typical SHH-based supercapacitors are summarized in **Table 5**. More studies on SHH supercapacitors can be referred to Ref. [335].

### 3.3. Self-Healing Hydrogel Display Devices

Self-healing flexible display devices represent an emerging application of SHHs, which can collect information from wearable sensors and display the retrieved data to users, playing an indispensable role in wearable electronics.[352] The diverse advantages, such as high mechanical compliance, excellent biocompatibility, liquid-like ionic conductivity, high transparency, and tunable

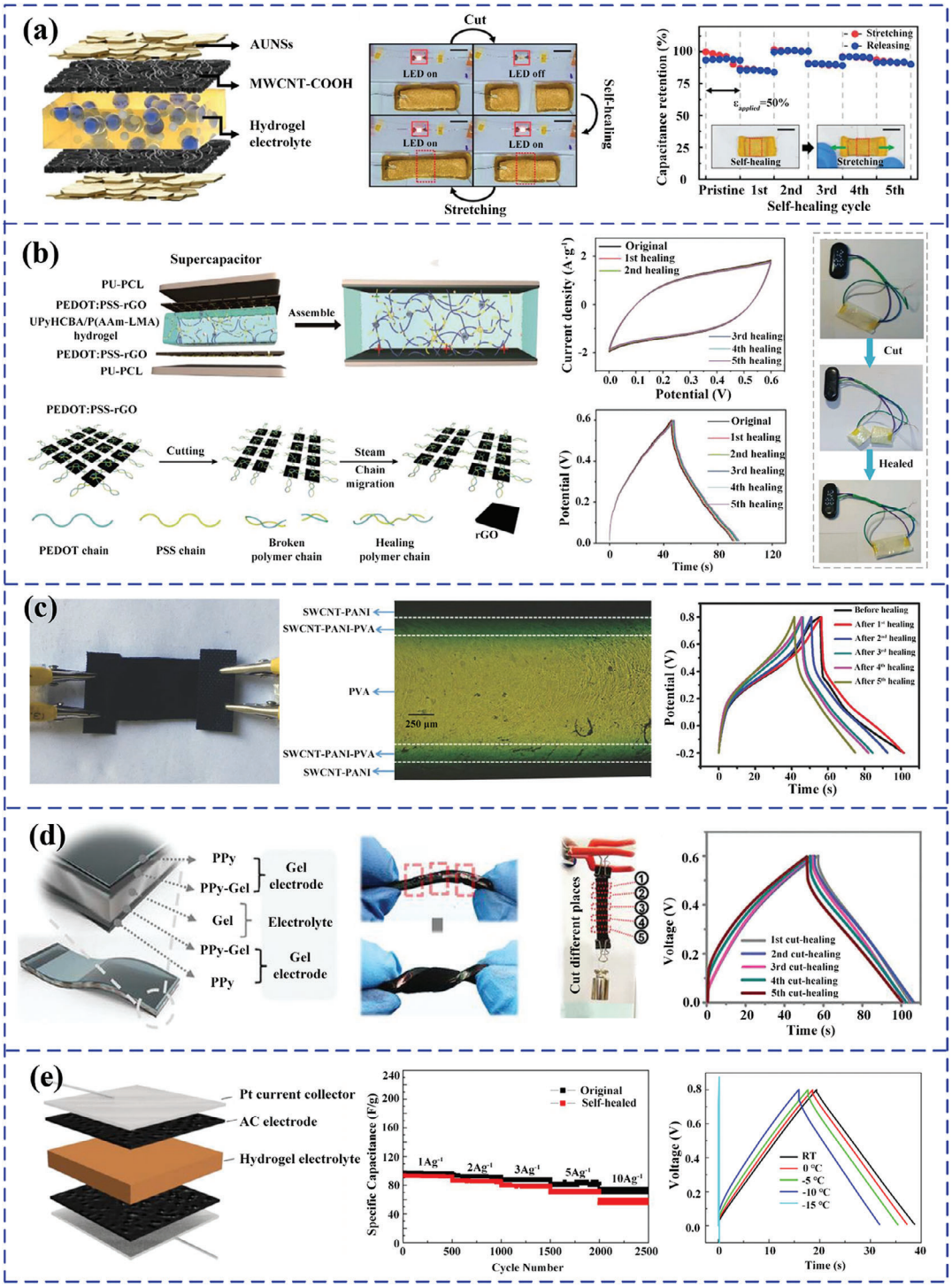


**Figure 18.** SHH-based supercapacitors. a) Structure schematic of self-healing supercapacitor, images of the process of powering the LED when breaking/healing, and the capacitance retention during 5 cutting-healing cycles. Reproduced with permission.[152] Copyright 2021, Elsevier. b) Structure schematic of a fully self-healing and shape-editable supercapacitor and the electrochemical self-healing performances after multiple healing cycles. Reproduced with permission.[341] Copyright 2022, John Wiley & Sons. c) The self-healable all-in-one supercapacitor by in situ polymerizing and depositing methods, the optical microscope of the prepared supercapacitor, and the electrochemical self-healing property after 5 healing cycles. Reproduced with permission.[342] Copyright 2018, John Wiley & Sons. d) Structure schematic of the self-healing non-laminated all-in-one supercapacitor by introducing chemical bonds, photographs of the non-laminated structure under twisting, and the electrochemical self-healing properties of the healed supercapacitor with different cutting places. Reproduced with permission.[345] Copyright 2021, John Wiley & Sons. e) Structure schematic of the self-healable cold-resistant supercapacitor, the electrochemical self-healing performance under multiple healing cycles and different temperatures. Reproduced with permission.[347] Copyright 2017, American Chemical Society.

**Table 5.** A summary on the main performances of typical SHH-based supercapacitors.

| Electrolyte material | Electrode material | Specific capacitance | Capacitance retention [Cycles] | Self-healing efficiency [Cycles] | Refs. |
|---|---|---|---|---|---|
| PEI/PVA/Bn/LiCl | MWCNTs | 11.5 mF $cm^{-2}$ at 0.05 mA $cm^{-2}$ | 86% [10 000] | – | [339] |
| Azo-PAM/α-CDP/LiCl | MWCNTs-COOH | 2.2 mF $cm^{-2}$ at 0.2 mA $cm^{-2}$ | 68% [10 000] | > 90% [5] | [152] |
| UPyHCBA/P(AM-*co*-LMA) | PEDOT:PSS-rGO | 52.2 F $cm^{-2}$ at 10 mV $s^{-1}$ | 95.8% [10 000] | 95% [5] | [341] |
| PVA/$H_2SO_4$ | SWCNTs/PANI | 15.8 mF $cm^{-2}$ at 0.044 mA $cm^{-2}$ | 82% [2396] | 80% [5] | [342] |
| PAA/PSBMA/$Fe^{3+}$/$H_2SO_4$ | CNTs/PANI | 109 mF $cm^{-2}$ at 0.2 mA $cm^{-2}$ | 85% [2000] | – | [343] |
| PAA-β-CD/SF(Lys, Tyr) | PPy/PAA-β-CD/SF | 0.37 F $cm^{-2}$ at 1 mA $cm^{-2}$ | 80.5% [4000] | 95.8% [30] | [345] |
| GNs/PAM | GNs/PAM/CNTs/PPy | 885 mF $cm^{-2}$ at 1 mA $cm^{-2}$ | 93% [10000] | 92% [1] | [261] |
| P(VI-*co*-HPA)/$NaNO_3$ | AC | 90.0 F $g^{-1}$ at 1.0 A $g^{-1}$ | 93.9% [20 000] | – | [348] |
| PVA/PHEA/$H_2SO_4$ | PANI/PVA/PHEA | 98 mF $cm^{-2}$ at 0.2 mA $cm^{-2}$ | 98% [8000] | 96% [4] | [350] |
| $Fe^{3+}$/PAA/$H_2SO_4$ | CWF/PANI | 217.4 F $g^{-1}$ at 1.67 A $g^{-1}$ | 80% [2000] | 86% [7] | [351] |
| PAA/PSBMA/$H_2SO_4$ | PANI | 430 mF $cm^{-2}$ at 0.5 mA $cm^{-2}$ | ≈90% [10 000] | 84.6% [10] | [344] |
| PVA/CPBA/$CaCl_2$ | PANI/PVA | 351 F $g^{-1}$ at 1 A $g^{-1}$ | 85.7% [1000] | 49.8% [1] | [346] |

light absorption, transmission, or reflection nature, make hydrogels an appealing building-block material for flexible display devices, especially for application on biological organisms.[26,353] Meanwhile, with the self-healing ability, the display devices can recover after damage and maintain their function and reusability. In recent years, with increasing efforts invested into this area, a diversity of SHH-based optical displays has been developed, which can be mainly categorized into electrochromic and electroluminescent devices. Detailed accounts of their progress are provided below.

SHH electrochromic devices (ECDs) have been extensively studied due to their simple configuration, high contrast, low driving voltage, and tunable optical properties. Generally, their structures are composed of an electrochromic electrode for light-emitting, a counter electrode for ion storage, and an intermediate electrolyte layer for ionic transportation.[353–355] SHHs were employed as the electrolyte layer because of their reduced risk of solution leakage compared to conventional liquid electrolytes and improved ionic conductivity in comparison with conventional solid electrolytes. Owing to the reconstruction of electrons and ions migration pathway, the electrochemical reactions between chromophores with different valence states and cathodic/anodic materials could recur, thus achieving the repair of ED properties. For instance, Wang et al. devised a SHH ECD by sandwiching a self-healable P(AA-VIm-VSNP) hydrogel electrolyte between a viologen derivative (Bpy) electrochromic electrode and a PANI/ITO-based counter electrode.[356] The SHH electrolyte was prepared by radically polymerizing AA, 1-vinylimidazole (VIm), vinyl hybrid silica nanoparticles (VSNP), and with the introduction of Bpy and lithium perchlorate ($LiClO_4$). The assembled ECD exhibited an optical contrast ratio ($\Delta T$) of over 45%, a fast switching time of 2.0 s and 1.8 s for coloring and bleaching, respectively, a coloration efficiency (CE) of 406.96 $cm^2$ C, and a cyclic stability of more than 5000 cycles. Importantly, due to the internal multiple H-bonds, the hydrogel electrolyte could recover over 90% of its original mechanical properties and had no observable gap in the healed interface after 20 min healing. However, as the electrodes lacked self-healing ability, the entire device could not self-repair after damage. Similarly, Chen et al. prepared a SHH-based ECD by sandwiching a SHH electrolyte between an electrochromic layer of poly(3,4-(2,2-dimethylpropylenedioxy) thiophene) (PProDOT-$Me_2$) and an ITO/PET counter electrode (**Figure 19a**).[357] The hydrogel electrolyte was synthesized by immersing the copolymer of glycerol monomethacrylate (GMA) and AAm into a mixed solution composed of borax, $LiClO_4$, and 3-((ferrocenylmethyl)dimethylammonio)-propane-1-sulfonate (Fc-S). The resultant hydrogel electrode exhibited superior multifunctions, such as a high stretchability of 1155%, a breaking toughness of 136.6 kJ·$m^{-3}$, a SHE of 97%, and an ionic conductivity of 4.5 mS·$cm^{-1}$. The ECD demonstrated stable mechanical and optical performances during more than 1000 operating cycles, gradual repair ability and reusability within 30 min under small cracks. Many other SHH-based ECDs can be seen in Ref. [358–360].

In addition, researchers also attempted to construct SHH-based electroluminescent devices (ELD). For instance, Liang et al. devised an omni-layer-healable ELD using a self-healable PAA/NaCl hydrogel as the electrode and self-healing PU/ZnS/boron nitride (BN) as the intermediate phosphor composite layer (Figure 19b).[361] The hydrogel electrode and phosphor composite layer could entirely restore their initial physicochemical performances when damaged. Consequently, the ELD achieved a high self-healing capacity with a SHE of 83.2% in luminescent performance after ten cycles of cutting and healing. By utilizing the inter-device healing ability, different shapes of light-emitting devices were further assembled. Except for the ELD, some other SHH-based light-emitting devices were also developed. For instance, Zhang et al. prepared a white-light-emitting hydrogel that is both self-healable and emitting-tunable.[362] The hydrogel was developed by mixing oxidized dextran and dithiodipropionate dihydrazide, and further doped with carbon dots, Riboflavin, and Rhodamine B (Figure 19c). The as-prepared hydrogel was covered on an ultraviolet light-emitting diode to convert UV light to white light. Impressively, the hydrogel could self-heal in 20 h under pH conditions (from 5 to 9, except 7), exhibiting a promising potential in flexible optical devices. Besides, some luminous SHHs were also invented and applied in white LEDs, optical information coding and encryption, etc.[363–366] A summary on the main performances of SHH-based ECDs and ELDs is given in **Table 6**

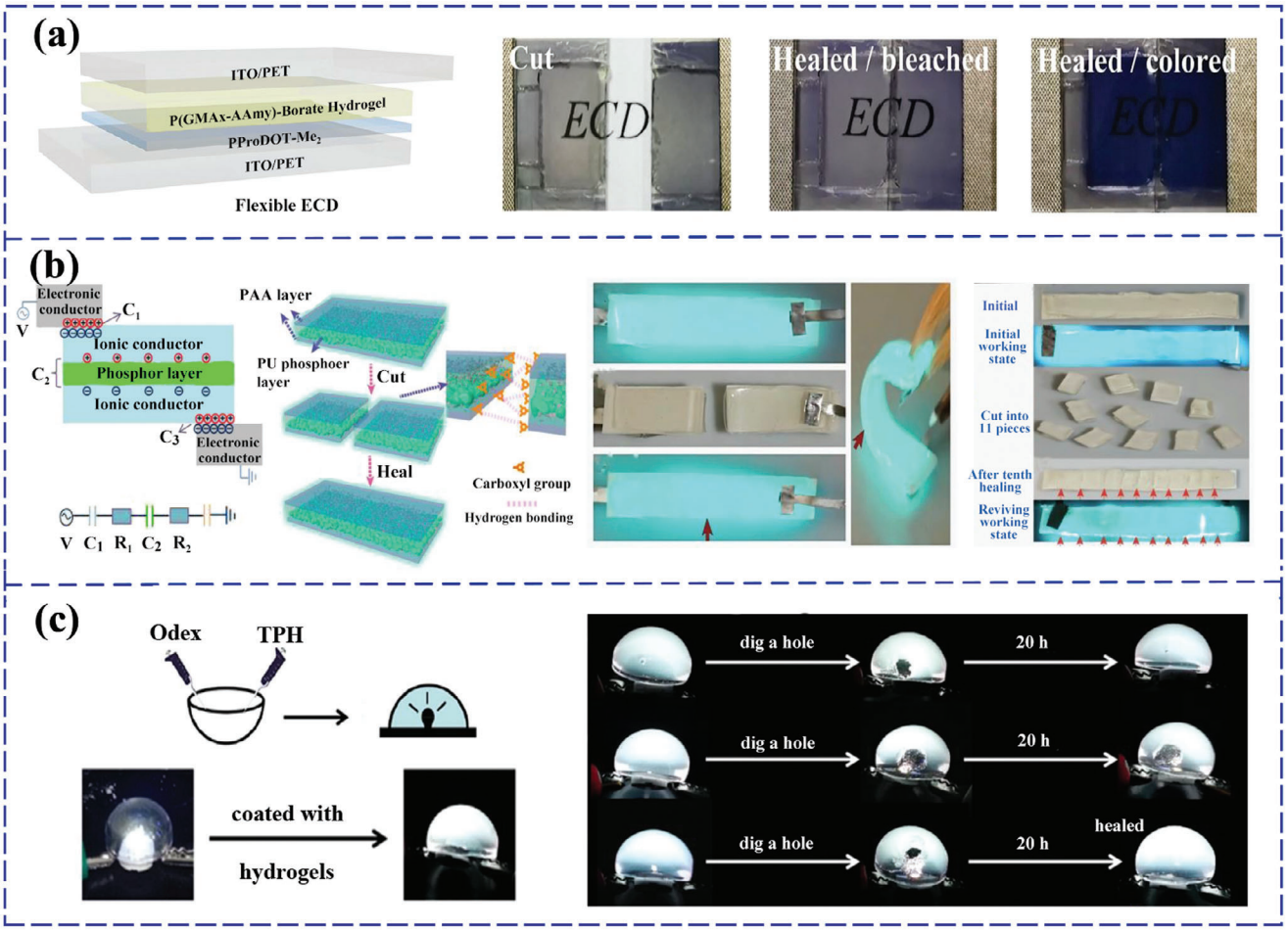


**Figure 19.** SHH-based display devices. a) Structure schematic of SHH-based ECD, photographs of the cutting-healing device. Reproduced with permission.[357] Copyright 2017, American Chemical Society. b) Schematics of the structure and healing mechanism of the SHH-based ELD, the electroluminescent photographs of the original and healed devices, and photographs of the healed device after being cut into 11 pieces. Reproduced with permission.[361] Copyright 2018, Springer Nature. c) Schematic diagram of the preparation of the white-light-emitting hydrogel and photographs of the original and healed hydrogels coated on an ultraviolet light-emitting diode. Reproduced with permission.[362] Copyright 2020, Elsevier.

**Table 6.** A summary on the comprehensive performances of SHH-based ECDs and ELDs.

| EC/EL materials | Hydrogel materials | $\Delta T$ [$\lambda$] | CE [$cm^2\ C^{-1}$] | Response time [s] | | Stability [Cycles] | Self-healing property | Self-healing efficiency | Refs. |
|---|---|---|---|---|---|---|---|---|---|
| | | | | Coloration | Bleaching | | | | |
| $PProDOT\text{-}Me_2$ | P(GMA-co-AAm)/$LiClO_4$/Borax/Fc-S | 49% (582 nm) | – | 1.6 | 2.0 | 1000 | tensile strain | 97%, 60 s | [357] |
| $WO_3$ | PAA-HPMC-$CaCl_2$ | 66% (633 nm) | 84.6 | 13 | 12 | 3000 | tensile strain | ≈100%, 8 h | [367] |
| Bpy | P(AA-VIm-VSN) | 45% (581 nm) | 406.96 | 2.0 | 1.8 | 5000 | tensile strength | 90.5%, 20 min | [356] |
| AVCOOEt | PVA-borax-$IL_{0.3}$ | 65.3% (406 nm) | 510 | 6.09 | 7.93 | 3000 | conductivity | ≈100%, 40 s | [368] |
| PA/FcA | CS/PEO-DBA/EG | 65% (600 nm) | – | 17 | 19 | 1000 | Macro | 20–240 s | [369] |
| KVO/MC | $LiClO_4$/propylene carbonate | 58.03% (500 nm) | 78.8 | 5.6 | 3.4 | 10 000 | – | – | [370] |
| $WO_3$ | P(MMA-co-DEA-co-AA)/[Emim]TFSI | 49.9% (650 nm) | 96.2 | 7 | 4 | 200 | tensile strain | 85%, 12 h | [371] |
| ZnS/Cu | PVA-BA/EmimCl | luminance: 114 cd $m^{-2}$, 50 V, 400 Hz | | | | 800 | tensile strain | 91%, 2 h | [372] |
| ZnS/BN | PAA/NaCl | luminance: 70.5 cd $m^{-2}$, 3 V/μm, 500 Hz | | | | – | luminance | 83.2%, 10 cycles | [361] |

### 3.4. Self-Healing Hydrogel TENGs

SHH-based TENGs have drawn increasing interest recently because they can combine the advantages of both hydrogels and TENGs, and overcome mechanical damage-induced performance degradation and function failure. In contrast to supercapacitors, TENGs are a type of energy harvester that can convert mechanical vibrations into electricity based on triboelectrification and electrostatic induction, providing wearable electronics and devices with renewable and sustainable power.[373,374] Hydrogels possessed the advantages of high transparency, high ionic conductivity under large deformation, excellent stretchability, and biocompatibility. Consequently, they are considered as promising electrode materials for TENGs and can be facilely integrated with other flexible wearable biomedical devices.[375] Furthermore, the self-healing capacity of hydrogels can solve the issue of device failure caused by continuous mechanical force stimulus (e.g., stretching) and repeated friction between different device layers during the energy collection process, enabling TENGs for practical engineering application.[376] Therefore, numerous efforts have been invested in SHH-based TENGs.

In most investigations, researchers were devoted to constructing TENGs working in a single-electrode mode with SHHs as the ionic conductive electrode and elastomers possessing high tribo-negativity (e.g., PDMS) as the triboelectric layer (**Figure 20a**).[377] Efforts were concentrated on simultaneously improving the multi-functionality of hydrogels, such as self-healing capacity, ionic conductivity, stretchability, mechanical toughness, etc., and thus the overall performance of TENGs. For instance, Long and co-workers constructed a self-healable single-electrode mode TENG using a stretchable and self-healable PAM/PDA hydrogel electrode and a polytetrafluoroethylene (PTFE) electrification film.[378] Compared to conventional copper electrodes, the hydrogel electrode could prominently enhance the output performance and stability even when seriously stretched. Furthermore, owing to the H-bonds between PAM and PDA chains, the TENG could self-heal in 5 h and achieve approximately 85% of its original electric output. To enhance the electrical output performance and achieve autonomous self-healing capacity, Guan et al. fabricated a SHH TENG by exploiting self-healable PVA/Agar/polydopamine particles (PDAPs)/MWCNTs hydrogels as the electrodes and silicone rubber as the triboelectric film.[379] The incorporation of PDAPs and MWCNTs in the hydrogel electrodes enabled the prepared TENGs to self-heal mechanically (a SHE of ≈93%) and electrically (a SHE of ≈100%) when they were exposed to NIR light for 1 min. It could harvest human motion energy and charge commercial LEDs sustainably, exhibiting a short-circuit charge ($Q_{sc}$) of ≈32 nC, an open circuit voltage ($V_{oc}$) of ≈95 V, and a short-circuit current ($I_{sc}$) of ≈1.5 µA. Liu and co-workers proposed a TENG with a PVA/PDAPs/graphene/Glycerol-based SHH as the electrode and a dielectric PDMS/CNTs as the triboelectric layer (Figure 20b).[380] The broken TENG could self-heal in 1 min without additional stimuli, and restore 94% and 92% of its original $Q_{sc}$ and $V_{oc}$, respectively. Compared with pure PDMS, incorporating CNTs in PDMS could significantly improve the $Q_{sc}$ and $V_{oc}$ , and power 37 LEDs simultaneously, exhibiting superior electrical output performance. Besides, similar TENGs based on various SHH electrodes, such as PAM/PAA/graphene/PEDOT:PSS,[381] PVA/SA,[377] and PAA/gelatin/NaCl,[382] were also developed.

Since their self-healing capacity mainly relied on the healing ability of the used hydrogel electrode, the aforementioned TENGs could not fully self-repair, resulting in limited performance recovery ability. To address this issue, researchers tried to explore fully self-healable TENGs, in which each layer of the device could self-heal after damage. For instance, Lai et al. presented an entirely self-healing TENG using healable PDMS and ionic conductive hydrogels as the triboelectric layer and electrode layer, respectively (Figure 20c).[383] The healable PDMS was synthesized based on the coordination interactions between the zinc ions and the condensation polymer of bis(3-aminopropyl)-terminated PDMS and bipyridine groups. The healable hydrogel was cross-linked by borate ester bonds between PVA and tetrahydro borate ions. On this foundation, the as-prepared TENG exhibited a fully self-healing capacity (100% efficiency at 900% strain in 30 min) and could retain its functionality after 500 cutting-healing cycles. Furthermore, it showed high transparency of 88.6% and inherent super-stretchability of more than 900%. The TENG could harvest low-frequency (1–4 Hz) mechanical energy and output a $V_{oc}$ of 20 V, an $I_{sc}$ of 240 µA $m^{-2}$, and a power of ≈5 mW $cm^{-2}$, respectively, and successfully power an electronic watch and calculator. Yang and co-authors proposed a multifunctional TENG with a rapid self-healing ability and photo-thermal property.[384] It was composed of PDA-CNTs/PVA/Borax-based SHHs electrodes and two self-healable silicone elastomer triboelectric layers. Due to the dynamic imine bonds in silicone elastomer and the H-bonds and borate ester bonds in hydrogel electrode, the whole TENG was able to self-repair and achieve 80% of its original electrical outputs within 10 min when damaged.

To endow SHH TENGs with anti-freezing and anti-drying performances for application in harsh environments, Guo et al. constructed anti-freezing zwitterionic SHH-based TENGs that could instantly recover upon damage in a wide temperature range.[278] The SHE of the hydrogel electrode in tensile strain and toughness reached 94.70% and 66.59% within 72 h, respectively, and the conductive SHE reached almost 100% under multiple cutting-healing cycles and different temperatures (−20 to 20 °C). The as-prepared TENG device demonstrated a typical $V_{oc}$ of 123 V, $I_{sc}$ of 5.1 µA, and $Q_{sc}$ of 42 nC. Its electric output performance could almost completely recover after 1 min healing at RT. Huang et al. utilized PAM/clay organohydrogels and healable PDMS as the electrode and charged layer, respectively, and prepared an ultrafast self-healing TENG with thermo-resistant, anti-drying, and anti-freezing performances (Figure 20d).[273] The self-healable organohydrogel was synthesized by incorporating glycerol into cross-linked PAM-clay hydrogels. It exhibited hydrophobic and icephobic properties, and could restrain the accumulation of water and ice layers on the device's surface. As a result, the healed TENGs demonstrated a high SHE above 95% in electric output after 1 s healing in a broad temperature range of −30 to 80 °C. Besides, other anti-freezing self-healing supramolecular gel and ionogel-based TENGs were also fabricated.[385,386]

Integration of TENGs with wearable sensors to realize self-power presents an emerging development trend for flexible wearable electronics, which is desirable for practical engineering applications. Bagchi and co-workers constructed a self-healing TENG composed of a healable AuNPs/PVA hydrogel electrode

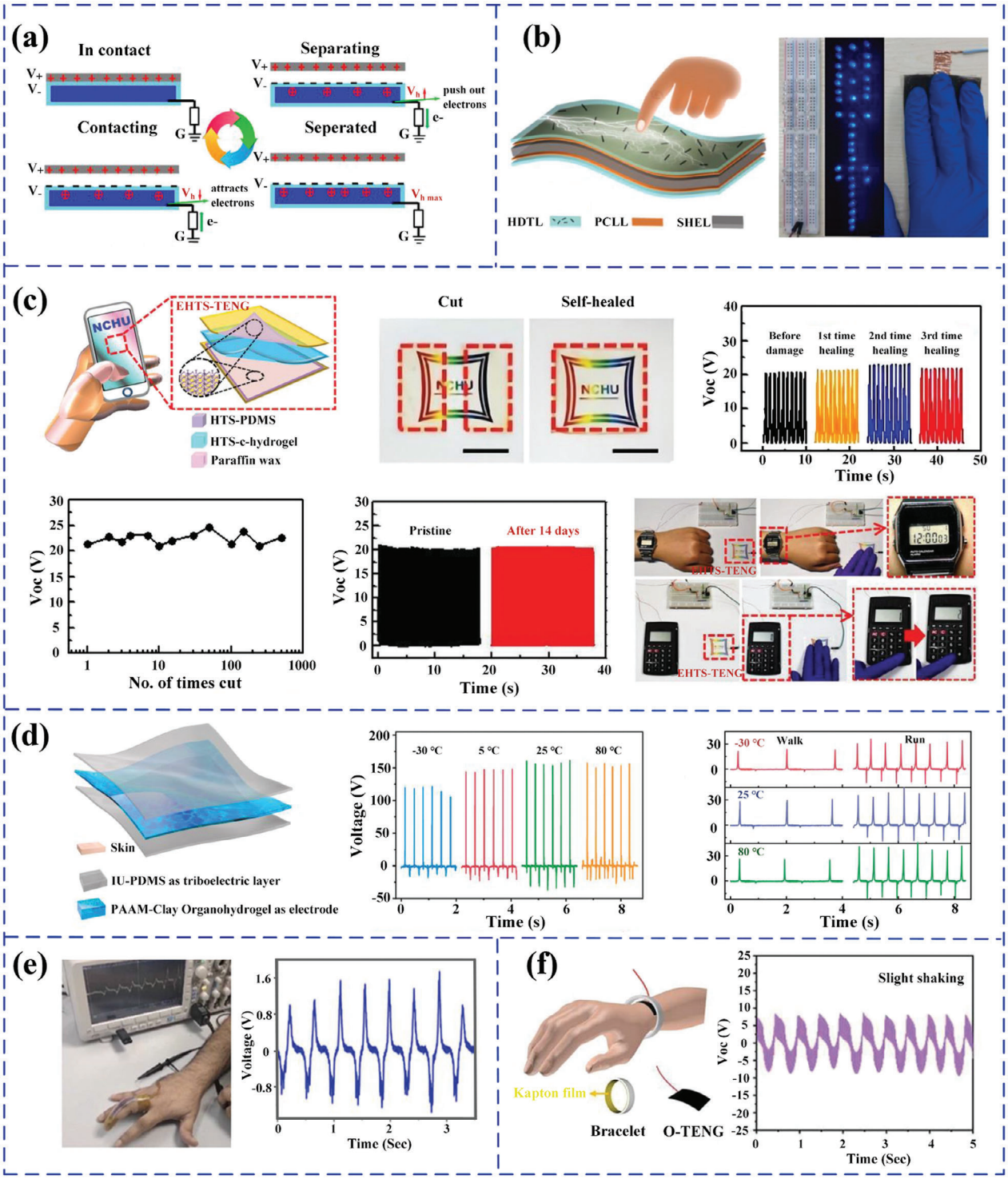


**Figure 20.** SHH-based TENGs. a) Schematics of the working principle of TENGs based on the single-electrode mode. Reproduced with permission.[377] Copyright 2020, American Chemical Society. b) Structure schematic of the self-healing TENGs using PVA/PDAPs/graphene/Glycerol hydrogel as the electrode, and the picture of the SH-TENG lighting 37 LEDs. Reproduced with permission.[380] Copyright 2021, Elsevier. c) i) Structure schematic of the self-healing EHTS-TENG, ii) performances of EHTS-TENG after self-repair, iii) the cycle self-healing capability and stability, and iv) the application of gathering energy to drive electronic watch and calculator. Reproduced with permission.[383] Copyright 2019, John Wiley & Sons. d) Structure schematic of the self-healing organohydrogel-based TENG, $V_{oc}$ of the OG-TENG at different temperatures, and the signals of OG-TENG (attached on one foot) during walking and running under different temperatures. Reproduced with permission.[273] Copyright 2020, Elsevier. e) Demonstration of finger bending movement detection capability of G3 TENG. Reproduced with permission.[387] Copyright 2023, Elsevier. f) Schematic illustration of wrist motion monitoring based on an O-TENG and $V_{oc}$ variation of slight wrist shaking. Reproduced with permission.[388] Copyright 2022, John Wiley & Sons.

**Table 7.** A summary on the main performances of SHH-based TENGs.

| Hydrogel material | Tribo-pair | Size [cm$^2$] | $Q_{SC}$ [nC] | $V_{OC}$ [V] | $I_{SC}$ [μA] | Self-healing properties | Self-healing efficiency | Refs. |
|---|---|---|---|---|---|---|---|---|
| PVA/Agarose/PDAPs/MWCNTs | Silicone rubber | 3 × 3 | ≈32 | ≈95 | ≈1.5 | $Q_{sc}$, $I_s$ | ≈100%, 1 min | [379] |
| PVA/PDAPs/Graphene/Glycerol | PDMS/CNTs | 2.5 × 2.5 | ≈44 | ≈132 | – | $Q_{sc}$; $V_{OC}$ | 94%, 1 min; 92%, 1 min | [380] |
| PVA/MXene/Borax | Ecoflex | 2 × 5 | 38 | 230 | 0.27 | – | – | [389] |
| PAM/PAA/Graphene/PEDOT: PSS | PDMS/CNTs | 42 | NA | 141 | 0.8 | $V_{OC}$; $I_{SC}$ | ≈96%, 12 h; ≈85%, 12 h | [381] |
| MDHS/HEMA/PAA/LiCl | PDMS | 4 × 5 | 42 | 123 | 5.1 | $V_{OC}$, $I_{SC}$ | ≈100%,1 min | [278] |
| HTS-c-hydrogel | HTS-PDMS | 4 × 2.5 | 7 | 20 | 0.24 | $V_{OC}$ | > 90%, 1 h | [383] |
| PAM/PDA | PTFE | 2.5 × 2.5 | 100 | 230 | 12 | $V_{OC}$ $I_{SC}$ | ≈84%, 5 h; ≈80%, 5 h | [378] |
| PAM/Clay/Glycerol | IU-PDMS | 4 × 4 | 29 | 157 | 16 | $V_{OC}$, $I_{SC}$ | > 95%, 1 s | [273] |
| PVA/PDA-CNTs | SH-AD-549 | – | 78.34 | 38.57 | 7.98 | $V_{OC}$; $Q_{SC}$ | ≈96%, 10 min; ≈80%, 10 min | [384] |
| PVA/PEI/LiCl | Silicone rubber | 3 × 5 | 47.48 | 78.44 | 1.42 | $V_{OC}$ | ≈100%, 1 min | [390] |
| PAA/Gelatin/NaCl | VHB | 2 × 3 | ≈6 | ≈22 | ≈0.4 | Electrical | 99%, 2.5 min | [382] |
| P(AMPS-*co*-AA-*co*-DMAPMA)/Laponite/Graphene/LiCl | PTFE | 2 × 2 | 25 | 75 | 0.6 | $V_{OC}$, $I_{SC}$ | ≈100%, 1 min | [391] |

and an Ecoflex-based triboelectric layer.[387] Because of its good conformability to the human body, the device could adhere to the finger joint, neck, and knee for energy acquisition (Figure 20e). Concurrently, the state of human motion was also detected during the process of energy acquisition. Besides, Zhang et al. proposed a self-healing O-TENG composed of a multifunctional Ag@rGO/PVA/PAM organohydrogel electrode layer for self-powered biomechanical sensing.[388] It identified handwriting via distinguishable and repeatable signature voltage signals responsive to different handwritings. Furthermore, it was adhered to the human wrist for biomechanical activity monitoring, successfully recognizing three amplitude levels of wrist movements (Figure 20f). **Table** 7 summarizes the main peoformances of virous SHH-based TENGs developed in recent years.

### 3.5. Self-Healing Hydrogel Implantable Bioelectronics

Implantable bioelectronics play an indispensable role in personalized healthcare because they can interface directly with the biological tissues or organs inside human bodies to implement vital bio-signals monitoring or chronic disease treatment, which generally can not be realized by those on-skin or wearable electronics mentioned before. Compared with those silicon-based conventional counterparts, hydrogel-based soft implantable bioelectronics are drawing increasing interest[392] because of their tissue-mimicking mechanical, electrical, and biocompatible properties, which successfully solve the issues of non-conformal contact with bio-tissues, mechanical mismatch at biotic-abiotic interfaces, and prominent immune reactions and rejection.[393–395] The self-healing function further endows the hydrogel implantable bioelectronics with the capacity to bear stress fatigue, and repair cyclic deformation-induced cracks and property degradation in harsh in vivo environments, and thus expand their lifetime, long-term stability, and sustainability. Therefore, self-healing hydrogel implantable bioelectronics provide an ideal solution to in vivo biomedical applications, which have sparked numerous research interests in recent years. To date, a diversity of self-healing hydrogel implantable bioelectronics have been developed for nerve signal recording, tissue repairing, and neuromodulation and therapy, including implantable electrodes, bioactuators, and sensors.

Among various implantable bioelectronics, SHH implantable electrodes have been extensively investigated owing to their widespread application in electrophysiological monitoring and disease treatment. Specifically, by exploiting the sensing function, SHH electrodes can be intimately and conformally attached to brain tissues, nerves, cardiac tissues, and muscles to monitor their electrical potential variations during life activities to diagnose their health status, e.g., electroencephalogram (EEG) signals, electromyographic (EMG) signals, and ECG signals.[396] By using its electrical conductivity, the electrode can operate as a simulator to apply electrical stimulation to the targeted brain regions, peripheral nerves, or specific muscle tissues for major diseases treatment or organ function assistance, such as epilepsy,[397,398] chronic pain,[399] muscular dystrophies.[400,401] For instance, Han and co-workers designed a self-adhesive, conductive, and self-healable PDA-pGO-PAM hydrogel as an implantable electrode for in vivo electrical signal detection (**Figure** 21a).[402] The SHH electrodes exhibited a high stretchability (3500%), toughness (4280 J m$^{-2}$), electrical conductivity (0.08 S cm$^{-1}$), self-healing ability (95% in electrical SHE), and excellent biocompatibility because of the introduction of the PDA chains and PDA partially reduced rGO. After implanting into the human dorsal muscle, the electrode successfully collected its electrical voltage variation, with a signal magnitude of 0.1–40 mV, which was much higher and more accurate than the signals detected by skin-attachable electrodes, demonstrating its efficiency in monitoring the electrical signal of deep muscle tissues. Choi et al. prepared an alginate-based conductive SHH implantable electrode for the electrical connection and signal transduction between muscles.[176] To evaluate the electrophysiological bridging effect of the prepared SHH electrode, an ex vivo muscle-hydrogel-muscle defect model was constructed, where one muscle was electrically stimulated and another one was used to extract EMG signals. Owing to the superior conductivity of the intermediate SHH electrode, the action potential produced by stimulated muscle tissue was effectively transferred to and detected from another

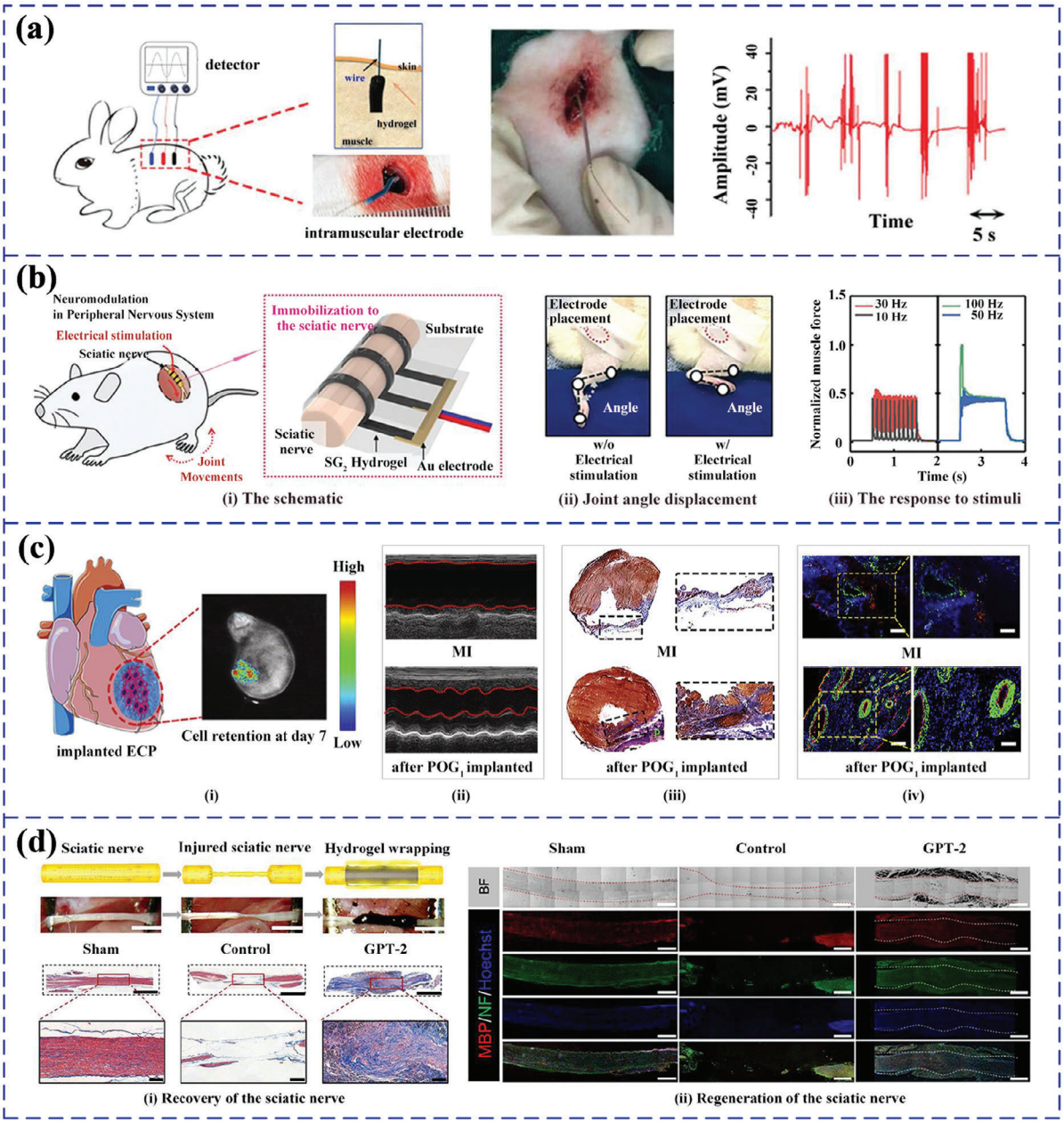


**Figure 21.** SHH-based implantable bioelectronics. a) Schematic of self-healable PDA-pGO-PAM hydrogel as the intramuscular electrode for EMG signal detection, the photograph of the practical implantation of the hydrogel, and the recorded EMG signal from the rabbit's muscle under external stimulation. Reproduced with permission.[402] Copyright 2016, John Wiley & Sons. b) Self-healable SG hydrogel biodevice for neuromodulation. i) Illustration of the Au/SG hydrogel biodevice for sciatic nerve modulation under electrostimulation; ii) Pictures of rat's joint bending angles with/without electrostimulation; iii) a plot of muscle force as a function of stimulation frequency. Reproduced with permission.[45] Copyright 2022, John Wiley & Sons. c) Self-healable $POG_1$ hydrogel-based ECP for MI repair. i) Illustration of the implanted hydrogel ECP for MI repair; ii) Echocardiographic images for hearts, iii) Masson's trichrome staining images, and iv) $\alpha$-SMA staining (green) and vWF staining (red) images of the MI areas without and with $POG_1$ hydrogel ECP transplantation at 4 weeks. Reproduced with permission.[46] Copyright 2021, Elsevier. d) Self-healing GPT hydrogel-based NGC for peripheral nerve regeneration. i) Schematic of hydrogel wrapping injured sciatic nerve and Masson's trichrome staining results of the sciatic nerve at 2 weeks; ii) Immunohistofluorescence images of the sciatic nerve at 2 weeks. Reproduced with permission.[405] Copyright 2021, Elsevier.

muscle. And the EMG amplitude and signal pattern were almost consistent with those extracted for another muscle-muscle defect model (the control group), demonstrating its tissue-like electrophysiological bridging capacity and great potential in the usage of SHH implantable electrical interconnectors.

Besides EMG signal monitoring of deep muscle tissues, electrophysiological signal detection and modulation of brain and nerves are other attractive applications of SHH implantable electrodes. In recent years, increasing efforts have been devoted to the development of SHH implantable bioelectrodes because of

their significance in EEG monitoring and the treatment and rehabilitation of neuropathic diseases. Sun et al. developed a self-healable multifunctional hydrogel with superior conductivity and good biointegration, and utilized it as an implantable bidirectional interface for both neural recording and therapeutic electrostimulation.[403] On this foundation, an SG hydrogel-based neuromodulatory electrode was invented and further implanted in the sciatic nerve of a rat model for function validation (Figure 21b). By applying different frequencies and intensities of electrical stimulations on the sciatic nerve, the ankle joint of the rat's leg could bend at different speeds and angles, demonstrating the neuromodulation capability of the SG hydrogel bioelectrode in the peripheral nervous system. More importantly, with the anti-swelling and self-healing capacities, the hydrogel-based bioelectrode implanted in the sciatic nerve could maintain steady under both dry and wet conditions, as well as a stable ankle joint movement under pulse electric stimulations with an intensity of 50 μA and a time of duration of 100 μs even after one week. The results demonstrated the long-term implantable capacity and great potential in the therapy of neurological diseases.

In addition, SHH implantable electronics have also been extensively investigated for tissue/organ repair and regeneration medicine (such as myocardial tissue repair, and peripheral nerve regeneration). For instance, Song et al. proposed a self-healable PAA/oxidized alginate/gelatin (POG) hydrogel-based engineering cardiac patch (ECP) for myocardial infarction repair.[46] Owing to the introduction of conductive PAA and entire biocompatible materials, the resultant POG SHHs exhibited excellent comprehensive performances, such as a similar Young's modulus with a mammalian heart (30–500 kPa), rapid self-healing capability, superior biocompatibility and microscopic ultra-homogenous ionic conductivity (highly stable conductivity under large deformations). As a result, the neonatal cardiomyocytes (CMs) cultured in the POG SHHs showed more oriented and elongated sarcomeres than those seeded in electronic conductive hydrogels, demonstrating their outstanding performance in CMs orientation growth and functionalization. A further in vivo experiment showed that the POG ECP could restrain the enlargement and remodeling of the left ventricular (Figure 21c(ii)), suppress cardiac fibrosis (Figure 21c(iii)), and induce angiogenesis in the MI area (Figure 21c(iv)), exhibiting desirable performance in MI repair and normal systolic function recover. Similarly, a self-healable zwitterionic hydrogel-based ECP was also constructed for MI treatment and cardiac function restoration.[404] These studies validated the function and efficiency of SHH patches in cardiac and other organ/tissue repair. Besides these, a large number of researchers were devoted to developing SHH implantable electronics for injured peripheral nerve repair, which was significant to human sensory and motor function therapy. For this, Kang et al. designed a shape-resistant gelatin/PPy/TA (GPT) SHH and utilized it to prepare a nerve guidance conduit (NGC).[405] The NGC could be implanted and conformally wrapped in the injured sciatic nerve in female mice. After two weeks of implantation, a lot of new neurofilaments emerged in the injured nerve regions (Figure 21d(i)). A further immunofluorescence staining experiment showed the presence of the high staining intensity of NF-200 protein and myelin basic protein (Figure 21d(ii)), which meant the regeneration of axons and myelin sheaths, and thus the regeneration of the sciatic nerve. These results indicated the positive efficacy of GPT hydrogel NGC on peripheral nerve regeneration and function recovery. Some other examples about the applications of SHH implantable electronics in regeneration engineering can be found in Ref. [406,407].

The aforementioned studies presented several typical SHH implantable electronics and demonstrated their efficiency and promising prospects for in vivo electrophysiological detection and disease treatment. However, the development of SHH implantable electronics is still in the infant stage. More types of implantable bioelectronics and applications in personalized healthcare and therapy are waiting to be explored. For instance, pH-responsive (or pH/catalyst-triggered) SHH implantable bioelectronics can be employed for tumor diagnosis by utilizing the sensitive response to the corresponding humoral environment conditions.[408] Controllable drug delivery based on SHH implantable bioelectronics is also another extensively investigated area because of its effective function in diseases and wound healing.[409] To realize the clinical transformation of SHH implantable electronics, more efforts should focus on constructing SHH with excellent comprehensive performances under in vivo environments, such as self-healing capacity, biocompatibility, anti-swelling, stretchability, ionic conductivity, self-adhesion, tissue-mimicking mechanical property, etc.

## 4. Challenges and Prospects

In this review, we have highlighted the most prominent mechanisms explored in synthesizing SHHs and their applications in developing soft bioelectronics in the past years. A diversity of self-healing mechanisms has been constructed, involving autonomous and external-stimuli triggered and in harsh environments (like low temperature or underwater circumstances). Exploiting these mechanisms, numerous SHHs have been demonstrated, exhibiting remarkable improvement in their SHE, recovery speed, and allowable self-healing cycles, as well as many other physiochemical performances (such as mechanical strength, stretchability, conductivity, anti-freezing ability, water retaining performance, etc.). Applications of these SHHs range from wearable sensors, optical displays, supercapacitors, and TENGs to implantable bioelectronics. Excellent performance-restoring capacities after mechanical damages have been demonstrated, significantly improving the reusability and lifetime of soft electronics. Although tremendous progress has been made, most of the developed self-healing electronics are in the proof-of-concept stage. Grand challenges need to be tackled before their ultimate engineering applications.

### 4.1. Deeper Insights into the Theories and Performance Evaluation of Self-Healing

Most current efforts focus on exploring possible self-healing mechanisms for hydrogels and experimentally demonstrating their macroscopic self-healing behavior. There is an absence of theoretical analysis or modeling on the self-healing kinetics at a molecular level, which can illustrate the effects of the types, kinetics, and concentration of molecules and environment parameters (like temperature, pH, etc.) on the formation of dynamic

bonds and thus bonding energy. It's desirable to develop theoretical models that can quantitatively compute the self-healing macro performances (like self-healing efficiency, time, and cycles) of hydrogels from their molecule constituent. These models can not only predict the self-healing performance under given conditions but also provide powerful design strategies toward targeted performance requirements with the help of machine learning and artificial intelligence. Besides, constructing performance evaluation standards and corresponding experimental testing methods will also be instrumental, enabling quantitative characterization and verification of self-healing performances of SHHs.

### 4.2. Toward Simultaneous Enhancement of Self-Healing Capacity and Other Desired Material Properties

For practical application in soft electronics, hydrogels should possess not only the self-healing capacity but also many other necessary performances, such as mechanical strength, stretchability, conductivity, etc. However, tremendous challenges exist in the concurrent improvement of these performances because of their contradictory requirements on material component design. One common challenge is the trade-off between the SHE and mechanical property, Young's modulus. A hydrogel with a high SHE rarely has enough Young's modulus under ambient temperature. This is because the high SHE requires fast segmental and chain dynamics, and readily breakable/exchangeable dynamic bonds, which usually comes at the cost of polymer chains with low modulus and weak dynamic bonds. Exploring new strategies to balance the contradictions among multiple functions, including self-healing ability, is instrumental in realizing practical engineering applications of hydrogels. A promising solution is to take advantage of both complex molecular designs combining different dynamic bonds and network architectures with specific morphologies.

### 4.3. Endowing SHHs with Environmental Adaptabilities

Due to their water-rich and hydrophilic nature, hydrogels are susceptible to dehydration at ambient or higher temperatures, freezing at low temperatures, and swelling in water. These factors can degrade the stability and reliability of hydrogel-based electronics and even result in device failure. On the premise of ensuring self-healing performance, tackling the issues of water loss, freezing, and swelling is crucial to self-healing hydrogel electronics, which can improve the device stability and reliability, and extend their application scope, such as at low temperatures, underwater circumstances, etc. Furthermore, SHHs with controllable degradability are promising in developing environmentally friendly and implantable self-healing soft devices.

### 4.4. Toward the Development of Soft Electronics with Fully Self-Healing Capacities

Although a diversity of self-healing soft electronics has been demonstrated in past years, few of them can implement self-healing of the whole device, especially for those with multiple or multi-layer structure components, such as capacitive sensors. To achieve full SHH electronics, each component layer of the device structure should possess self-healing capability. That is, apart from SHHs, many other materials required for the device construction should be imparted with self-healing ability. Furthermore, it's more challenging to overcome the deformation, stripping, and dislocation caused by function failure during the healing process of the device because of the mismatching in the self-healing performance (SHE, speed, repeated cycles, and conditions). Tremendous efforts should be put into constructing effective strategies for this issue. Besides, the interface adhesion/bonding and interface self-healing between different layers are also instrumental to maintaining device structure robustness and implementing full performance restoration after damage.

### 4.5. Exploring Fabrication Technologies of Self-Healing Hydrogel Electronics

Manufacturing techniques are essential to developing self-healing hydrogel electronics, which bridge the gap between device concepts and their practical application. Presently, most self-healing hydrogel-based electronics are fabricated from bulk self-healing hydrogel with simple structure designs, and the patterning and integration are conducted manually. The first urgent mission that needs to be tackled is exploring fabrication technologies that can realize graphical patterning, device-to-device consistency, and integration manufacturing. In this aspect, 3D/4D printing, soft lithography, screen printing, direct ink writing, and inkjet printing possess great potential in manufacturing self-healing hydrogel electronics with complex structures and consistent performances. Furthermore, miniaturization and scalable fabrication can shrink the device size, enable highly dense integration (imparting one single device with multiple functions), and reduce the cost, which is in high demand for self-healing soft electronics. Fabrication of self-healing hydrogel devices with micro/nano thickness and good breathability could improve user comfort during long-term usage.

### 4.6. Endowing Self-Healing Hydrogel Bioelectronics with New Functions for More Extensive and Revolutionary Applications

With SHH-based flexible electronics going into the deep of human life, new and revolutionary functions will be continuously required to extend the application scope and innovate the existing way. For example, SHH bioelectronics with shape memory function can memorize complicated shapes and return to their initial ones with programmable approaches under external stimuli, which can be broadly used in the situations which need controllable activating capability in device structure and performances, such as minimally invasive surgery, biomedical devices, and smart soft bioactuators. With imparted shape-editable and self-adhesive abilities, SHH electronics can conformally adhere to the surfaces of tissues or complex organs with the desired shapes to achieve long-term physiological information monitoring, and further apply for artificial nerve, brain-machine interfaces, and brain disease therapy. Moreover, SHH electronics can be integrated with self-healing supercapacitors and self-healing

TENGs to realize self-power and thus continuous operation. For example, self-healing wearable sensors integrated with TENGs can implement continuous, long-term, and wearable medical monitoring, which is the ultimate goal of the development of flexible electronics.

### 4.7. Prospects

Owing to their soft nature, hydrogel-based bioelectronics are prone to mechanical damage during their usage, severely restricting their practical applications. Self-healing provides an effective solution to this issue, imparting soft bioelectronics with skin-like restoring ability and reusability, and expanding their lifetime. Previous research has perfectly demonstrated this point, and verified its feasibility and effectiveness in a concept of proof way. Once the key challenges are tackled, we can envision that SHHs with superior comprehensive properties will be constructed by rationally combining multiple self-healing mechanisms and topological structure designs. SHH bioelectronics will be able to fully restore their performance under thousands of times of damage and simultaneously possess many other excellent performances, such as enough mechanical strength, high stretchability, superior electrical conductivity, desirable stability, reliability, etc. With their rapid development, the clinical translation or commercialization of self-healing hydrogels bioelectronics can be found in fields of wearable physiological signal monitoring, in vivo drug delivery, tissue engineering scaffolds, electrophysiological signal sensing of human organs, wound dressing, contact lenses, neural signal recording and regulation, and major neurological disease treatment. It can be foreseen that, in the near future, SHH bioelectronics will fuse into the daily life of human beings and make revolutionary changes in the way people live.

## Acknowledgements

This work was partially supported the National Natural Science Foundation of China (52275570, 52103320), the Project of Shaanxi Provincial Science and Technology New Star(2023KJXX-001), the Collaborative Research Fund of Research Grants Council (C7005-23Y), and Shenzhen-Hong Kong-Macau Technology Research Programme (SGDX20210823103537034).

## Conflict of Interest

The authors declare no conflict of interest.

## Author Contributions

Z.K.L. initiated the idea to write this review, which was later supported by Y.M.X. and S.M.Z. based on their collaborations in self-healing hydrogel-based bioelectronics. J.J.L. was in charge of the investigation, manuscript writing, and all the figures preparation. Z.K.L. was in charge of conceptualization, investigation, logically writing, editing, and supervision. Y.M.X. and S.M.Z. revised the manuscript. T.J. made all the tables and revised the figures. K.Z., B.W., B.Q.J., and J.X.W. were in charge of the manuscript formatting, expressions, and references. L.B.Z. and Academician Z.D.J. were in charge of supervision, project administration, and funding acquisition.

## Keywords

self-healing hydrogels, self-healing mechanisms, wearable sensors, soft display devices, flexible supercapacitors, flexible TENGs, implantable bioelectronics

Received: June 30, 2023
Revised: October 7, 2023
Published online: February 12, 2024

[1] O. A. Araromi, M. A. Graule, K. L. Dorsey, S. Castellanos, J. R. Foster, W. H. Hsu, A. E. Passy, J. J. Vlassak, J. C. Weaver, C. J. Walsh, R. J. Wood, *Nature* **2020**, *587*, 219.
[2] V. Cacucciolo, J. Shintake, Y. Kuwajima, S. Maeda, D. Floreano, H. Shea, *Nature* **2019**, *572*, 516.
[3] S. Xu, A. Jayaraman, J. A. Rogers, *Nature* **2019**, *571*, 319.
[4] B. Yin, X. Liu, H. Gao, T. Fu, J. Yao, *Nat. Commun.* **2018**, *9*, 5161.
[5] G. Cai, J. Wang, K. Qian, J. Chen, S. Li, P. S. Lee, *Adv. Sci.* **2017**, *4*, 1600190.
[6] M. Kaltenbrunner, T. Sekitani, J. Reeder, T. Yokota, K. Kuribara, T. Tokuhara, M. Drack, R. Schwodiauer, I. Graz, S. Bauer-Gogonea, S. Bauer, T. Someya, *Nature* **2013**, *499*, 458.
[7] S. Lee, S. Franklin, F. A. Hassani, T. Yokota, O. G. Nayeem, Y. Wang, R. Leib, G. Cheng, D. W. Franklin, T. Someya, *Science* **2020**, *370*, 966.
[8] Y. Khan, A. E. Ostfeld, C. M. Lochner, A. Pierre, A. C. Arias, *Adv. Mater.* **2016**, *28*, 4373.
[9] H. Liu, S. Zhang, Z. Li, T. Lu, H. Lin, Y. Zhu, S. Ahadian, S. Emaminejad, M. R. Dokmeci, F. Xu, A. Khademhosseini, *Matter* **2021**, *4*, 2886.
[10] M. Bariya, H. Y. Y. Nyein, A. Javey, *Nat. Electron.* **2018**, *1*, 160.
[11] J. Kim, A. S. Campbell, B. E. F. de Avila, J. Wang, *Nat. Biotechnol.* **2019**, *37*, 389.
[12] H. Joo, Y. Lee, J. Kim, J.-S. Yoo, S. Yoo, S. Kim, A. K. Arya, S. Kim, S. H. Choi, N. Lu, H. S. Lee, S. Kim, S.-T. Lee, D.-H. Kim, *Sci. Adv.* **2021**, *7*, eabd4639.
[13] Y. Li, G. Huang, B. Gao, M. Li, G. M. Genin, T. J. Lu, F. Xu, *NPG Asia Mater* **2016**, *8*, e238.
[14] D. Afanasenkau, D. Kalinina, V. Lyakhovetskii, C. Tondera, O. Gorsky, S. Moosavi, N. Pavlova, N. Merkulyeva, A. V. Kalueff, I. R. Minev, P. Musienko, *Nat. Biomed. Eng.* **2020**, *4*, 1010.
[15] H. U. Chung, B. H. Kim, J. Y. Lee, J. Lee, Z. Xie, E. M. Ibler, K. Lee, A. Banks, J. Y. Jeong, J. Kim, C. Ogle, D. Grande, Y. Yu, H. Jang, P. Assem, D. Ryu, J. W. Kwak, M. Namkoong, J. B. Park, Y. Lee, D. H. Kim, A. Ryu, J. Jeong, K. You, B. Ji, Z. Liu, Q. Huo, X. Feng, Y. Deng, Y. Xu, et al., *Science* **2019**, *363*, 947.
[16] W. Gao, S. Emaminejad, H. Y. Y. Nyein, S. Challa, K. V. Chen, A. Peck, H. M. Fahad, H. Ota, H. Shiraki, D. Kiriya, D. H. Lien, G. A. Brooks, R. W. Davis, A. Javey, *Nature* **2016**, *529*, 509.
[17] Y. Liu, J. Liu, S. Chen, T. Lei, Y. Kim, S. Niu, H. Wang, X. Wang, A. M. Foudeh, J. B. H. Tok, Z. Bao, *Nat. Biomed. Eng.* **2019**, *3*, 58.
[18] J. Lee, H. Kwon, J. Seo, S. Shin, J. H. Koo, C. Pang, S. Son, J. H. Kim, Y. H. Jang, D. E. Kim, T. Lee, *Adv. Mater.* **2015**, *27*, 2433.
[19] E. Roh, B. U. Hwang, D. Kim, B. Y. Kim, N. E. Lee, *ACS Nano* **2015**, *9*, 6252.
[20] K. Y. Chun, Y. Oh, J. Rho, J. H. Ahn, Y. J. Kim, H. R. Choi, S. Baik, *Nat. Nanotechnol.* **2010**, *5*, 853.
[21] S. H. Kim, H. Seo, J. Kang, J. Hong, D. Seong, H.-J. Kim, J. Kim, J. Mun, I. Youn, J. Kim, Y.-C. Kim, H.-K. Seok, C. Lee, J. B. H. Tok, Z. Bao, D. Son, *ACS Nano* **2019**, *13*, 6531.
[22] I. Jeon, J. Cui, W. R. K. Illeperuma, J. Aizenberg, J. J. Vlassak, *Adv. Mater.* **2016**, *28*, 4678.

[23] Z. Li, S. Zhang, Y. Chen, H. Ling, L. Zhao, G. Luo, X. Wang, M. C. Hartel, H. Liu, Y. Xue, R. Haghniaz, K. Lee, W. Sun, H. Kim, J. Lee, Y. Zhao, Y. Zhao, S. Emaminejad, S. Ahadian, N. Ashammakhi, M. R. Dokmeci, Z. Jiang, A. Khademhosseini, *Adv. Funct. Mater.* **2020**, *30*, 2003601.
[24] S. Lin, H. Yuk, T. Zhang, G. A. Parada, H. Koo, C. Yu, X. Zhao, *Adv. Mater.* **2016**, *28*, 4497.
[25] R. Feiner, T. Dvir, *Nat. Rev. Mater.* **2018**, *3*, 1.
[26] X. Liu, J. Liu, S. Lin, X. Zhao, *Mater. Today* **2020**, *36*, 102.
[27] C. Yang, Z. Suo, *Nat. Rev. Mater.* **2018**, *3*, 125.
[28] H. Yuk, B. Lu, X. Zhao, *Chem. Soc. Rev.* **2019**, *48*, 1642.
[29] M. Kharaziha, A. Baidya, N. Annabi, *Adv. Mater.* **2021**, *33*, 2100176.
[30] Q. Shi, H. Liu, D. Tang, Y. Li, X. Li, F. Xu, *NPG Asia Mater* **2019**, *11*, 64.
[31] T. L. Sun, K. P. Cui, *Adv. Polym. Sci.* **2020**, *285*, 295.
[32] M. X. Wang, P. Y. Zhang, M. Shamsi, J. L. Thelen, W. Qian, V. K. Truong, J. Ma, J. Hu, M. D. Dickey, *Nat. Mater.* **2022**, *21*, 359.
[33] X. Ding, L. Fan, L. Wang, M. Zhou, Y. Wang, Y. Zhao, *Mater. Horiz.* **2023**, *10*, 3929.
[34] Z. Wei, J. Yang, J. Zhou, F. Xu, M. Zrinyi, P. H. Dussault, Y. Osada, Y. Chen, *Chem. Soc. Rev.* **2014**, *43*, 8114.
[35] Q. Li, C. Liu, J. Wen, Y. Wu, Y. Shan, J. Liao, *Chin. Chem. Lett.* **2017**, *28*, 1857.
[36] S. Talebian, M. Mehrali, N. Taebnia, C. P. Pennisi, F. B. Kadumudi, J. Foroughi, M. Hasany, M. Nikkhah, M. Akbari, G. Orive, A. Dolatshahi-Pirouz, *Adv. Sci.* **2019**, *6*, 1801664.
[37] A. D. V. K. R. Shyam, A. Palaniappan, A. K. Jaiswal, T. H. Oh, A. J. Nathanael, *Polymers-Basel* **2021**, *13*, 3782.
[38] Y. Ou, M. Tian, *J. Mater. Chem. B* **2021**, *9*, 7955.
[39] P. Bertsch, M. Diba, D. J. Mooney, S. C. G. Leeuwenburgh, *Chem. Rev.* **2022**, *123*, 834.
[40] Y. Yang, L. Xu, J. Wang, Q. Meng, S. Zhong, Y. Gao, X. Cui, *Carbohydr. Polym.* **2022**, *283*, 119161.
[41] P. Kanokpaka, Y.-H. Chang, C.-C. Chang, M. Rinawati, P.-C. Wang, L.-Y. Chang, M.-H. Yeh, *Nano Energy* **2023**, *112*.
[42] M. S. Kim, J. W. Kim, J. Yun, Y. R. Jeong, S. W. Jin, G. Lee, H. Lee, D. S. Kim, K. Keum, J. S. Ha, *Appl. Surf. Sci.* **2020**, *515*, 146018.
[43] C. Larson, B. Peele, S. Li, S. Robinson, M. Totaro, L. Beccai, B. Mazzolai, R. Shepherd, *Science* **2016**, *351*, 1071.
[44] C. Chen, H. Guo, L. Chen, Y.-C. Wang, X. Pu, W. Yu, F. Wang, Z. Du, Z. L. Wang, *ACS Nano* **2020**, *14*, 4585.
[45] I. K. Han, K. I. Song, S. M. Jung, Y. Jo, J. Kwon, T. Chung, S. Yoo, J. Jang, Y. T. Kim, D. S. Hwang, Y. S. Kim, *Adv. Mater.* **2022**, *35*, 2203431.
[46] X. Song, X. Wang, J. Zhang, S. Shen, W. Yin, G. Ye, L. Wang, H. Hou, X. Qiu, *Biomaterials* **2021**, *273*, 120811.
[47] Z. Deng, H. Wang, P. Ma, B. Guo, *Nanoscale* **2020**, *12*, 1224.
[48] J. Kang, J. B. H. Tok, Z. Bao, *Nat. Electron.* **2019**, *2*, 144.
[49] J. Li, L. Geng, G. Wang, H. Chu, H. Wei, *Chem. Mater.* **2017**, *29*, 8932.
[50] J. Dahlke, S. Zechel, M. D. Hager, U. S. Schubert, *Adv. Mater. Interfaces* **2018**, *5*, 1800051.
[51] S. J. Garcia, *Eur. Polym. J.* **2014**, *53*, 118.
[52] W. Li, B. Dong, Z. Yang, J. Xu, Q. Chen, H. Li, F. Xing, Z. Jiang, *Adv. Mater.* **2018**, *30*, 1705679.
[53] Y. Zhang, A. Khademhosseini, *Science* **2017**, *356*, eaaf3627.
[54] S. Azevedo, A. M. S. Costa, A. Andersen, I. S. Choi, H. Birkedal, J. F. Mono, *Adv. Mater.* **2017**, *29*, 1700759.
[55] D. L. Taylor, M. I. H. Panhuis, *Adv. Mater.* **2016**, *28*, 9060.
[56] C. Li, J. Zuo, *Adv. Mater.* **2020**, *32*, 1903762.
[57] N. Zheng, Y. Xu, Q. Zhao, T. Xie, *Chem. Rev.* **2021**, *121*, 1716.
[58] J. Cui, A. del Campo, *Chem. Commun.* **2012**, *48*, 9302.
[59] Y. Lin, G. Li, *J. Mater. Chem. B* **2014**, *2*, 6878.
[60] D. C. Tuncaboylu, A. Argun, M. Sahin, M. Sari, O. Okay, *Polymer* **2012**, *53*, 5513.
[61] H. Zhang, H. Xia, Y. Zhao, *ACS Macro Lett.* **2012**, *1*, 1233.
[62] M. Gharakhloo, M. Karbarz, *Eur. Polym. J.* **2022**, *165*, 111004.
[63] D. Myung, D. Waters, M. Wiseman, P. E. Duhamel, J. Noolandi, C. N. Ta, C. W. Frank, *Polym. Adv. Technol.* **2008**, *19*, 647.
[64] J. P. Gong, Y. Katsuyama, T. Kurokawa, Y. Osada, *Adv. Mater.* **2003**, *15*, 1155.
[65] N. Yuan, L. Xu, H. Wang, Y. Fu, Z. Zhang, L. Liu, C. Wang, J. Zhao, J. Rong, *ACS Appl. Mater. Interfaces* **2016**, *8*, 34034.
[66] D. Zhao, M. Feng, L. Zhang, B. He, X. Chen, J. Sun, *Carbohydr. Polym.* **2021**, *256*, 117580.
[67] Z. Feng, H. Zuo, W. Gao, N. Ning, M. Tian, L. Zhang, *Macromol. Rapid Commun.* **2018**, *39*, 1800138.
[68] Z. Gong, G. Zhang, X. Zeng, J. H. Li, G. Li, W. Huang, R. Sun, C. Wong, *ACS Appl. Mater. Interfaces* **2016**, *8*, 24030.
[69] J. Wu, S. Han, T. Yang, Z. Li, Z. Wu, X. Gui, K. Tao, J. Miao, L. K. Norford, C. Liu, F. Huo, *ACS Appl. Mater. Interfaces* **2018**, *10*, 19097.
[70] X. Yan, Q. Chen, L. Zhu, H. Chen, D. Wei, F. Chen, Z. Tang, J. Yang, J. Zheng, *J. Mater. Chem. B* **2017**, *5*, 7683.
[71] H. Fan, J. Wang, Z. Jin, *Macromolecules* **2018**, *51*, 1696.
[72] L. Liu, X. Li, X. Ren, G. Wu, *Polymer* **2020**, *202*, 122657.
[73] C. Zhang, M. Wang, C. Jiang, P. Zhu, B. Sun, Q. Gao, C. Gao, R. Liu, *Nano Energy* **2022**, *95*, 106991.
[74] M. Caprioli, I. Roppolo, A. Chiappone, L. Larush, C. F. Pirri, S. Magdassi, *Nat. Commun.* **2021**, *12*, 2462.
[75] B. Liu, Y. Wang, Y. Miao, X. Zhang, Z. Fan, G. Singh, X. Zhang, K. Xu, B. Li, Z. Hu, M. Xing, *Biomaterials* **2018**, *171*, 83.
[76] H. G. Nam, M. G. Nam, P. J. Yoo, J. H. Kim, *Soft Matter* **2019**, *15*, 785.
[77] X. Gao, Q. Hu, K. Sun, H. Peng, X. Xie, H. A. Hamouda, G. Ma, *J. Alloys Compd.* **2021**, *888*, 161554.
[78] J. Chen, Q. Peng, T. Thundat, H. Zeng, *Chem. Mater.* **2019**, *31*, 4553.
[79] G. Zhang, L. Lv, Y. Deng, C. Wang, *Macromol. Rapid Commun.* **2017**, *38*, 1700018.
[80] S. Hou, X. Wang, S. Park, X. Jin, P. Ma, *Adv. Healthcare Mater.* **2015**, *4*, 1491.
[81] H. J. Won, B. Ryplida, S. G. Kim, G. Lee, J. H. Ryu, S. Y. Park, *ACS Nano* **2020**, *14*, 8409.
[82] L. Zhao, J. Zhao, F. Zhang, Z. Xu, F. Chen, Y. Shi, C. Hou, Y. Huang, C. Lin, R. Yu, W. Guo, *Adv. Healthcare Mater.* **2021**, *10*, 2002083.
[83] Q. Zhang, M. Wu, X. Hu, W. Lu, M. Wang, T. Li, Y. Zhao, *Macromol. Chem. Phys.* **2020**, *221*, 106991.
[84] J. Wang, F. Tang, Y. Wang, Q. Lu, S. Liu, L. Li, *ACS Appl. Mater. Interfaces* **2020**, *12*, 1558.
[85] H. Y. Yin, F. F. Liu, T. Abdiryim, X. Liu, *ACS Mater. Lett.* **2023**, *5*, 1787.
[86] A. Phadke, C. Zhang, B. Arman, C. C. Hsu, R. A. Mashelkar, A. K. Lele, M. J. Tauber, G. Arya, S. Varghese, *Proc. Natl. Acad. Sci. U.S.A.* **2012**, *109*, 4383.
[87] H. Wei, S. Du, Y. Liu, H. Zhao, C. Chen, Z. Li, J. Lin, Y. Zhang, J. Zhang, X. Wan, *Chem. Commun.* **2014**, *50*, 1447.
[88] S. Wang, J. Lei, X. Yi, L. Yuan, L. Ge, D. Li, C. Mu, *ACS Appl Polym Mater* **2020**, *2*, 3016.
[89] M. A. Darabi, A. Khosrozadeh, R. Mbeleck, Y. Liu, Q. Chang, J. Jiang, J. Cai, Q. Wang, G. Luo, M. Xing, *Adv. Mater.* **2017**, *29*, 1700533.
[90] C. Shao, L. Meng, C. Cui, J. Yang, *J. Mater. Chem. C* **2019**, *7*, 15208.
[91] Y. Zhu, L. Lin, Y. Chen, Y. Song, W. Lu, Y. Guo, *Soft Matter* **2020**, *16*, 2238.
[92] D. Yang, Y. Wang, Z. Li, Y. Xu, F. Cheng, P. Li, H. Li, *J. Mater. Chem. C* **2018**, *6*, 1153.
[93] X. Li, L. He, Y. Li, M. Chao, M. Li, P. Wan, L. Zhang, *ACS Nano* **2021**, *15*, 12453.
[94] T. Yu, X. Lei, Y. Zhou, H. Chen, *Polym. Adv. Technol.* **2021**, *32*, 3167.
[95] Y. Zhu, J. Liu, T. Guo, J. Wang, X. Tang, V. Nicolosi, *ACS Nano* **2021**, *15*, 1465.
[96] Z. Zhang, T. Chao, S. Jiang, *J. Phys. Chem. B* **2008**, *112*, 5327.

[97] Q. Li, C. Wen, J. Yang, X. Zhou, Y. Zhu, J. Zheng, G. Cheng, J. Bai, T. Xu, J. Ji, S. Jiang, L. Zhang, P. Zhang, *Chem. Rev.* **2022**, *122*, 17073.
[98] X. Pei, H. Zhang, Y. Zhou, L. Zhou, J. Fu, *Mater. Horiz.* **2020**, *7*, 1872.
[99] Y. Sun, S. Lu, Q. Li, Y. Ren, Y. Ding, H. Wu, X. He, Y. Shang, *Eur. Polym. J.* **2020**, *133*, 109761.
[100] L. Wang, G. Gao, Y. Zhou, T. Xu, J. Chen, R. Wang, R. Zhang, J. Fu, *ACS Appl. Mater. Interfaces* **2019**, *11*, 3506.
[101] M. Wu, J. Chen, W. Huang, B. Yan, Q. Peng, J. Liu, L. Chen, H. Zeng, *Biomacromolecules* **2020**, *21*, 2409.
[102] J. Zhao, D. D. Diaz, M. Wu, Y. Peng, J. Wang, H. Zeng, W. Duan, L. Kong, X. Hao, R. Narain, *Biomacromolecules* **2021**, *22*, 800.
[103] Y. Chen, W. Wang, D. Wu, M. Nagao, D. Hall, T. Thundat, R. Narain, *Biomacromolecules* **2018**, *19*, 596.
[104] S. Zhang, Y. Chen, H. Liu, Z. Wang, H. Ling, C. Wang, J. Ni, B. Çelebi-Saltik, X. Wang, X. Meng, H. J. Kim, A. Baidya, S. Ahadian, N. Ashammakhi, M. R. Dokmeci, J. Travas-Sejdic, A. Khademhosseini, *Adv. Mater.* **2020**, *32*, 1904752.
[105] Z. Deng, Y. He, Y. Wang, Y. Zhao, L. Chen, *Soft Matter* **2020**, *16*, 6128.
[106] J. Zheng, P. Xiao, W. Liu, J. Zhang, Y. Huang, T. Chen, *Macromol. Rapid Commun.* **2016**, *37*, 265.
[107] F. Luo, T. Sun, T. Nakajima, T. Kurokawa, Y. Zhao, K. Sato, A. Bin Ihsan, X. Li, H. Guo, J. Gong, *Adv. Mater.* **2015**, *27*, 2722.
[108] S. Wu, J. Guo, Y. Wang, H. Xie, S. Zhou, *ACS Appl. Mater. Interfaces* **2022**, *14*, 42317.
[109] S. Wang, M. W. Urban, *Nat. Rev. Mater.* **2020**, *5*, 562.
[110] D. L. Taylor, M. Het Panhuis, *Adv. Mater.* **2016**, *28*, 9060.
[111] T. Qin, W. Liao, L. Yu, J. Zhu, M. Wu, Q. Peng, L. Han, H. Zeng, *J. Polym Sci.* **2022**, *60*, 2607.
[112] S. Wu, M. Qiu, Z. Tang, B. Guo, *J. Phys. Chem. C* **2017**, *121*, 28594.
[113] S. Yanagisawa, I. Hamada, K. Lee, D. C. Langreth, Y. Morikawa, *Phys. Rev. B* **2011**, *83*, 113401.
[114] Y. Rao, A. Chortos, R. Pfattner, F. Lissel, Y. C. Chiu, V. Feig, J. Xu, T. Kurosawa, X. Gu, C. Wang, M. He, J. Chung, Z. Bao, *J. Am. Chem. Soc.* **2016**, *138*, 6020.
[115] I. Hussain, S. M. Sayed, S. Liu, F. Yao, O. Oderinde, G. Fu, *Eur. Polym. J.* **2018**, *100*, 219.
[116] Z. Zhang, Z. Gao, Y. Wang, L. Guo, C. Yin, X. Zhang, J. Hao, G. Zhang, L. Chen, *Macromolecules* **2019**, *52*, 2531.
[117] L. Zhao, X. Li, Y. Li, X. Wang, W. Yang, J. Ren, *Biomacromolecules* **2021**, *22*, 1273.
[118] Y. Jiao, K. Lu, Y. Lu, Y. Yue, X. Xu, H. Xiao, J. Li, J. Han, *Cellulose* **2021**, *28*, 4295.
[119] J. Cao, P. Wu, Q. Cheng, C. He, Y. Chen, J. Zhou, *ACS Appl. Mater. Interfaces* **2021**, *13*, 24095.
[120] M. A. Darabi, A. Khosrozadeh, R. Mbeleck, Y. Liu, Q. Chang, J. Jiang, J. Cai, Q. Wang, G. Luo, M. Xing, *Adv. Mater.* **2018**, *30*, 1700533.
[121] C. Shao, H. Chang, M. Wang, F. Xu, J. Yang, *ACS Appl. Mater. Interfaces* **2017**, *9*, 28305.
[122] N. Holten-Andersen, M. J. Harrington, H. Birkedal, B. P. Lee, P. B. Messersmith, K. Y. C. Lee, J. H. Waite, *Proc. Natl. Acad. Sci. U.S.A.* **2011**, *108*, 2651.
[123] X. Zhao, Y. Liang, Y. Huang, J. He, Y. Han, B. Guo, *Adv. Funct. Mater.* **2020**, *30*, 1910748.
[124] Y. Liang, Z. Li, Y. Huang, R. Yu, B. Guo, *ACS Nano* **2021**, *15*, 7078.
[125] Z. Jia, Y. Zeng, P. Tang, D. Gan, W. Xing, Y. Hou, K. Wang, C. Xie, X. Lu, *Chem. Mater.* **2019**, *31*, 5625.
[126] S. Jin, Y. Kim, D. Son, M. Shin, *Gels* **2022**, *8*, 336.
[127] J. Shin, S. An, S. Choi, M. Shin, J. S. Lee, J. H. Cho, H. Lee, S.-W. Cho, *Nano Lett.* **2023**, *23*, 5934.
[128] M. Krogsgaard, V. Nue, H. Birkedal, *Chem. - Eur. J.* **2016**, *22*, 844.
[129] I. Tunn, M. J. Harrington, K. G. Blank, *Biomimetics* **2019**, *4*, 25.
[130] X. Xu, V. V. Jerca, R. Hoogenboom, *Macromol. Rapid Commun.* **2020**, *41*, 1900457.
[131] H. Qin, T. Zhang, H. Li, H. Cong, M. Antonietti, S. Yu, *Chem* **2017**, *3*, 691.
[132] L. Shi, Y. Zhao, Q. Xie, C. Fan, J. Hilborn, J. Dai, D. A. Ossipov, *Adv. Healthcare Mater.* **2018**, *7*, 1700973.
[133] L. Shi, P. Ding, Y. Wang, Y. Zhang, D. Ossipov, J. Hilborn, *Macromol. Rapid Commun.* **2019**, *40*, 1800837.
[134] Y. Jia, M. Zhang, X. Zhu, *Macromolecules* **2017**, *50*, 9696.
[135] M. Zhang, D. Xu, X. Yan, J. Chen, S. Dong, B. Zheng, F. Huang, *Angew. Chem., Int. Ed.* **2012**, *51*, 7011.
[136] J. Jin, L. Cai, Y. Jia, S. Liu, Y. Chen, L. Ren, *J. Mater. Chem. B* **2019**, *7*, 1637.
[137] X. Ma, Y. Zhao, *Chem. Rev.* **2015**, *115*, 7794.
[138] H. Yang, B. Yuan, X. Zhang, O. A. Scherman, *Acc. Chem. Res.* **2014**, *47*, 2106.
[139] Q. Gao, J. Hu, J. Shi, W. Wu, D. K. Debeli, P. Pan, G. Shan, *Soft Matter* **2020**, *16*, 10558.
[140] Y. Jia, J. Jin, S. Liu, L. Ren, J. Luo, X. Zhu, *Biomacromolecules* **2018**, *19*, 626.
[141] Z. Yu, J. Liu, C. S. Y. Tan, O. A. Scherman, C. Abell, *Angew. Chem., Int. Ed.* **2018**, *57*, 3079.
[142] X. Liu, Z. Ren, F. Liu, L. Zhao, Q. Ling, H. Gu, *ACS Appl. Mater. Interfaces* **2021**, *13*, 14625.
[143] X. Ma, N. Zhou, T. Zhang, W. Hu, N. Gu, *Mater. Sci. Eng. C* **2017**, *73*, 357.
[144] M. S. de Luna, V. Marturano, M. Manganelli, C. Santillo, V. Ambrogi, G. Filippone, P. Cerruti, *J. Colloid Interface Sci.* **2020**, *568*, 16.
[145] M. Mohamadhoseini, Z. Mohamadnia, *Coord. Chem. Rev.* **2021**, *432*, 213711.
[146] M. Nakahata, Y. Takashima, H. Yamaguchi, A. Harada, *Nat. Commun.* **2011**, *2*, 511.
[147] K. Miyamae, M. Nakahata, Y. Takashima, A. Harada, *Angew. Chem., Int. Ed.* **2015**, *54*, 8984.
[148] Z. Wang, Y. Ren, Y. Zhu, L. Hao, Y. Chen, G. An, H. Wu, X. Shi, C. Mao, *Angew. Chem., Int. Ed.* **2018**, *57*, 9008.
[149] Z. Wang, G. An, Y. Zhu, X. Liu, Y. Chen, H. Wu, Y. Wang, X. Shi, C. Mao, *Mater. Horiz.* **2019**, *6*, 733.
[150] H. Xiong, Y. Li, H. Ye, G. Huang, D. Zhou, Y. Huang, *J. Mater. Chem. B* **2020**, *8*, 10309.
[151] R. Yu, Y. Yang, J. He, M. Li, B. Guo, *Chem. Eng. J.* **2021**, *417*, 128278.
[152] J. Kim, J. W. Kim, S. Kim, K. Keum, J. Park, Y. R. Jeong, S. W. Jin, J. S. Ha, *Chem. Eng. J.* **2021**, *422*, 130121.
[153] P. Chakma, D. Konkolewicz, *Angew. Chem., Int. Ed.* **2019**, *58*, 9682.
[154] H. Wang, S. C. Heilshorn, *Adv. Mater.* **2015**, *27*, 3717.
[155] J. Ye, S. Fu, S. Zhou, M. Li, K. Li, W. Sun, Y. Zhai, *Eur. Polym. J.* **2020**, *139*, 110024.
[156] A. Chao, J. Negulescu, D. Zhang, *Macromolecules* **2016**, *49*, 6277.
[157] K. Deng, S. Zhou, Z. Xu, M. Xiao, Y. Meng, *Chem. Eng. J.* **2022**, *428*, 131224.
[158] H. Guo, S. Huang, A. Xu, W. Xue, *Chem. Mater.* **2022**, *34*, 2655.
[159] H. Guo, S. Huang, X. Yang, J. Wu, T. B. Kirk, J. Xu, A. Xu, W. Xue, *ACS Appl. Mater. Interfaces* **2021**, *13*, 61638.
[160] Y. Liu, S. Lin, W. Chuang, N. Dai, S. H. Hsu, *ACS Appl. Mater. Interfaces* **2022**, *14*, 16032.
[161] W. Huang, Y. Wang, Y. Chen, Y. Zhao, Q. Zhang, X. Zheng, L. Chen, L. Zhang, *Adv. Healthcare Mater.* **2016**, *5*, 2813.
[162] Z. Jiang, B. Diggle, I. C. G. Shackleford, L. A. Connal, *Adv. Mater.* **2019**, *31*, 1904956.
[163] W. Wang, L. Xiang, L. Gong, W. Hu, W. Huang, Y. Chen, A. B. Asha, S. Srinivas, L. Chen, R. Narain, H. Zeng, *Chem. Mater.* **2019**, *31*, 2366.
[164] G. Xiao, Y. Wang, H. Zhang, L. Chen, S. Fu, *Carbohydr. Polym.* **2019**, *218*, 68.
[165] M. S. Q. Zhu, H. Jin, T. Shao, Y. Li, J. Liu, L. Gan, M. Long, *Mater. Des.* **2020**, *192*, 108723.

[166] X. Jiang, X. Yang, B. Yang, L. Zhang, A. Lu, *Carbohydr. Polym.* **2021**, *273*, 118547.
[167] L. Qiao, C. Liu, C. Liu, L. Zong, H. Gu, C. Wang, X. Jian, *Eur. Polym. J.* **2022**, *162*, 110838.
[168] C. Sun, H. Jia, K. Lei, D. Zhu, Y. Gao, Z. Zheng, X. Wang, *Polymer* **2019**, *160*, 246.
[169] X. Yang, G. Liu, L. Peng, J. Guo, L. Tao, J. Yuan, C. Chang, Y. Wei, L. Zhang, *Adv. Funct. Mater.* **2017**, *27*, 1703174.
[170] M. Chen, J. Tian, Y. Liu, H. Cao, R. Li, J. Wang, J. Wu, Q. Zhang, *Chem. Eng. J.* **2019**, *373*, 413.
[171] S. W. Kim, D. Y. Kim, H. H. Roh, H. S. Kim, J. W. Lee, K. Y. Lee, *Biomacromolecules* **2019**, *20*, 1860.
[172] Z. Wei, J. Yang, Z. Liu, F. Xu, J. Zhou, M. Zrinyi, Y. Osada, Y. Chen, *Adv. Funct. Mater.* **2015**, *25*, 1352.
[173] S. Mukherjee, M. R. Hill, B. S. Sumerlin, *Soft Matter* **2015**, *11*, 6152.
[174] M. Nadgorny, J. Collins, Z. Xiao, P. J. Scales, L. A. Connal, *Polym. Chem.* **2018**, *9*, 1684.
[175] S. H. Hong, S. Kim, J. P. Park, M. Shin, K. Kim, J. H. Ryu, H. Lee, *Biomacromolecules* **2018**, *19*, 2053.
[176] Y. Choi, K. Park, H. Choi, D. Son, M. Shin, *Polymers-Basel* **2021**, *13*, 1133.
[177] H. Zheng, N. Lin, Y. He, B. Zuo, *ACS Appl. Mater. Interfaces* **2021**, *13*, 40013.
[178] X. Zhou, A. Rajeev, A. Subramanian, Y. Li, N. Rossetti, G. Natale, G. A. Lodygensky, F. Cicoira, *Acta Biomater.* **2022**, *139*, 296.
[179] A. Chae, G. Murali, S. Y. Lee, J. Gwak, S. J. Kim, Y. J. Jeong, H. Kang, S. Park, A. S. Lee, D. Y. Koh, I. In, S. J. Park, *Adv. Funct. Mater.* **2023**, 33.
[180] Z. Nie, K. Peng, L. Lin, J. Yang, Z. Cheng, Q. Gan, Y. Chen, C. Feng, *Chem. Eng. J.* **2023**, 454.
[181] X. Chai, J. Tang, Y. Li, Y. Cao, X. Chen, T. Chen, Z. Zhang, *ACS Appl. Mater. Interfaces* **2023**, *15*, 18262.
[182] M. M. Perera, N. Ayres, *Polym. Chem.* **2020**, *11*, 1410.
[183] Z. Wei, J. Yang, J. Zhou, F. Xu, M. Zrinyi, P. Dussault, Y. Osada, Y. Chen, *Chem. Soc. Rev.* **2014**, *43*, 8114.
[184] F. Ji, J. Li, G. Zhang, W. Lan, R. Sun, C. Wong, *Polymer* **2019**, *184*, 121882.
[185] G. Bovone, O. Y. Dudaryeva, B. Marco-Dufort, M. W. Tibbitt, *ACS Biomater. Sci. Eng.* **2021**, *7*, 4048.
[186] S. Shahi, H. Roghani-Mamaqani, S. Talebi, H. Mardani, *Coord. Chem. Rev.* **2022**, *455*, 214368.
[187] Z. Jiang, A. Bhaskaran, H. M. Aitken, I. C. G. Shackleford, L. A. Connal, *Macromol. Rapid Commun.* **2019**, *40*, 1900038.
[188] S. Das, P. Martin, G. Vasilyev, R. Nandi, N. Amdursky, E. Zussman, *Macromolecules* **2020**, *53*, 11130.
[189] J. Pan, Y. Jin, S. Lai, L. Shi, W. Fan, Y. Shen, *Chem. Eng. J.* **2019**, *370*, 1228.
[190] J. Mo, Y. Dai, C. Zhang, Y. Zhou, W. Li, Y. Song, C. Wu, Z. A. K. Wang, *Mater. Horiz.* **2021**, *8*, 3409.
[191] Q. Zhang, C. Shi, D. Qu, Y. Long, B. Feringa, H. Tian, *Sci. Adv.* **2018**, *4*, eaat8192.
[192] X. Huang, G. Ge, M. She, Q. Ma, Y. Lu, W. Zhao, Q. Shen, Q. Wang, J. Shao, *Appl. Surf. Sci.* **2022**, *598*, 153803.
[193] M. Wu, J. Chen, Y. Ma, B. Yan, M. Pan, Q. Peng, W. Wang, L. Han, J. Liu, H. Zeng, *J. Mater. Chem. A* **2020**, *8*, 24718.
[194] Q. Wang, J. L. Mynar, M. Yoshida, E. Lee, M. Lee, K. Okuro, K. Kinbara, T. Aida, *Nature* **2010**, *463*, 339.
[195] Y. Shen, Z. Wang, Y. Wang, Z. Meng, Z. Zhao, *Carbohydr. Polym.* **2021**, *274*, 118642.
[196] M. M. Ghobashy, N. E. A. A. El-Sattar, *Macromol. Chem. Phys.* **2020**, *221*, 2000218.
[197] L. Zhao, Z. Ren, X. Liu, Q. Ling, Z. Li, H. Gu, *ACS Appl. Mater. Interfaces* **2021**, *13*, 11344.
[198] H. Fu, B. Wang, J. Li, J. Xu, J. Li, J. Zeng, W. Gao, K. Chen, *Mater Horiz.* **2022**, 1412.
[199] U. Gulyuz, O. Okay, *Macromolecules* **2014**, *47*, 6889.
[200] S. Ramesh, S. Khan, Y. Park, E. Ford, S. Menegatti, J. Genzer, *Mater. Today* **2022**, *54*, 90.
[201] N. D. Watuthanthrige, B. Ahmed, M. T. Dolan, Q. H. Fang, J. Wu, J. L. Sparks, M. B. Zanjani, D. Konkolewicz, Z. Ye, *Mater. Horiz.* **2020**, *7*, 1581.
[202] Y. Yang, X. Ding, M. W. Urban, *Prog. Polym. Sci.* **2015**, *49*, 34.
[203] P. Cordier, F. Tournilhac, C. Soulie-Ziakovic, L. Leibler, *Nature* **2008**, *451*, 977.
[204] X. He, Y. Zeng, G. Liu, Y. Tian, Y. Wei, L. Zhao, L. Yang, L. Tao, *ACS Macro Lett.* **2022**, *11*, 39.
[205] T. Liu, F. Wang, Q. Wu, T. Chen, P. Sun, *Mater. Horiz.* **2021**, *8*, 3096.
[206] Y. Zhang, B. Yang, X. Zhang, L. Xu, L. Tao, S. Li, Y. Wei, *Chem. Commun.* **2012**, *48*, 9305.
[207] Y. Yang, M. W. Urban, *Chem. Soc. Rev.* **2013**, *42*, 7446.
[208] X. Chen, M. Dam, K. Ono, A. Mal, H. Shen, S. Nutt, K. Sheran, F. Wudl, *Science* **2002**, *295*, 1698.
[209] Z. Wei, J. Yang, X. Du, F. Xu, M. Zrinyi, Y. Osada, F. Li, Y. Chen, *Macromol. Rapid Commun.* **2013**, *34*, 1464.
[210] Q. Zhang, J. Duan, Q. Guo, J. Zhang, D. Zheng, F. Yi, X. Yang, Y. Duan, Q. Tang, *Angew. Chem., Int. Ed.* **2022**, *61*, 202116632.
[211] Y. Jin, C. Yu, R. J. Denman, W. Zhang, *Chem. Soc. Rev.* **2013**, *42*, 6634.
[212] N. Zhong, W. Post, *Compos. Part a-Appl. S.* **2015**, *69*, 226.
[213] S. Terryn, J. Langenbach, E. Roels, J. Brancart, C. Bakkali-Hassani, Q. A. Poutrel, A. Georgopoulou, T. G. Thuruthel, A. Safaei, P. Ferrentino, T. Sebastian, S. Norvez, F. Iida, A. W. Bosman, F. Tournilhac, F. Clemens, G. Van Assche, B. Vanderborght, *Mater. Today* **2021**, *47*, 187.
[214] G. Hizal, U. Tunca, A. Sanyal, *J Polym Sci A Polym Chem* **2011**, *49*, 4103.
[215] C. Shao, M. Wang, H. Chang, F. Xu, J. Yang, *ACS Sustainable Chem. Eng.* **2017**, *5*, 6167.
[216] Y. Zhang, Q. Wang, Z. Wang, D. Zhang, J. Gu, K. Ye, D. Su, Y. Zhang, J. Chen, M. Barboiu, *ChemPlusChem* **2021**, *86*, 1524.
[217] D. Li, S. Wang, Y. Meng, Z. Guo, M. Cheng, J. Li, *Carbohydr. Polym.* **2021**, *268*, 118244.
[218] X. Dai, Y. Zhang, L. Gao, T. Bai, W. Wang, Y. Cui, W. Liu, *Adv. Mater.* **2015**, *27*, 3566.
[219] J. Yang, V. Cristian, A. Dong, J. Zhang, *Macromol. Chem. Phys.* **2021**, *222*, 2000429.
[220] Y. Guo, M. He, Y. Peng, Q. Zhang, L. Yan, X. Zan, *J. Mater. Sci.* **2020**, *55*, 9109.
[221] Z. Wang, H. Zhou, W. Chen, Q. Li, B. Yan, X. Jin, A. Ma, H. Liu, W. Zhao, *ACS Appl. Mater. Interfaces* **2018**, *10*, 14045.
[222] Z. Mousavikhamene, G. C. Schatz, *ACS Appl. Nano Mater.* **2022**, *5*, 13649.
[223] J. Wu, Z. Wu, Y. Wei, H. Ding, W. Huang, X. Gui, W. Shi, Y. Shen, K. Tao, X. Xie, *ACS Appl. Mater. Interfaces* **2020**, *12*, 19069.
[224] D. Habault, H. Zhang, Y. Zhao, *Chem. Soc. Rev.* **2013**, *42*, 7244.
[225] L. Yang, Z. Wang, G. Fei, H. Xia, *Macromol. Rapid Commun.* **2017**, *38*, 1700421.
[226] M. A. Azagarsamy, D. D. McKinnon, D. L. Alge, K. S. Anseth, *ACS Macro Lett.* **2014**, *3*, 515.
[227] L. Yu, K. Xu, L. Ge, W. Wan, A. Darabi, M. Xing, W. Zhong, *Macromol. Biosci.* **2016**, *16*, 1381.
[228] V. X. Truong, F. Y. Li, F. Ercole, J. S. Forsythe, *ACS Macro Lett.* **2018**, *7*, 464.
[229] Y. Wang, Q. Liu, J. Li, L. Ling, G. Zhang, R. Sun, C. Wong, *Polymer* **2019**, *172*, 187.
[230] L. Li, J. M. Scheiger, P. A. Levkin, *Adv. Mater.* **2019**, *31*, 1807333.
[231] T. Li, Z. Zhang, M. Rong, M. Zhang, *J. Appl. Polym. Sci.* **2019**, *136*, 47700.

[232] S. L. Banerjee, K. Bhattacharya, S. Samanta, N. K. Singha, *ACS Appl. Mater. Interfaces* **2018**, *10*, 27391.
[233] P. Dong, K. Cui, F. Xu, T. Jiang, Z. Ma, *Polym. Int.* **2018**, *67*, 868.
[234] B. Zhang, J. He, M. Shi, Y. Liang, B. Guo, *Chem. Eng. J.* **2020**, *400*, 125994.
[235] E. Zhang, T. Wang, L. Zhao, W. Sun, X. Liu, Z. Tong, *ACS Appl. Mater. Interfaces* **2014**, *6*, 22855.
[236] W. Xu, W. Wang, S. Chen, R. Zhang, Y. Wang, Q. Zhang, L. Yuwen, W. Yang, L. Wang, *J. Colloid Interface Sci.* **2021**, *586*, 601.
[237] X. Cao, H. Liu, X. Yang, J. Tian, B. Luo, M. Liu, *Compos. Sci. Technol.* **2020**, *191*, 108071.
[238] W. Yang, X. Wang, R. Zhang, Y. Wang, Q. Qiu, L. Yuwen, L. Wang, *J. Mater. Chem. B* **2021**, *9*, 2266.
[239] B. Li, L. Kan, S. Zhang, Z. Liu, C. Li, W. Li, X. Zhang, H. Wei, N. Ma, *Nanoscale* **2019**, *11*, 467.
[240] L. Wang, Q. Cao, X. Wang, D. Wu, *Soft Matter* **2022**, *18*, 3004.
[241] W. Xu, M. Rong, M. Zhang, *J. Mater. Chem. A* **2016**, *4*, 10683.
[242] X. Zhang, X. Liang, Q. Huang, H. Zhang, C. Liu, Y. Liu, *Soft Matter* **2020**, *16*, 9833.
[243] Z. Wei, Y. Deng, M. Yu, H. Yu, *Liq. Cryst.* **2020**, *47*, 1170.
[244] M. Wang, C. Nie, J. Liu, S. Wu, *Nat. Commun.* **2023**, *14*, 1000.
[245] L. Hu, P. L. Chee, S. Sugiarto, Y. Yu, C. Shi, R. Yan, Z. Yao, X. Shi, J. Zhi, D. Kai, H. D. Yu, W. Huang, *Adv. Mater.* **2023**, *35*, 2205326.
[246] T. Liu, S. Zou, C. Hang, J. Li, X. Di, X. Li, Q. Wu, F. Wang, P. Sun, *Polym. Chem.* **2020**, *11*, 1906.
[247] P. Guo, J. Liang, Y. Li, X. Lu, H. Fu, H. Jing, S. Guan, D. Han, L. Niu, *Colloid. Surface. A.* **2019**, *571*, 64.
[248] A. Shit, S. G. Kim, I. In, S. Y. Park, *Chem. Eng. J.* **2021**, *426*, 131846.
[249] F. Fu, Z. Chen, Z. Zhao, H. Wang, L. Shang, Z. Gu, Y. Zhao, *Proc. Natl. Acad. Sci. U.S.A.* **2017**, *114*, 5900.
[250] G. He, H. Lei, W. Sun, J. Gu, W. Yu, D. Zhang, H. Chen, Y. Li, M. Qin, B. Xue, W. Wang, Y. Cao, *Angew. Chem., Int. Ed.* **2022**, *61*, 202201765.
[251] P. Li, Y. Zhong, X. Wang, J. Hao, *ACS Cent. Sci.* **2020**, *6*, 1507.
[252] Z. Han, P. Wang, G. Mao, T. Yin, D. Zhong, B. Yiming, X. Hu, Z. Jia, G. Nian, S. Qu, W. Yang, *ACS Appl. Mater. Interfaces* **2020**, *12*, 12010.
[253] X. Lu, G. Fei, H. Xia, Y. Zhao, *J. Mater. Chem. A* **2014**, *2*, 16051.
[254] A. V. Shibaev, M. E. Smirnova, D. E. Kessel, S. A. Bedin, I. V. Razumovskaya, O. E. Philippova, *Nanomaterials* **2021**, *11*, 1271.
[255] B. Zhao, Z. Bai, H. Lv, Z. Yan, Y. Du, X. Guo, J. Zhang, L. Wu, J. Deng, D. Zhang, R. Che, *Nanomicro Lett* **2023**, *15*, 79.
[256] H. Qin, P. Liu, C. Chen, H. Cong, S. Yu, *Nat. Commun.* **2021**, *12*, 4297.
[257] W. Pu, D. Fu, Z. Wang, X. Gan, X. Lu, L. Yang, H. Xia, *Adv. Sci.* **2018**, *5*, 1800101.
[258] H. Wang, Y. Yang, M. Zhang, Q. Wang, K. Xia, Z. Yin, Y. Wei, Y. Ji, Y. Zhang, *ACS Appl. Mater. Interfaces* **2020**, *12*, 14315.
[259] T. Wang, W. Yu, W. Sun, L. Jia, J. Gao, J. Tang, H. Su, D. Yan, Z. Li, *Compos. Sci. Technol.* **2020**, *200*, 108446.
[260] L. Huang, N. Yi, Y. Wu, Y. Zhang, Q. Zhang, Y. Huang, Y. Ma, Y. Chen, *Adv. Mater.* **2013**, *25*, 2224.
[261] C. Chen, H. Qin, H. Cong, S. Yu, *Adv. Mater.* **2019**, *31*, 1900573.
[262] Y. Zhou, G. T. Liu, S. Y. Guo, *J. Mater. Chem. B* **2022**, *10*, 3947.
[263] Y. Li, G. Huang, X. Zhang, B. Li, Y. Chen, T. Lu, T. J. Lu, F. Xu, *Adv. Funct. Mater.* **2013**, *23*, 660.
[264] L. Y. Z. Shuai, Z. H. Guo, P. P. Zhang, J. M. Wan, X. Pu, Z. L. Wang, *Nano Energy* **2020**, *78*, 105389.
[265] L. Zhou, C. Dai, L. Fan, Y. Jiang, C. Liu, Z. Zhou, P. Guan, Y. Tian, J. Xing, X. Li, Y. Luo, P. Yu, C. Ning, G. Tan, *Adv. Funct. Mater.* **2021**, *31*, 2007457.
[266] C. Wang, Y. Liu, X. Qu, B. Shi, Q. Zheng, X. Lin, S. Chao, C. Wang, J. Zhou, Y. Sun, G. Mao, Z. Li, *Adv. Mater.* **2022**, *34*, 2105416.
[267] Q. Rong, W. Lei, L. Chen, Y. Yin, J. Zhou, M. Liu, *Angew. Chem., Int. Ed.* **2017**, *56*, 14159.
[268] X. Su, H. Wang, Z. Tian, X. Duan, Z. Chai, Y. Feng, Y. Wang, Y. Fan, J. Huang, *ACS Appl. Mater. Interfaces* **2020**, *12*, 29757.
[269] W. Zheng, L. Xu, Y. Li, Y. Huang, B. Li, Z. Jiang, G. Gao, *J. Colloid Interface Sci.* **2021**, *594*, 584.
[270] H. Gao, Z. Zhao, Y. Cai, J. Zhou, W. Hua, L. Chen, L. Wang, J. Zhang, D. Han, M. Liu, L. Jiang, *Nat. Commun.* **2017**, *8*, 15911.
[271] H. Liao, X. Guo, P. Wan, G. Yu, *Adv. Funct. Mater.* **2019**, *29*, 1904507.
[272] Y. Wang, B. Pang, R. Wang, Y. Gao, Y. Liu, C. Gao, *Compos. Part a-Appl. S.* **2022**, *160*, 107039.
[273] L. Huang, X. Dai, Z. Sun, M. Wong, S. Pang, J. Han, Q. Zheng, C. Zhao, J. Kong, J. Hao, *Nano Energy* **2021**, *82*, 105724.
[274] T. Ke, L. Zhao, X. Fan, H. Gu, *J. Mater. Sci. Technol.* **2023**, *135*, 199.
[275] S. Xue, Y. Wu, M. Guo, Y. Xia, D. Liu, H. Zhou, W. Lei, *Soft Matter* **2019**, *15*, 3680.
[276] Y. Zhang, T. Li, L. Miao, P. Kaur, S. Men, Q. Wang, X. Gong, Y. Fang, C. Zhai, S. Zhang, L. Zhang, L. Ye, *J. Mater. Chem. A* **2022**, *10*, 3970.
[277] W. Zhang, B. Wu, S. Sun, P. Wu, *Nat. Commun.* **2021**, *12*, 4082.
[278] X. Guo, F. Yang, X. Sun, Y. Bai, G. Liu, W. Liu, R. Wang, X. He, *Adv. Funct. Mater.* **2022**, *32*, 2201230.
[279] Q. Fan, Y. Nie, Q. Sun, W. Wang, L. Bai, H. Chen, L. Yang, H. Yang, D. Wei, *ACS Appl Polym Mater* **2022**, *4*, 1626.
[280] Z. Liu, Y. Wang, Y. Ren, G. Jin, C. Zhang, W. Chen, F. Yan, *Mater. Horiz.* **2020**, *7*, 919.
[281] X. Zhang, X. Ma, T. Hou, K. Guo, J. Yin, Z. Wang, L. Shu, M. He, J. Yao, *Angew. Chem., Int. Ed.* **2019**, *58*, 7366.
[282] B. K. Ahn, D. W. Lee, J. N. Israelachvili, J. H. Waite, *Nat. Mater.* **2014**, *13*, 867.
[283] W. Chen, D. Hao, W. Hao, X. Guo, L. Jiang, *ACS Appl. Mater. Interfaces* **2018**, *10*, 1258.
[284] Y. Wang, H. Huang, J. Wu, L. Han, Z. Yang, Z. Jiang, R. Wang, Z. Huang, M. Xu, *ACS Sustainable Chem. Eng.* **2020**, *8*, 18506.
[285] X. Wei, D. Chen, X. Zhao, J. Luo, H. Wang, P. Jia, *ACS Appl Polym Mater* **2021**, *3*, 837.
[286] X. Su, Y. Luo, Z. Tian, Z. Yuan, Y. Han, R. Dong, L. Xu, Y. Feng, X. Liu, J. Huang, *Mater. Horiz.* **2020**, *7*, 2651.
[287] R. Fu, Y. Guan, C. Xiao, L. Fan, Z. Wang, Y. Li, P. Yu, L. Tu, G. Tan, J. Zhai, L. Zhou, C. Ning, *Small Methods* **2022**, *6*, 2101513.
[288] Y. Cao, H. Wu, S. I. Allec, B. Wong, D. S. Nguyen, C. Wang, *Adv. Mater.* **2018**, *30*, 1804602.
[289] Z. Yu, P. Wu, *Adv. Mater.* **2021**, *33*, 2008479.
[290] X. Liu, Q. Zhang, F. Jia, G. Gao, *Sci. China Mater.* **2021**, *64*, 3069.
[291] Y. Liu, M. Su, Y. Fu, P. Zhao, M. Xia, Y. Zhang, B. He, P. He, *Chem. Eng. J.* **2018**, *354*, 1185.
[292] Q. Ling, W. Liu, J. Liu, L. Zhao, Z. Ren, H. Gu, *ACS Appl. Mater. Interfaces* **2022**, *14*, 24741.
[293] S. Deng, L. Wang, C. Zhao, D. Xiang, H. Li, B. Wang, Z. Li, H. Zhou, Y. Wu, *Colloid. Surface. A.* **2023**, *656*, 130380.
[294] C. M. Boutry, A. Nguyen, Q. O. Lawal, A. Chortos, S. Rondeau-Gagne, Z. Bao, *Adv. Mater.* **2015**, *27*, 6954.
[295] K. Meng, X. Xiao, W. Wei, G. Chen, A. Nashalian, S. Shen, X. Xiao, J. Chen, *Adv. Mater.* **2022**, *34*, 2109357.
[296] X. Wang, Z. Liu, T. Zhang, *Small* **2017**, *13*, 1602790.
[297] B. Ying, X. Liu, *iScience* **2021**, *24*, 103174.
[298] Y. Liu, W. Cao, M. Ma, P. Wan, *ACS Appl. Mater. Interfaces* **2017**, *9*, 25559.
[299] X. Li, L. He, Y. Li, M. Chao, M. Li, P. Wan, L. Zhang, *ACS Nano* **2021**, *15*, 7765.
[300] W. Zhao, D. Zhang, Y. Yang, C. Du, B. Zhang, *J. Mater. Chem. A* **2021**, *9*, 22082.
[301] C. Zheng, K. Lu, Y. Lu, S. Zhu, Y. Yue, X. Xu, C. Mei, H. Xiao, Q. Wu, J. Han, *Carbohydr. Polym.* **2020**, *250*, 116905.
[302] X. Jing, H. Mi, Y. Lin, E. Enriquez, X. Peng, L. S. Turng, *ACS Appl. Mater. Interfaces* **2018**, *10*, 20897.

[303] J. Xu, G. Wang, Y. Wu, X. Ren, G. Gao, *ACS Appl. Mater. Interfaces* **2019**, *11*, 25613.
[304] X. Yao, S. Zhang, L. Qian, N. Wei, V. Nica, S. Coseri, F. Han, *Adv. Funct. Mater.* **2022**, *32*, 2204565.
[305] T. Li, Y. Wang, S. Li, X. Liu, J. Sun, *Adv. Mater.* **2020**, *32*, 2002706.
[306] G. Su, S. Yin, Y. Guo, F. Zhao, Q. Guo, X. Zhang, T. Zhou, G. Yu, *Mater. Horiz.* **2021**, *8*, 1795.
[307] C. Yang, J. Yin, Z. Chen, H. Du, M. Tian, M. Zhang, J. Zheng, L. Ding, P. Zhang, X. Zhang, K. Deng, *Macromol. Mater. Eng.* **2020**, *305*, 2000479.
[308] J. Chen, X. Xu, M. Liu, Y. Li, D. Yu, Y. Lu, M. Xiong, I. Wyman, X. Xu, X. Wu, *Carbohydr. Polym.* **2021**, *264*, 1900285.
[309] L. Xu, Z. Huang, Z. Deng, Z. Du, T. Sun, Z. Guo, K. Yue, *Adv. Mater.* **2021**, *33*, 2105306.
[310] S. Li, H. Pan, Y. Wang, J. Sun, *J. Mater. Chem. A* **2020**, *8*, 3667.
[311] J. Zhang, L. Wan, Y. Gao, X. Fang, T. Lu, L. Pan, F. Xuan, *Adv. Electron. Mater.* **2019**, *5*, 1900285.
[312] Z. Lei, Q. Wang, S. Sun, W. Zhu, P. Wu, *Adv. Mater.* **2017**, *29*, 1700321.
[313] C. Zhang, Y. Zhou, H. Han, H. Zheng, W. Xu, Z. Wang, *ACS Nano* **2021**, *15*, 1785.
[314] J. Wei, J. Xie, P. Zhang, Z. Zou, H. Ping, W. Wang, H. Xie, J. Shen, L. Lei, Z. Fu, *ACS Appl. Mater. Interfaces* **2021**, *13*, 2952.
[315] X. Jing, H. Li, H. Mi, Y. Liu, P. Feng, Y. Tan, L. S. Turng, *Sens. Actuators, B* **2019**, *295*, 159.
[316] V. K. Rao, N. Shauloff, X. Sui, H. D. Wagner, R. Jelinek, *J. Mater. Chem. C* **2020**, *8*, 6034.
[317] Z. Zhang, L. Tang, C. Chen, H. Yu, H. Bai, L. Wang, M. Qin, Y. Feng, W. Feng, *J. Mater. Chem. A* **2021**, *9*, 875.
[318] P. Jiang, H. Qin, J. Dai, S. Yu, H. Cong, *Nano Lett.* **2022**, *22*, 1433.
[319] G. Ge, Y. Lu, X. Qu, W. Zhao, Y. Ren, W. Wang, Q. Wang, W. Huang, X. Dong, *ACS Nano* **2020**, *14*, 218.
[320] H. Zhu, J. Xu, X. Sun, Q. Guo, Q. Guo, M. Jiang, K. Wu, R. Cai, K. Qian, *J. Mater. Chem. A* **2022**, *10*, 23366.
[321] P. Wei, T. Chen, G. Chen, H. Liu, I. T. Mugaanire, K. Hou, M. Zhu, *ACS Appl. Mater. Interfaces* **2020**, *12*, 3068.
[322] J. Zhang, C. Wu, Y. Xu, J. Chen, N. Ning, Z. Yang, Y. Guo, X. Hu, Y. Wang, *ACS Appl. Mater. Interfaces* **2020**, *12*, 40990.
[323] Q. Ding, H. Wang, Z. Zhou, Z. Wu, K. Tao, X. Gui, C. Liu, W. Shi, J. Wu, *SmartMat* **2023**, *4*, 1147.
[324] J. Wu, Z. Wu, H. Xu, Q. Wu, C. Liu, B. Yang, X. Gui, X. Xie, K. Tao, Y. Shen, J. M. Miao, L. K. Norford, *Mater. Horiz.* **2020**, *7*, 595.
[325] A. J. Bandodkar, W. J. Jeang, R. Ghaffari, J. A. Rogers, *Annu. Rev. Anal. Chem.* **2019**, *12*, 1.
[326] Y. Luo, M. R. Abidian, J.-H. Ahn, D. Akinwande, A. M. Andrews, M. Antonietti, Z. Bao, M. Berggren, C. A. Berkey, C. J. Bettinger, J. Chen, P. Chen, W. Cheng, X. Cheng, S.-J. Choi, A. Chortos, C. Dagdeviren, R. H. Dauskardt, C. Di, M. D. Dickey, et al., *ACS Nano* **2023**, *17*, 5211.
[327] Z. Liang, J. Zhang, C. Wu, X. Hu, Y. Lu, G. Wang, F. Yu, X. Zhang, Y. Wang, *Biosens. Bioelectron.* **2020**, *155*, 112105.
[328] Y. Qin, J. Mo, Y. Liu, S. Zhang, J. Wang, Q. Fu, S. Wang, S. Nie, *Adv. Funct. Mater.* **2022**, *32*, 2201846.
[329] Z. Wu, L. Rong, J. Yang, Y. Wei, K. Tao, Y. Zhou, B. Yang, X. Xie, J. Wu, *Small* **2021**, *17*, 2104997.
[330] Y. Liang, Z. Wu, Y. Wei, Q. Ding, M. Zilberman, K. Tao, X. Xie, J. Wu, *Nanomicro Lett* **2022**, *14*, 52.
[331] L. T. Duy, H. Seo, *Sens. Actuators, B* **2020**, *321*, 128507.
[332] Y. Guo, J. Bae, F. Zhao, G. Yu, *Trends Chem.* **2019**, *1*, 335.
[333] Q. Xue, J. Sun, Y. Huang, M. Zhu, Z. Pei, H. Li, Y. Wang, N. Li, H. Zhang, C. Zhi, *Small* **2017**, *13*, 1701827.
[334] R. T. Yadlapalli, R. R. Alla, R. Kandipati, A. Kotapati, *J. Energy Storage* **2022**, *49*, 104194.
[335] T. Cheng, Y. Zhang, S. Wang, Y. Chen, S. Gao, F. Wang, W. Lai, W. Huang, *Adv. Funct. Mater.* **2021**, *31*, 2101303.
[336] Z. Wang, H. Li, Z. Tang, Z. Liu, Z. Ruan, L. Ma, Q. Yang, D. Wang, C. Zhi, *Adv. Funct. Mater.* **2018**, *28*, 1804560.
[337] T. Xu, K. Liu, N. Sheng, M. Zhang, W. Liu, H. Liu, L. Dai, X. Zhang, C. Si, H. Du, K. Zhang, *Energy Stor. Mater.* **2022**, *48*, 244.
[338] M. Li, S. Zhou, L. Cheng, F. Mo, L. Chen, S. Yu, J. Wei, *Adv. Funct. Mater.* **2023**, *33*, 2208034.
[339] J. Liu, J. Huang, Q. Cai, Y. Yang, W. Luo, B. Zeng, Y. Xu, C. Yuan, L. Dai, *ACS Appl. Mater. Interfaces* **2020**, *12*, 20479.
[340] Z. Gao, L. Kong, R. Jin, X. Liu, W. Hu, G. Gao, *J. Mater. Chem. C* **2020**, *8*, 11119.
[341] Y. Zhao, Q. Liang, S. M. Mugo, L. An, Q. Zhang, Y. Lu, *Adv. Sci.* **2022**, *9*, 2201039.
[342] Y. Guo, K. Zheng, P. Wan, *Small* **2018**, *14*, 1704497.
[343] T. Cheng, L. Li, Y. Chen, S. Yang, X. Yang, Z. Liu, J. Qu, C. Meng, Y. Zhang, W. Lai, *Adv. Mater. Interfaces* **2022**, *9*, 2201137.
[344] Y. Shi, Y. Zhang, L. Jia, B. Zhang, X. Xu, *ACS Appl. Mater. Interfaces* **2018**, *10*, 36028.
[345] F. Mo, Q. Li, G. Liang, Y. Zhao, D. Wang, Y. Huang, J. Wei, C. Zhi, *Adv. Sci.* **2021**, *8*, 2100072.
[346] Y. Zou, C. Chen, Y. Sun, S. Gan, L. Dong, J. Zhao, J. Rong, *Chem. Eng. J.* **2021**, *418*, 128616.
[347] F. Tao, L. Qin, Z. Wang, Q. Pan, *ACS Appl. Mater. Interfaces* **2017**, *9*, 15541.
[348] J. Wang, F. Liu, F. Tao, Q. Pan, *ACS Appl. Mater. Interfaces* **2017**, *9*, 27745.
[349] H. Peng, X. Gao, K. Sun, X. Xie, G. Ma, X. Zhou, Z. Lei, *Chem. Eng. J.* **2021**, *422*, 130353.
[350] J. Yang, X. Yu, X. Sun, Q. Kang, L. Zhu, G. Qin, A. Zhou, G. Sun, Q. Chen, *ACS Appl. Mater. Interfaces* **2020**, *12*, 9736.
[351] Y. Lin, H. Zhang, H. Liao, Y. Zhao, K. Li, *Chem. Eng. J.* **2019**, *367*, 139.
[352] J. H. Koo, D. C. Kim, H. J. Shim, T. H. Kim, D. H. Kim, *Adv. Funct. Mater.* **2018**, *28*, 1801834.
[353] Y. Zhou, X. Dong, Y. Mi, F. Fan, Q. Xu, H. Zhao, S. Wang, Y. Long, *J. Mater. Chem. A* **2020**, *8*, 10007.
[354] C. G. Granqvist, *J. Eur. Ceram. Soc.* **2005**, *25*, 2907.
[355] V. K. Thakur, G. Ding, J. Ma, P. S. Lee, X. Lu, *Adv. Mater.* **2012**, *24*, 4071.
[356] Y. Wang, R. Zheng, J. Luo, H. A. Malik, Z. Wan, C. Jia, X. Weng, J. Xie, L. Deng, X. Yao, *Electrochim. Acta* **2019**, *320*, 134489.
[357] Q. Chen, Y. Shi, K. Sheng, J. Zheng, C. Xu, *ACS Appl. Mater. Interfaces* **2021**, *13*, 56544.
[358] J. W. Kim, S. Kim, Y. R. Jeong, J. Kim, D. S. Kim, K. Keum, H. Lee, J. S. Ha, *Chem. Eng. J.* **2022**, *430*, 132685.
[359] J. Ko, A. Surendran, B. Febriansyah, W. L. Leong, *Org. Electron.* **2019**, *71*, 199.
[360] G. Li, L. Gao, L. Li, L. Guo, *J. Alloys Compd.* **2019**, *786*, 40.
[361] G. Liang, Z. Liu, F. Mo, Z. Tang, H. Li, Z. Wang, V. Sarangi, A. Pramanick, J. Fan, C. Zhi, *Light Sci Appl* **2018**, *7*, 102.
[362] Y. Zhang, Z. Ding, Y. Liu, Y. Zhang, S. Jiang, *J. Colloid Interface Sci.* **2021**, *582*, 825.
[363] H. Zhi, X. Fei, J. Tian, M. Jing, L. Xu, X. Wang, D. Liu, Y. Wang, J. Liu, *J. Mater. Chem. B* **2017**, *5*, 5738.
[364] Y. Wang, Z. Chen, N. Li, H. Zhang, J. Wei, *Eur. Polym. J.* **2022**, *166*, 111025.
[365] J. Shen, X. Wang, H. An, L. Chang, Y. Wang, W. Li, J. Qin, *J Polym Sci A Polym Chem* **2019**, *57*, 869.
[366] X. Hu, J. Liu, X. Du, R. Cheng, Q. Li, S. Chen, *J. Mater. Chem. C* **2019**, *7*, 10988.
[367] W. Li, Y. Cui, *Sol. Energy Mater. Sol. Cells* **2023**, *250*, 112071.
[368] J. Liu, Q. He, M. Pan, K. Du, C. Gong, Q. Tang, *J. Mater. Chem. A* **2022**, *10*, 25118.

[369] Q. Chen, J. Zhao, J. Zheng, C. Xu, *Electrochim. Acta* **2022**, *431*, 141156.
[370] S. Sun, X. Xia, F. Wang, M. Gao, W. Wei, S. Cui, Q. Zhu, *Electrochim. Acta* **2023**, *466*, 143006.
[371] W. Chen, S. Liu, L. Guo, G. Zhang, H. Zhang, M. Cao, L. Wu, T. Xiang, Y. Peng, *Polymers-Basel* **2021**, *13*, 742.
[372] G. Zhang, Y. Guo, Y. Fang, Y. Chu, Z. Liu, *J. Mater. Chem. C* **2023**, *11*, 5882.
[373] C. Chan, Z. Wang, H. Jia, P. Ng, L. Chow, B. Fei, *J. Mater. Chem. A* **2021**, *9*, 2043.
[374] W. Y. Toh, Y. K. Tan, W. S. Koh, L. Siek, *IEEE Sens. J.* **2014**, *14*, 2299.
[375] F. G. Torres, O. P. Troncoso, G. E. De-la-Torre, *Int. J. Energy Res.* **2022**, *46*, 5603.
[376] Y. Wu, Y. Luo, T. J. Cuthbert, A. V. Shokurov, P. Chu, S. Feng, C. Menon, *Adv. Sci.* **2022**, *9*, 2106008.
[377] X. Jing, H. Li, H. Mi, P. Feng, X. Tao, Y. Liu, C. Liu, C. Shen, *ACS Appl. Mater. Interfaces* **2020**, *12*, 23474.
[378] Y. Long, Y. Chen, Y. Liu, G. Chen, W. Guo, X. Kang, X. Pu, W. Hu, Z. Wang, *Nanoscale* **2020**, *12*, 12753.
[379] Q. Guan, G. Lin, Y. Gong, J. Wang, W. Tan, D. Bao, Y. Liu, Z. You, X. Sun, Z. Wen, Y. Pan, *J. Mater. Chem. A* **2019**, *7*, 13948.
[380] P. Liu, N. Sun, Y. Mi, X. Luo, X. Dong, J. Cai, X. Jia, M. A. Ramos, T. Hu, Q. Xu, *Compos. Sci. Technol.* **2021**, *208*, 108733.
[381] L. Dong, M. Wang, J. Wu, C. Zhu, J. Shi, H. Morikawa, *ACS Appl. Mater. Interfaces* **2022**, *14*, 9126.
[382] X. Han, D. Jiang, X. Qu, Y. Bai, Y. Cao, R. Luo, Z. Li, *Materials* **2021**, *14*, 1689.
[383] Y. Lai, H. Wu, H. Lin, C. Chang, H. Chou, Y. C. Hsiao, Y. Wu, *Adv. Funct. Mater.* **2019**, *29*, 1904626.
[384] D. Yang, Y. Ni, X. Kong, S. Li, X. Chen, L. Zhang, Z. Wang, *ACS Nano* **2021**, *15*, 14653.
[385] A. Khan, S. Ginnaram, C. Wu, H. Lu, Y. Pu, J. Wu, D. Gupta, Y. Lai, H. Lin, *Nano Energy* **2021**, *90*, 106525.
[386] W. Liao, X. Liu, Y. Li, X. Xu, J. Jiang, S. Lu, D. Bao, Z. Wen, X. Sun, *Nano Res.* **2022**, *15*, 2060.
[387] B. Bagchi, P. Datta, C. S. Fernandez, L. Xu, P. Gupta, W. Huang, A. L. David, D. Siassakos, H. V. S., M. K. Tiwari, *Nano Energy* **2023**, *107*, 108127.
[388] J. Zhang, X. Zhao, Z. Wang, Z. Liu, S. Yao, L. Li, *Adv. Mater. Interfaces* **2022**, *9*, 2200290.
[389] X. Luo, L. Zhu, Y. Wang, J. Li, J. Nie, Z. Wang, *Adv. Funct. Mater.* **2021**, *31*, 2104928.
[390] C. Wang, X. Qu, Q. Zheng, Y. Liu, P. C. A. Tan, B. Shi, H. Ouyang, S. Chao, Y. Zou, C. Zhao, Z. Liu, Y. Li, Z. Li, *ACS Nano* **2021**, *15*, 10130.
[391] G. Li, L. Li, P. Zhang, C. Chang, F. Xu, X. Pu, *RSC Adv.* **2021**, *11*, 17437.
[392] Y. Li, N. Li, N. D. Oliveira, S. H. Wang, *Matter* **2021**, *4*, 1125.
[393] J. H. Koo, J.-K. Song, D.-H. Kim, D. Son, *ACS Mater. Lett.* **2021**, *3*, 1528.
[394] S. Li, Y. Cong, J. Fu, *J. Mater. Chem. B* **2021**, *9*, 4423.
[395] X. Zhang, X. Chen, Z. Ye, W. Liu, X. Liu, X. Wang, *J. Mater. Chem. C* **2023**, *11*, 10785.
[396] Q. D. Liang, X. J. Xia, X. G. Sun, D. H. Yu, X. R. Huang, G. H. Han, S. M. Mugo, W. Chen, Q. Zhang, *Adv. Sci.* **2022**, *9*, 2201059.
[397] G. D. Spyropoulos, J. Savarin, E. F. Gomez, D. T. Simon, M. Berggren, J. N. Gelinas, E. Stavrinidou, D. Khodagholy, *Adv. Mater. Technol.* **2019**, *5*, 1900652.
[398] J. Ding, Z. Chen, X. Liu, Y. Tian, J. Jiang, Z. Qiao, Y. Zhang, Z. Xiao, D. Wei, J. Sun, F. Luo, L. Zhou, H. Fan, *Mater. Horiz.* **2022**, *9*, 2215.
[399] M. Dong, B. Shi, D. Liu, J.-H. Liu, D. Zhao, Z.-H. Yu, X.-Q. Shen, J.-M. Gan, B.-l. Shi, Y. Qiu, C.-C. Wang, Z.-Z. Zhu, Q.-D. Shen, *ACS Nano* **2020**, *14*, 16565.
[400] G. W. Tian, D. Yang, C. Y. Liang, Y. Liu, J. H. Chen, Q. Y. Zhao, S. L. Tang, J. P. Huang, P. Xu, Z. Y. Liu, D. P. Qi, *Adv. Mater.* **2023**, *35*, 2212302.
[401] Y. X. Liu, J. Liu, S. C. Chen, T. Lei, Y. Kim, S. M. Niu, H. L. Wang, X. Wang, A. M. Foudeh, J. B. H. Tok, Z. N. Bao, *Nat. Biomed. Eng.* **2019**, *3*, 58.
[402] L. Han, X. Lu, M. Wang, D. Gan, W. Deng, K. Wang, L. Fang, K. Liu, C. W. Chan, Y. Tang, L. Weng, H. Yuan, *Small* **2017**, *13*, 1601916.
[403] J. Sun, X. Wu, J. Xiao, Y. Zhang, J. Ding, J. Jiang, Z. Chen, X. Liu, D. Wei, L. Zhou, H. Fan, *ACS Appl. Mater. Interfaces* **2023**, *15*, 5897.
[404] X. Hu, P. Zhang, J. Liu, H. Guan, R. Xie, L. Cai, J. Guo, L. Wang, Y. Tian, X. Qiu, *Chem. Eng. J.* **2022**, *446*, 136988.
[405] X. Kang, X. Li, C. Liu, M. Cai, P. Guan, Y. Luo, Y. Guan, Y. Tian, K. Ren, C. Ning, L. Fan, G. Tan, L. Zhou, *J. Mater. Sci. Technol.* **2023**, *142*, 134.
[406] M. Shi, R. Dong, J. Hu, B. Guo, *Chem. Eng. J.* **2023**, *457*, 141110.
[407] H. Xuan, S. Wu, Y. Jin, S. Wei, F. Xiong, Y. Xue, B. Li, Y. Yang, H. Yuan, *Adv. Sci.* **2023**, 2302519.
[408] K. Roy, S. Jiang, E.-J. Jin, S. Y. Park, *Chem. Eng. J.* **2023**, *475*, 146168.
[409] H. An, Y. Yang, Z. Zhou, Y. Bo, Y. Wang, Y. He, D. Wang, J. Qin, *Acta Biomater* **2021**, *131*, 149.

**Zhikang Li** is currently an associate professor with the School of Instrument Science and Technology, Xi'an Jiaotong University. He received his Ph.D. in mechanical engineering from Xi'an Jiaotong University in 2017 and carried out his postdoctoral research with the groups of Prof. Ali Khademhosseini and Prof. Tzung Hsiai at the Department of Bioengineering, UCLA. His current research interests include skin-like electronics, flexible wearable biosensors, and micromachined ultrasonic transducers (MUTs) for non-invasively vital physiological signal detection and ultrasonic therapy.

**Jijian Lu** received his Bachelor's degree from Ocean University of China (OUC) in 2021. He is presently a second-year graduate student at the Institute of Precision Engineering, Xi'an Jiaotong University. His research interest focuses on self-healing hydrogel and its application in flexible/wearable tactile sensors.

**Yumeng Xue** received her Ph.D. in Frontier Institute of Science and Technology from Xi'an Jiaotong University in 2020. She is currently an associate professor at School of Materials Science and Engineering, Northwestern Polytechnical University. Her research interests focus on the design of new nanomaterials and the construction of multifunctional biomaterial systems, the exploration of new methods of material preparation, and its application and mechanism in biological imaging, tissue repair, disease diagnosis, and treatment.

**Libo Zhao** is a professor at School of Instrument Science and Technology, Xi'an Jiaotong University. He received his B.S., M.S., and Ph.D. degrees from Xi'an Jiaotong University, and carried out his postdoctoral research at Tsinghua University. Now his research interests include high-end MEMS sensors,MEMS ultrasonic transducers, flexible sensors, quantum sensors.

**Shiming Zhang** is currently an assistant professor at the University of Hong Kong (HKU). He is the PI of the wearable, intelligent, and soft electronics (WISE) research group. Before joining HKU, he spent 3 years at UCLA as a postdoctoral scholar and obtained his Ph.D. (first honor) from Ecole Polytechnique, University of Montreal, Canada, and B.S. and M.S. (first honor) from Jilin University, China. He is known for his pioneering contributions in designing tissue-like organic bioelectronics, focusing on soft and healable organic electrochemical transistors (OECTs). He demonstrated the world's first: stretchable OECTs, self-healable OECTs, and OECTs-based wearable biosensors.

**Zhuangde Jiang** is a professor with the School of Mechanical Engineering, Xi'an Jiaotong University, China. He is also an Academician of the Chinese Academy of Engineering and Honorary Professor with University of Birmingham, UK. He has been engaged in the research of micro-nano-manufacturing, microelectromechanical systems (MEMS), ultraprecision machining technology, sensing technology, and instrumentation for decades. His research interests also cover quantum sensing, biological detection technology, and biomedical instruments.